Dipl.-Ing. Levent TÜMBEK

Nucleation and thin film growth of the rod-like molecules hexaphenyl and pentacene on mica substrates

DOCTORAL THESIS

For obtaining the academic degree
Doktor der Technischen Wissenschaften“

Graz University of Technology

Supervisor:

Ao. Univ.-Prof. Dipl.-Ing. Dr. techn. Adolf Winkler

Institute of Solid State Physics

Graz,June 2017

Deutsche Fassung:
Beschluss der Curricula-Kommission für Bachelor-, Master- und Diplomstudien vom 10.11.2008
Genehmigung des Senates am 1.12.2008

EIDESSTATTLICHE ERKLÄRUNG

Ich erkläre an Eides statt, dass ich die vorliegende Arbeit selbstständig verfasst, andere als die angegebenen Quellen/Hilfsmittel nicht benutzt, und die den benutzten Quellen wörtlich und inhaltlich entnommene Stellen als solche kenntlich gemacht habe.

Graz, am …… ……
(Unterscrift)

Englische Fassung:

STATUTORY DECLARATION

I declare that I have authored this thesis independently, that I have not used other than the declared sources / resources, and that I have explicitly marked all material which has been quoted either literally or by content from the used sources.

…… ……
Date (signature)

Acknowledgments

I express my deepest gratitude to people and institutions who supported me during my Ph.D., without whom I could not have finished this work:

Austrian Academy of Science, Austrian Science Fund: For financially supporting my Ph.D. thesis.

Special thanks to Adolf Winkler: For truly excellent supervision, guidance and support throughout my thesis, including the chance to visit research institutes and conferences. Special thanks for having an open mind to any kind of new ideas and being the constant source of good atmosphere in our group.

Apart from the scientific part of my work, I would like to mention here that I enjoyed working in such an amicable atmosphere at this institute. In this context I would like to thank my lab mates Erkan Demirci, Thomas Potocar, Roman Lassnig, Boris Scherwitzl, and Bernhard Putsche for many pleasant hours of working in a climate of friendship.

Additionally, I have to thank Mathias, Dana and my mother for giving bravery to finish my Ph.D.

Abstract

Organic thin films have recently attracted considerable interest due to their potential applicability for flexible organic electronics. In particular, the understanding of the initial steps of film formation, nucleation, adsorption, diffusion and desorption is of utmost importance for a proper tailoring of organic films. The question arises whether large, anisotropic organic molecules behave in the nucleation process similarly as point-like atoms. Although this has been frequently assumed to describe organic film growth, some recent experimental results required a rethinking on this issue. In this thesis, I present some recent results on the nucleation of rod-like molecules (pentacene (5A) and para-hexaphenyl (6P)) on amorphous mica and draw some general conclusions on this subject. The organic molecules were deposited on sputter amorphized mica by physical vapor deposition in ultra-high vacuum (UHV). A quartz microbalance was used to quantify the deposited amount. Thermal desorption spectroscopy (TDS) was applied to obtain information on the energetics and kinetics of adsorption, nucleation and desorption. Ex-situ atomic force microscopy (AFM) was used to determine the morphology, island density and island size distribution of the sub-monolayer films. Both types of molecules formed islands, composed of standing molecules, on the sputter amorphized mica surface. This is typical for organic film growth on weakly interacting substrates, e.g. on silicon dioxide, as frequently used in fundamental and application studies.

Kurzfassung

Organische dünne Schichten haben wegen ihrer vielfältigen Anwendbarkeit im Zusammenhang mit flexibler organischer Elektronik in letzter Zeit besonderes Interesse erhalten. Insbesondere ist ein tieferes Verständnis der grundlegenden Prozesse des Schichtwachstums, der Nukleation, Diffusion und Desorption, wichtig um das Schichtwachstum gezielt beeinflussen zu können. Es erhebt sich nun die Frage ob sich große, anisotrope organische Moleküle bei der Nukleation gleich verhalten wie punktförmige Atome. Dies wurde in der Literatur bisher angenommen, unsere experimentellen Ergebnisse haben allerdings gezeigt, daß es erhebliche Unterschiede in diesem Zusammenhang gibt. In der vorliegenden Dissertation werden experimentelle Ergebnisse zur Nukleation und zum Schichtwachstum der stäbchenförmigen organischen Moleküle para-Hexaphenyl (6P) und Pentacene (5A) auf amorphem Glimmer vorgestellt und daraus einige allgemeine Schlüsse zum Schichtwachstum organischer Moleküle gezogen.

Die organischen Moleküle wurden mittels Dampfphasenabscheidung (PVD) unter Ultrahochvakuumbedingungen auf Glimmeroberflächen aufgebracht, die durch Sputtern amorphisiert wurden. Eine Quartz-Mikrowaage wurde für die Quantifizierung der aufgebrachten Menge eingesetzt. Die Thermische Desorptionsspektroskopie (TDS) wurde angewendet, um die Energetik und Kinetik der Adsorption, Nukleation und Desorption der organischen Moleküle zu untersuchen. Zur Bestimmung der Morphologie, Dichte und Größenverteilung inselförmiger ultradünner Schichten wurde die Atomkraftmikroskopie (AFM) eingesetzt. Beide Arten der untersuchten Moleküle (6P, 5A) bilden auf amorphisierten Glimmeroberflächen inselförmige Schichten die aus stehenden Molekülen bestehen. Dies ist typisch für organisches Schichtwachstum auf schwach reaktiven Oberflächen, wie zum Beispiel auch auf amorphem Silizium Dioxid, welches häufig eingesetzt wird, sowohl für das Studium fundamentaler Prozesse des Schichtwachstums wie auch für Anwendungen in der organischen Elektronik.

Initiatory Statement Regarding the Structure of this Thesis

The following work is a so-called cumulative Ph.D. thesis. As such, it is based on peer-reviewed scientific articles to which the author of the thesis has extensively contributed during the scientific work associated with the Ph.D. study. According to the structure suggested for such a thesis by the "Doctoral School of Physics" at Graz University of Technology, the associated articles are enclosed in the main part of the thesis in their original and published form. Moreover, an introduction is put into the main part in the context of previous work, and a summary is given in the light of the main findings of this thesis.

List of Enclosed Publications

Paper I [P1]

"Attachment limited versus diffusion limited nucleation of organic molecules: Hexaphenyl on sputter-modified mica"

L. Tumbek, A. Winkler

Surface Sci. 606 (2012) L55-L58.

Paper II [P2]

"Origin of the bimodal island size distribution in ultra-thin films of para-hexaphenyl on mica"

L. Tumbek, C. Gleichweit, K. Zojer, A. Winkler

Phys. Rev. B 86 (2012) 085402

Paper III [P3]

"Nucleation of organic molecules via a hot-precursor state: Pentacene on amorphous mica"

A. Winkler, L. Tumbek

J. Phys. Chem. Lett. 4 (2013) 4080

Paper IV [P4]

"Scaling and exponent equalities in island nucleation: Novel results and application to organic films "

A. Pimpinelli, L. Tumbek, A. Winkler

J. Phys. Chem. Lett. 5 (2014) 995-998

Paper V [P5]

"The influence of potassium on the growth of ultra-thin films of para-hexaphenyl on muscovite mica(001)"

B. Putsche, L. Tumbek and A. Winkler

J. Chem. Phys., 137 (2012) 134701

Paper VI [P6]

"Initial stages of para-hexaphenyl film growth on amorphous mica"

T. Potocar, S. Lorbek, D. Nabok, Q. Shen, L. Tumbek, G. Hlawacek, P. Puschnig, C. Ambrosch-Draxl, C. Teichert, A. Winkler

Phys. Rev. B 83 (2011) 075423.

Author Contributions

Paper I

The nucleation and growth of organic molecules is usually discussed in the framework of diffusion limited aggregation (DLA). In this letter we demonstrate for the rod-like organic molecules hexaphenyl (6P) on sputtered mica, that under specific experimental conditions the nucleation has to be described by attachment limited aggregation (ALA).

L.Tümbek performed all calculations and experiments. A.Winkler and L.Tümbek interpreted and analysed the experimental data. L.Tümbek prepared the figures. First version of manuscript was written by A.Winkler. Published version of the manuscript was improved in close cooporation with A.Winkler and L.Tümbek. A.Winkler supervised the project.

Paper II

The bimodal island size density, which is frequently observed when a sub-monolayer of 6P is deposited on muscovite mica, has been investigated in detail. Kinetic Monte Carlo Simulation has been applied; in particular to simulate the venting-induced subsequent nucleation process, by assuming that an initially immobile monomer phase becomes mobile at the venting.
A. Winkler conceived the idea to investigate the origin of bimodal island size distribution in ultrathin films of para-hexaphenyl on mica. L.Tümbek performed all the experiments. L. Tümbek and A.Winkler analysed the experimental data. L.Tümbek prepared the figures. Kinetic Monte Carlo Simulations calculations were performed by C. Gleichweit under the guidance of K. Zojer. A. Winkler wrote the first version of manuscript. The manuscript was then further improved with the help of all authors.
Adolf Winkler supervised the project.

Paper III

The classical scenario for thin film nucleation is the diffusion–limited aggregation (DLA). Recently, it has been shown that organic thin film growth is better described by attachment-limited aggregation (ALA). However, in both cases, unusual relationship between the island density and the substrate temperature was observed. In this manuscript, an aggregation model has been presented that goes beyond the classical DLA or ALA models to explain this behavior. We propose that the (hot) molecules impinging on the surface cannot immediately equilibrate to the substrate temperature but remain in a hot precursor state. In this state, the molecules can migrate considerable distances before attaching to a stable or unstable island. This results in a significantly smaller island density than expected by assuming fast equilibration and random diffusion. We have applied our model to pentacene film growth on amorphous Muscovite mica.

L. Tümbek performed all calculations and experiments. A. Winkler and L. Tümbek interpreted and analysed the experimental data. L. Tümbek prepared the figures. The first version of manuscript was written by L. Tümbek. Published version of the manuscript was improved in close corporation with A. Winkler and L. Tümbek. Adolf Winkler supervised the project.

Paper IV

Recently, Pimpinelli and Einstein have proposed an alternative analytic approach for extracting values of critical island size based on the capture zone distribution. In the manuscript, it has been shown that the Pimpinelli and Einstein approach can be generalized to any kind of aggregation mechanism.

L. Tümbek performed all the experiments. L. Tümbek and A. Winkler analysed the experimental data. L. Tümbek prepared the figures. The theoretical calculations were performed by A. Pimpinelli. A. Winkler wrote the manuscript in close corporation with A. Pimpinelli. A. Winkler and A. Pimpinelli equally contributed to this publication.

Paper V

Freshly cleaved mica, which is frequently used as a substrate for thin film growth studies, contains half a monolayer of potassium on the surface. In this work, we focus on the role of surface potassium on the layer growth of 6P on muscovite mica. It is assumed that after cleavage in air half a monolayer of potassium remains on the surface. However, since no superstructure can be observed in low energy electron diffraction (LEED), potassium is apparently randomly distributed. In the atomic force microscopy (AFM) investigations of this work it was found that actually domains with and without potassium exist on the mica surface, resulting in positively and negatively charged areas.
L. Tümbek performed all AFM investigations. B. Putsche, L. Tümbek and A. Winkler analysed the experimental data. L. Tümbek and B. Purtsche prepared the figures. First version of the manuscript was written by B. Putsche and L. Tümbek. Published version of the manuscript was improved in close corporation with A. Winkler. Adolf Winkler supervised the project.

Paper VI

We focus on the nucleation and submonolayer growth of 6P on a modified mica(001) surface, which has been amorphized by Ar+ ion sputtering. The 6P film formation on as-received mica(001) (typically produced by cleaving a mica sheet) has been intensively studied by several groups. The main observation was that in this case the rodlike molecules first forms a wetting layer of flat-lying molecules, and on top of this layer, needle like islands-that are also composed of flat-lying molecules- grow (Stransky-Krastanov growth). Recently, we discovered that a modification of the mica surface by gentle sputtering or by

covering the surface with a submonolayer of carbon results in a totally different growth behavior. On such a modified surface no wetting layer exists and the molecules start to form mounds consisting of standing molecules (Volmer-Weber growth).
L. Tümbek performed all TDS investigations. L. Tümbek and T. Potocar prepared the figures. The calculations were done by P. Puschnig. A. Winkler wrote the manuscript in close corporation with C.Teichert and C. Ambrosch-Draxl. A. Winkler supervised the project.

Contents

List of Acronyms

6P	Para-hexaphenyl
5A	Pentacene
α-peak	Multilayer peak, desorption of zero order
β-peak	Monolayer peak, desorption of first order
Θ	Coverage
acc. to	According to
AES	Auger electron spectroscopy
AFM	Atomic force microscopy
chap	Chapter
corr	Corrected
DLA	Diffusion limited aggregation
E_{des}	Desorption energy
equ	Equation
eV	Electron volt (1 eV = $1.602 \cdot 10^{-19}$ J)
Fig	Figure
i	Critical cluster size for nucleation
LED	Light emitting diode
LN2	Liquid nitrogen
ML	Monolayer
MW	Average value
PVD	Physical vapour deposition
QMS	Quadrupole mass spectrometer
R	Deposition rate
r	Desorption rate
SEM	Scanning electron microscope
T	Temperature
t	(Deposition) time
Tab	Table
TDS	Thermal desorption spectroscopy
u	Atomic mass unit ($1\ u = 1.66 \cdot 10^{-27}\ kg$)
UHV	Ultra-high vacuum
uncorr	Uncorrected
k	Boltzmann constant

1. Introduction

Organic thin films have recently attracted considerable interest due to their potential applicability for flexible organic electronics. In addition, the morphology of the organic films plays a crucial role for their electrical and electro-optical properties. Frequently used organic molecules, like oligo-acenes or oligo-phenylenes, are of rod-like shape; such molecules can be arranged in thin films either predominantly parallel or normal to the substrate surface. For the application as active layers in organic field effect transistors the films should be composed of standing molecules, because the charge carrier transport will mainly occur along the direction of the π-π bonds. On the other hand, the fluorescence emission of rod-like organic molecules will be most intense normal to the long molecule axis, requiring molecule orientation parallel to the substrate for organic light emitting diodes. It has been shown that the preferred orientation of rod-like organic molecules can be significantly influenced by a change of the chemical and/or geometrical composition of the substrate. Typically, on contaminated and/or rough surfaces islands composed of standing molecules will be dominant, whereas on clean, reactive surfaces the molecules will be forced to lie parallel to the surface.

In particular, the understanding of the initial steps of film formation, nucleation, adsorption, diffusion and desorption is of utmost importance for a proper tailoring of organic films. The question arises whether large, anisotropic organic molecules behave in the nucleation process similarly as point-like atoms. Although this has been frequently assumed to describe organic film growth, some recent experimental results required a rethinking on this issue. In this contribution we present new results on the nucleation of rod-like molecules (pentacene (5A) and para-hexaphenyl (6P)) on amorphous mica and draw some general conclusions on this subject.

The experiments were done under ultra-high vacuum conditions. The following experimental techniques were used: Auger electron spectroscopy (AES), quartz microbalance, thermal desorption spectroscopy (TDS) and ex-situ atomic force microscopy (AFM).

2. Theoretical Background

2.1. Growth behaviour

2.1.1 Growth modes

One can differentiate between three possible modes of crystal growth on surfaces as illustrated in fig 2.1 for three different coverages Θ, indicated in monolayer (ML) [1].

Frank van der Merwe Growth

In fig 2.1(a) the 'layer' or 'Frank van der Merwe' growth mode is shown. In this connection the atoms or molecules of the deposit are more strongly bound to the substrate, than to each other. First, a wetting layer (complete monolayer) is formed on the surface, the following layers are less tightly bound (monotonic decrease), toward the value for a bulk crystal of the deposit. This growth mode occurs in the case of adsorbed gases on graphite and several metals, in some metal-metal and semi-conductor systems.

Stranski- Krastanov Growth

In the 'layer plus islands' or 'Stranski-Krastanov' growth mode (b), a wetting layer is formed on the substrate. With increasing coverage, islands are formed on top of this layer. This growth mode occurs in metal-metal, semiconductor-metal systems, including 6P and 5A on unsputtered mica.

Volmer-Weber Growth

In the 'island' or 'Volmer-Weber' growth mode (c), islands are formed directly on the substrate surface. The atoms or molecules of the deposit are more strongly bound to each other than to the substrate. The growth mode occurs in many systems of metals on insulators and also for 6P and 5A on sputtered mica.

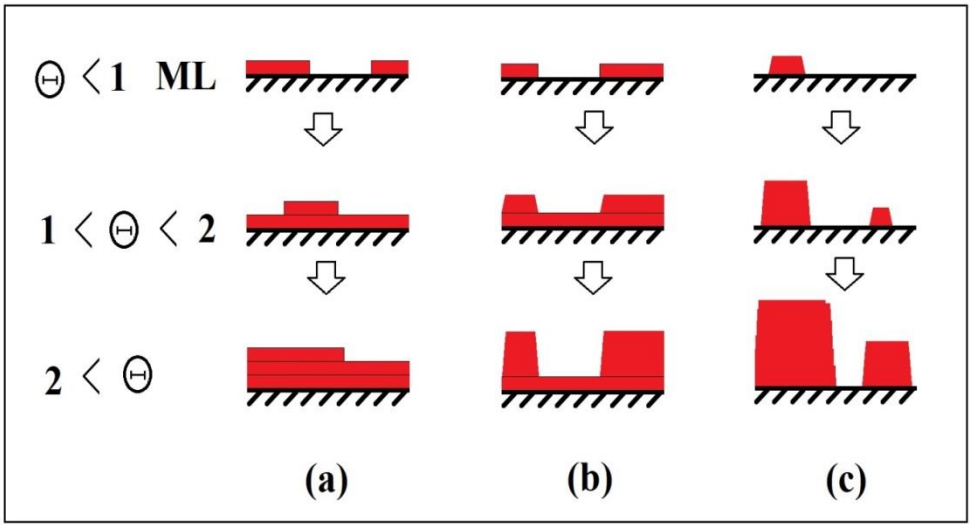

Figure 2.1: Sketch of the three crystal growth modes. (a) 'Frank van der Merwe' or 'layer' growth, (b) 'Stranski-Krastanov' or 'layer plus islands' growth, (c) 'Volmer-Weber ' or 'island' growth, Θ ; coverage/ ML [1]

2.1.2 Critical cluster size for nucleation

On the substrate, impinging molecules are diffusing on the surface as long as they do not encounter some other molecules. Not till then, the molecules start to form stable nuclei.
One less than the number of molecules which are necessary to form a stable nucleus, is called the critical cluster size for nucleation. Note that for 6P and 5A the particles are not point like. The nucleation can be described by the diffusion mediated growth, which involves four different steps [2]:

- **First step**
  Initially, monomers diffuse on an almost bare substrate, and when a critical number of them meet, a stable nucleus is formed.

- **Second step**
  In a second (intermediate) step, adsorbents still nucleate new islands but also start aggregating into existing ones.

- **Third step**
  Then, in the aggregation regime, the incoming material only aggregates into existing islands.

- **Fourth step**
  Finally, islands are growing together (coalescence).

The island density increases until the 3rd step is reached, in this so called aggregation regime (saturated island density) 3 different methods are used to determine the critical nucleation size in our publications. These methods are different growth rates, scaling theory and Voronoi analysis.

Different growth rates

The island density n_x (n_0 is the available adsorption sites) can be changed experimentally by variation of the deposition rate *R* and substrate temperature *T* in the following form [1]:

$$\frac{n_x}{n_0} = \eta(\Theta, i)\left(\frac{4R}{\nu_0 N_0}\right)^{\alpha} exp\left(\frac{iE_{diff}+E_i}{(i+2)kT}\right) \quad (2.1)$$

This equation is valid in case of complete condensation, i.e. when desorption of the monomers can be ignored. η is a weak function of Θ (≈ 0.1 − 1). ν_0 is the hopping frequency for diffusion, E_{diff} the diffusion energy of adatoms and E_i the binding energy of the critical cluster. In the exponent α = *i* / (*i* + 2), *i* means the critical cluster size for nucleation. To determine the critical cluster size, one has to plot $ln(n_x)$ vs. r, the slope *B* of a linear fit is therefore:

$$B = \alpha = \frac{i}{i+2} \quad (2.2)$$

As a result one gets for the critical nucleation size:

$$i = \frac{2}{\frac{1}{B}-1} \quad (2.3)$$

A drawback of this method is that one must produce a couple of samples for only one result at a fixed temperature.

Scaling theory

Another way to obtain the critical cluster size is given by the so called scaling theory, where the distribution of the island areas is used [2], [3], [4], [5]. The distribution of islands of size *a* per unit area (denoted as N_a in μm^{-4}) can be measured by AFM and can be plotted for different coverages Θ. Each graph has a well-defined maximum at A (mean value of a), which increases with increasing coverage and the distribution broadens. After rescaling acc. to:

$$N_a(\Theta) = \Theta A(\theta)^{-2} f(u) \quad (2.4)$$

the different distributions collaps into only one empirical scaling function $f(u)$. An analytical expression for the scaled island size distribution is given in the following term:

$$f(u) = C_i u^i \exp(-b_i i u^{1/b_i}) \quad (2.5)$$

with $u = a/A$. The numerical values of the parameters are fixed by the implicit hyper-geometrical equations:

$$\frac{\Gamma[(i+2)b_i]}{\Gamma[(i+1)b_i]} = (ib_i)^{b_i} \tag{2.6}$$

and

$$C_i = \frac{(ib_i)^{(i+1)b_i}}{b_i\Gamma[(i+1)b_i]} \tag{2.7}$$

An illustration of the scaling function (equ.2.5) is given in fig.2.2 where one can compare the different critical nucleation sizes from i = 1 to 6. The best fit of the measured size distribution to equ.2.5 for different i gives the critical island size.

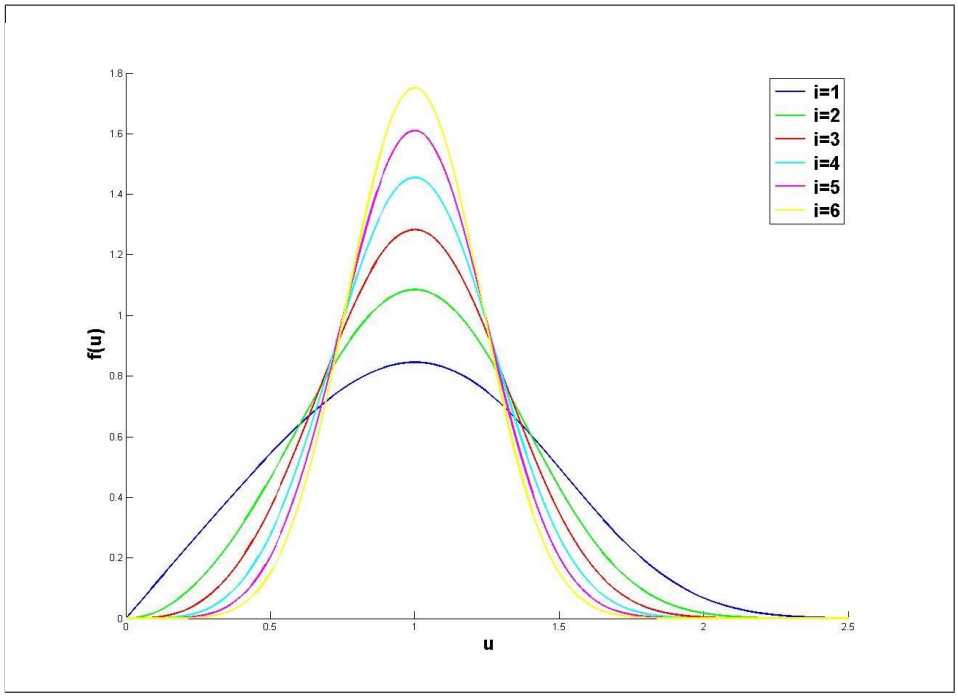

Figure 2.2: Scaling function with different critical nucleation sizes from i = 1 to 6 acc. to $f(u) = C_i\, u^i\, exp(-b_i\, i\, u^{1/bi})$, $u = a/A$ (a: island size, A: mean value of a).

Voronoi analysis

Another evaluation method is based on the so called Voronoi tesselation, where the critical island size can be derived from the islands capture zone distribution [6]. These zones can roughly be described by Voronoi polygons as illustrated in fig.2.3.

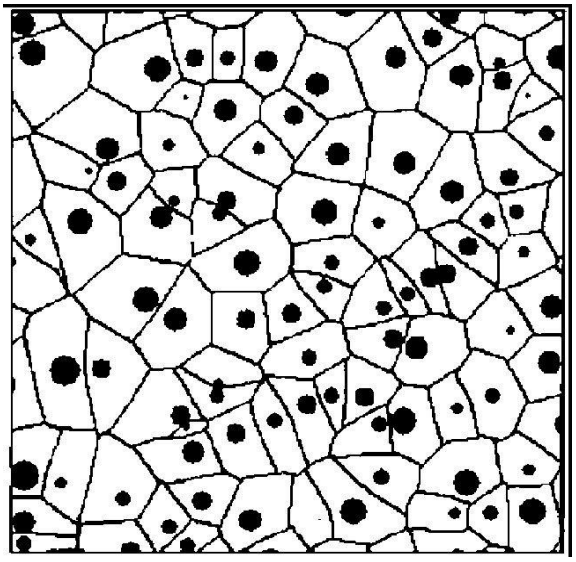

Figure 2.3: Voronoi tesselation. The boundaries of a Voronoi polygon of an island (black circles) are in the half distance between the nearest neighbour islands [6].

The size distribution *P* of the capture zones can be described by the generalized Wigner surmise:

$$P_\beta(s) = a_\beta s^\beta exp(-b_\beta s^2) \tag{2.8}$$

with $s = v/V$ (v: Voronoi polygon size, V : mean value of v) and the parameter

$$\beta = i + 2 \tag{2.9}$$

The two constants a_β and b_β are given by:

$$a_\beta = 2\Gamma\left(\frac{\beta+2}{2}\right)^{\beta+1} \Big/ \Gamma\left(\frac{\beta+1}{2}\right)^{\beta+2} \tag{2.10}$$

$$b_\beta = \left[\Gamma\left(\frac{\beta+2}{2}\right) / \Gamma\left(\frac{\beta+1}{2}\right)\right]^2 \tag{2.11}$$

As like as in the scaling theory, the best fit of the measured size distribution with equ.2.8 for different *i* gives the critical island size.

2.2. Analytical methods

2.2.1. Auger electron spectroscopy (AES)

Auger electron spectroscopy (AES) is a common analytical technique to measure the chemical composition of a surface. Underlying the spectroscopic technique is the Auger effect, where an impinging electron (2-10 keV) from an electron gun ionizes an atom in the material, which is to be examined. The so created hole in one of the inner shells (core hole) is filled either by an electron from an energetically higher level, where the energy is released by emitting a characteristic X-ray photon, or an outer electron, where the energy is transmitted in a radiationless process (Auger effect) to another electron.
This so-called Auger electron leaves the atom with a characteristic kinetic energy and can be classified by the involved energy levels. For instance, a KL_1L_2 Auger electron means that the atom is primarily ionized in the K shell, this hole is filled by an electron of the L_1 shell and the emitted electron comes from the L_2 shell. Therefore, three electrons are involved in the Auger process; hence H and He do not produce Auger electrons. The kinetic energy of course depends on the involved energy levels and can be approximated as follows:

$$E_{KL_1L_2} = E_K - E_{L_1} - E_{L_2} - \Phi - \Delta E_r \qquad (2.12)$$

Φ is the necessary energy to bring an electron to the vacuum level from the Fermi level (work function). Furthermore, one must take into account that the energy levels of the ionized atom shift in comparison to the neutral atom, expressed with the relaxation energy ΔE_r .The Auger spectra for all elements are recorded in a so-called Auger atlas [7]. Further information can be found in the corresponding literature [8].

2.2.2. X-ray photoelectron spectroscopy (XPS)

One of the most frequently used methods to probe the chemical composition of a sample surface is XPS, often also denoted as electron spectroscopy for chemical analysis (ESCA). This method involves irradiation of a solid in the vacuum with monoenergetic soft X-rays and sorting the emitted photoelectrons by their kinetic energy.

$$E_{kin} = h\upsilon - E_{Bind} - \psi_s \qquad (2.13)$$

ψ_s is the work function of the spectrometer. The kinetic energy E_{kin} of photoelectrons emitted upon irradiation of the sample with photons with a known energy of $h\upsilon$ depends on the binding energy of the involved photoelectron state E_{Bind} and is therefore

characteristic for each element and thus allows to identify the components of the sample surface. The fundamental process of generating photoelectrons is illustrated in **Fig. 2.4**. The spectrum obtained is a plot of the number of emitted electrons as a function of their kinetic energy.
Further details on this technique can be found in the literature [9-11].

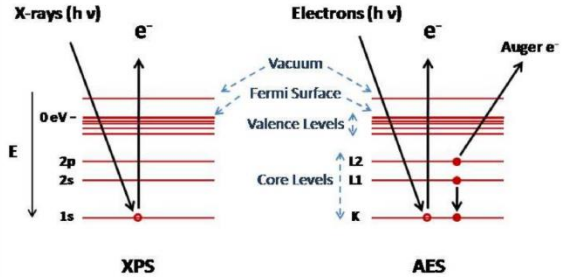

Fig. 2.4: Schematic view of the X-ray induced photoelectron (left) and the electron beam induced Auger electron (right) emission [12].

For the realization of the XPS experiments, a combined XPS/AES system by *Leybold Inc*. containing a concentric hemispherical analyser (CHA) was used. The X-ray source could be switched between Mg K_α (1253.6 eV) and Al K_α (1486.6 eV) radiation. Standard operating parameters were a source voltage of 10.5 kV and an emission current of 30 mA.

2.2.3. Atomic force microscopy (AFM)

The atomic force microscope is part of the family of scanning probe microscopes [10]. The first scanning probe microscope, the scanning tunnelling microscope (STM, 1981) restricted to electrically conducting surfaces [10]. With the AFM it became possible to get a three dimensional picture of surfaces also of insulating materials. Unfortunately very rough samples cannot be investigated.
The surface is scanned by a small sharp tip, which is mounted on a cantilever. The distance between the tip and the sample surface is so small that atomic-range forces act between them. This force can be determined by detecting the deflection of the cantilever by several methods:

- Optical interferometry
- An STM measures the cantilever deflection
- Laser beam with a position sensitive photo detector
- Capacitance change between cantilever and an additional electrode
- Electrically by a cantilever fabricated from piezo resistive material

The cantilever is typically 150-250 μm long, normal tips are 7 -15 μm high and have an end radius of 5-10 *nm* (fig. 2.5). The tip is moved over the sample (or the sample under the tip) by a piezoelectric scanner. The image size is therefore small compared to SEM (max. 100*x*100 μm).

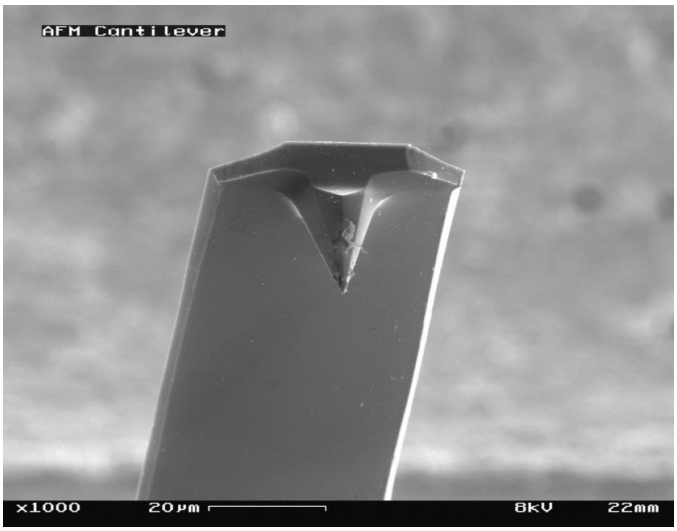

Figure 2.5: Cantilever in Atomic Force Microscope [13].

The AFM can be used in different modes. The distance from tip to sample used for AFM imaging defines the mode of operation (fig.2.5):

- Contact mode
- Non-contact mode
- Intermittent-contact mode

AFM contact mode

The tip to sample distance is only a few Angstrom (soft contact). The tip is affected by a repulsive force as shown in fig.2.6 (Lennard-Jones potential). For this mode one uses a cantilever with a low spring constant to avoid damaging of the probed surface. The tip-sample interaction causes the cantilever to bend following the change in surface topography.
Concerning the use of a feedback control one can distinguish between the constant height mode and the constant-force mode. To create an image in the constant-height mode, the scanner height is fixed and the cantilever deflection is monitored (fast scan speed). In constant-force mode, the cantilever deflection is fixed and the scanner height is monitored (limited scan speed).

AFM non-contact mode

The tip to sample distance is $1 - 10$ *nm* (little or no contact). The tip is affected by a weak attractive force. For this mode, stiffer cantilevers are necessary. The cantilever is in vibration near its resonant frequency ($100-400$ *kHz*), with a typical amplitude of a few tens

of Å. The cantilever resonance frequency is changed according the interaction with the surface. The non-contact mode is advantageous for studying soft or elastic samples.

AFM intermittent-contact mode

The tip is closer to the sample and vibrates with greater amplitude than that in the non-contact mode. This mode is also called 'tapping-mode', because the cantilever tip barely touches (taps) the surface. This mode is advantageous for surfaces with high topographical corrugation. In our AFM researches this tapping mode was used.

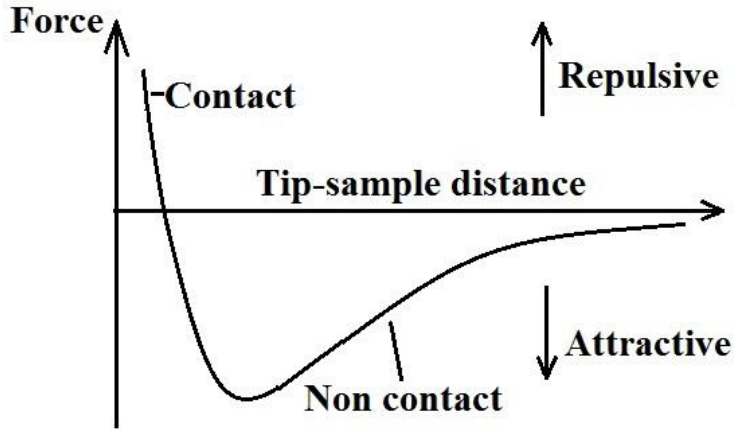

Figure 2.6: Force on the AFM tip versus distance from the sample surface (Lennard-Jones potential). In contact mode the distance of the tip from the sample is only a few Å (repulsive force). In non-contact mode the distance is 1 −10 nm (weak attractive force).

2.1.4. Thermal desorption spectroscopy (TDS)

To obtain thermal desorption spectra, a sample with previously adsorbed particles is heated with a temperature program in UHV. In the temperature program the heating rate β, the start and end temperature can be chosen. The desorbing particles can be detected by a mass spectrometer. This partial pressure versus temperature or time provides information for the determination of kinetic and thermodynamic parameters of desorption processes, such as:

- Desorption order from the peak shape
- Desorption energy from the peak temperature
- Number of desorption states from the number of desorption peaks
- Coverage from the peak area

A general relation between desorption rate r and temperature T is given by the Polanyi-Wigner equation [10].

$$r = -\frac{d\Theta}{dt} = \nu_n \Theta^n \, exp(-\frac{E_{Des}}{k \cdot T}) \quad (2.14)$$

Here, ν_n is the frequency factor, n the desorption order, Θ the coverage, E_{Des} the desorption energy and k the Boltzmann constant.

Coverage

The coverage is defined as

$$\Theta = \frac{N_{ad}}{N_{ad}^{max}} \quad (2.15)$$

N_{ad} is the number of adsorbed particles and N_{ad}^{max} the maximum number of adsorbable particles.

Frequency factor

ν_n is the frequency factor, one can interpret ν_1 as frequency of attempts of the adsorbed particle to desorb. For atoms and small molecules, the frequency factor can be correlated with the attempt frequency for desorption, which is in the order of 10^{13} s^{-1}. However, according to transition state theory, the pre-exponential factor contains the ratio of the partition functions of the molecules in the gaseous phase and the adsorbed phase. Due to the many rotational and vibrational degrees of freedom in the gas phase, the pre-exponential factor for large organic molecules is by orders of magnitudes larger than 10^{13} s^{-1}.

Desorption order

i. Desorption of zero order (n = 0)

In this case the desorption rate is independent of the coverage. The zero order desorption occurs in the multilayer regime and has the following characteristics:

- Exponential increase of r vs. temperature
- Steep decrease of r, if the adsorbate is no longer available
- The maximum of desorption shifts to higher temperature with increasing coverage

ii. Desorption of first order (n = 1)

The first order desorption occurs if single particles desorb directly and has the following characteristics:

- Asymmetric spectrum with steeper decrease at higher temperature

- The temperature of the desorption rate maximum is independent of coverage
- The temperature of the desorption rate maximum is dependent of the heating rate

iii. Desorption of second order (n = 2)

The second order desorption occurs if two atoms recombine during desorption and has the following characteristics:

- Symmetric peaks
- Peak maximum shifts with increasing initial coverage to lower temperatures

Determination of the desorption energy for zero order desorption

One can obtain the desorption energy from a simple analysis [14]. A plot $ln(r)$ vs. $1/T$ of the TD spectra gives with the logarithmic Polanyi-Wigner equation 2.14 for zero order desorption ($n = 0$):

$$ln(r) = ln(\nu_0) + ln(\Theta_{max}) - \frac{E_{Des}}{k} \cdot \frac{1}{T} \qquad (2.16)$$

the desorption energy from the slope of this plot. The frequency factor ν_0 can be determined from the intercept.

Determination of the desorption energy for first order desorption

A simple method to approximate the desorption energy E_{Des} for $n = 1$ is given by the Redhead equation [10]:

$$E_{Des} = k \cdot T_m \cdot [\, ln(\frac{\nu_1 T_m}{\beta}) - ln(\frac{E_{Des}}{kT_m})] \qquad (2.17)$$

3. Experimental Setup

Most of the experimental results shown in this work were produced in our laboratory. While AFM was performed ex-situ under ambient atmospheric conditions, thermal desorption spectroscopy (TDS), X-ray photoelectron spectroscopy (XPS) and Auger electron spectroscopy (AES) had to be accomplished under ultra-high vacuum (UHV) conditions. All these UHV experiments were conducted in our laboratory.

3.1 The UHV chamber

A schematic view as well as a more detailed description of the chamber and the sample holder can be found in ref [15]. The base pressure in the UHV chamber ~ 10^{-10} mbar could be reached after bake-out. The UHV was generated and maintained by rotary pumps and turbo pumps and monitored via a *Ionivac IM 520* ionisation gauge.
The sample was placed on a turn able sample holder which was located in the center of the chamber. The sample holder could be cooled down to about 100 K via a liquid nitrogen cooling finger attached to the sample holder. The above mentioned surface probing devices and a sputter gun for specimen cleaning were arranged within a measuring plane and could be addressed by rotating the sample holder.

3.2 Atomic force microscopy

After the removal of the ready samples from the vacuum chamber the surface was investigated by atomic force microscopy at five different positions. A tutorial of the used AFM (Figure 3.1) is given in [15], detailed information can be found in the manuals of the manufacturer [16] and [17]. The treatment and evaluation of the AFM pictures were done by Gwyddion (chap.A.4) [18]

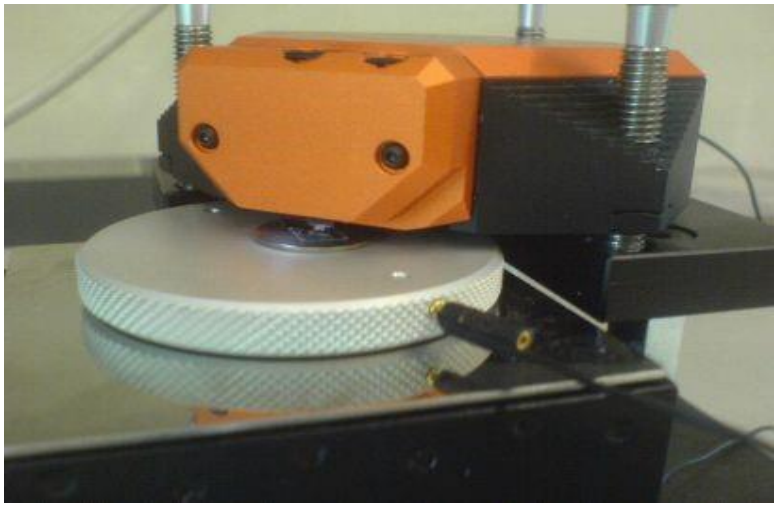

Figure 3.1 AFM

The ex-situ AFM Nanosurf easyScan2 was used in the dynamic force mode with a NCLR cantilever. For a better measurement the AFM is placed on an anti-vibration system (active vibration isolation system TS 150, fig.3.2).

Figure 3.2 Vibration isolation system TS 150.

4. Original Publications

Paper I [P1]

"Attachment limited versus diffusion limited nucleation of organic molecules: Hexaphenyl on sputter-modified mica"

L. Tumbek, A. Winkler

Surface Sci. 606 (2012) L55-L58.

Surface Science 606 (2012) L55–L58

Contents lists available at SciVerse ScienceDirect

Surface Science

journal homepage: www.elsevier.com/locate/susc

Surface Science Letters

Attachment limited versus diffusion limited nucleation of organic molecules: Hexaphenyl on sputter-modified mica

L. Tumbek, A. Winkler *

Institute of Solid State Physics, Graz University of Technology, Petersgasse 16, A-8010 Graz, Austria

ARTICLE INFO

Article history:
Received 13 February 2012
Accepted 22 March 2012
Available online 29 March 2012

Keywords:
Nucleation
Diffusion limited aggregation
Attachment limited aggregation
Hexaphenyl
Mica
Sputtering

ABSTRACT

The nucleation and growth of organic molecules is usually discussed in the framework of diffusion limited aggregation (DLA). In this letter we demonstrate for the rod-like organic molecules hexaphenyl (6P) on sputter-modified mica, that under specific experimental conditions the nucleation has to be described by attachment limited aggregation (ALA). The crucial parameter for the growth mode is the roughness of the substrate surface, as induced by ion sputtering. With decreasing surface roughness the diffusion probability of the molecules increases and the growth mode changes from DLA to ALA. This was derived from the deposition rate dependence of the island density. A critical size of $i=7$ molecules was determined for the nucleation of 6P on a moderately sputtered mica surface.

1. Introduction

The understanding and tailoring of organic thin film growth is a challenging issue in the context of modern organic electronics. Whereas the nucleation and growth of (metal) atoms is well understood [1–3], there is still lack of a comprehensive description for the nucleation and growth of larger (anisotropic) organic molecules. Although experimental evidence exists that in many cases organic film growth can be described sufficiently well with the models developed for single atom nucleation [4–7], there are also indications that substantial differences exist [8,9]. It is obvious, that the specific features of organic molecules (weak molecule–molecule and molecule-substrate interactions, low diffusion energies, diffusion anisotropy, many degrees of freedom, etc.) can lead to a larger variety of growth mechanisms than for point like particles.

In this letter we describe the nucleation and sub-monolayer formation of para-hexaphenyl (6P) on sputter-modified Muscovite mica(001) surfaces as a model system for the interaction of rod-like organic molecules with weakly interacting substrates. The merit of mica as a model substrate is the easy preparation of a rather clean, atomically flat single crystalline surface by just cleaving a mica sheet. It has been shown previously that on a freshly cleaved mica surface 6P forms needle like islands which are composed of flat lying molecules [10,11]. However, a modification of the mica surface by argon ion sputtering changes the film formation drastically: dendritic islands form which are composed of standing molecules [12]. Molecular dynamics calculations revealed that also in this case first clusters of lying molecules develop, which then reorient into the upright position at a cluster size of about 10–15 molecules [9]. From the island density as a function of the deposition rate, as well as from island size distributions (ISD) and capture zone distributions (CZD), a critical island size of 2–3 molecules was obtained for deposition at room temperature [9], by applying the nucleation model of diffusion limited aggregation (DLA) [3]. However, the temperature dependence of the island density exhibited some unusual features and it was argued that the anisotropic diffusion probability and/or orientation dependent attachment probability of the monomers at the rim of the islands might be responsible for these features. Here we demonstrate that in addition to the diffusion limitation the attachment limitation governs the nucleation and growth of 6P on mica(001), depending on the surface preparation by ion sputtering. We believe that the findings on this model system are relevant for many similar, more application related organic film/substrate systems, e.g. pentacene on silicon oxide [4,5,13,14], where typically the dielectric substrates are plasma treated prior to deposition of the organic semiconductor [15].

2. Experimental

The mica(001) samples ($10\times10\times\sim0.01$ mm^3) were prepared by cleaving them with adhesive tape in air and then attaching them to a steel plate sample holder, which was immediately installed inside a UHV chamber. The sample holder could be heated resistively and cooled by LN_2 to obtain sample temperatures between 150 K and 800 K. Surface characterization was performed by low energy electron diffraction (LEED), X-ray photoelectron spectroscopy (XPS),

* Corresponding author: Tel.: +43 316 873 8463; fax: +43 316 873 8466.
E-mail addresses: ltumbek@tugraz.at (L. Tumbek), a.winkler@tugraz.at (A. Winkler).

0039-6028/$ – see front matter © 2012 Elsevier B.V. All rights reserved.
doi:10.1016/j.susc.2012.03.018

Auger electron spectroscopy (AES) and thermal desorption spectroscopy (TDS), with respect to surface crystallography, surface chemical composition and thermal stability, respectively. The 6P films were deposited by physical vapor deposition (PVD) from a Knudsen cell. A quartz microbalance was used to determine the 6P film thickness quantitatively. For the modification of the mica surface to obtain exclusively layers with standing 6P molecules, the surface was sputtered with 500 eV Ar^+ ions, using an argon partial pressure of 5×10^{-5} mbar.[1] After the in-situ preparation and characterization of the 6P films on mica, the samples were investigated ex-situ by atomic force microscopy (AFM), by applying the tapping mode (Nanosurf, EasyScan2). More details regarding the sample holder, sample preparation and characterization of the samples with surface analytical techniques have been described elsewhere [9,12].

3. Results and discussion

In Fig. 1 three AFM images of sub-monolayer 6P films are shown, where about 0.1 monolayer (ML) were adsorbed on differently sputter-modified mica(001) surfaces, with a deposition rate of 0.1 ML/min at room temperature. Sputtering was performed with the above mentioned parameters, with sputter times of 3 min (a), 10 min (b) and 60 min (c), respectively. We could show that a sputter time of 3 min was sufficient to change the 6P layer growth from needle like islands, consisting of flat lying molecules, to dendritic islands composed of standing molecules. Also, a LEED analysis showed that after 3 min sputtering the distinct LEED spots of the freshly cleaved mica have already disappeared. However, from XPS and AES we observed that the chemical composition of the surface (silicon, aluminum, oxygen, potassium) was not significantly changed. Only small amounts of initially adsorbed carbon were removed. But even for extended sputtering the chemical composition of the near surface region remained the same, in particular the potassium signal did not change. Thus, one has to assume that in this case a change of the surface geometric structure is responsible for the changed 6P layer growth, rather than a change of the chemical composition.

The aggregation mode and the critical island size can be experimentally determined by the measurement of the island density N_x as a function of the deposition rate R. In Fig. 2 we present selected AFM images as obtained for different deposition rates at 200 K, to demonstrate the morphological development of the sub-monolayer 6P films. Similar series of AFM images were obtained for 6P films prepared at 150 K, 300 K and 400 K substrate temperature, respectively, over a wide range of deposition rates. The final coverage was held in the range between 0.1 and 0.3 ML, to stay in the aggregation regime. Below this coverage the film growth would be in the nucleation regime where the island density still increases with coverage; above about 0.5 ML the island density starts to decrease due to coalescence. In all cases the mica(001) surface was modified prior to 6P deposition by 10 min Ar^+ sputtering.

The most frequently applied model to describe nucleation is that for diffusion limited aggregation [16]. According to Venables et al. [3] the island density N_x in the aggregation regime can be described as a function of the deposition rate R by a power law [3]:

$$\frac{N_x}{N_0} = \eta(\Theta, i)\left(\frac{4R}{\nu_0 N_0}\right)^{\frac{i}{i+2}} \exp\left(\frac{iE_d + E_i}{(i+2)kT}\right). \quad (1)$$

Here N_0 is the number of adsorption sites per unit area (4.4×10^{14} 6P molecules cm^{-2} in the (001) plane), η is a weak function of the

[1] In this work a different sputter gun was used than in Ref. 9. In that work the sputter gas was introduced through the sputter gun, whereas in this work the gas was introduced via a separate leak valve. Therefore, in this work the effective ion flux is smaller for comparable equilibrium Ar pressure and sputter time.

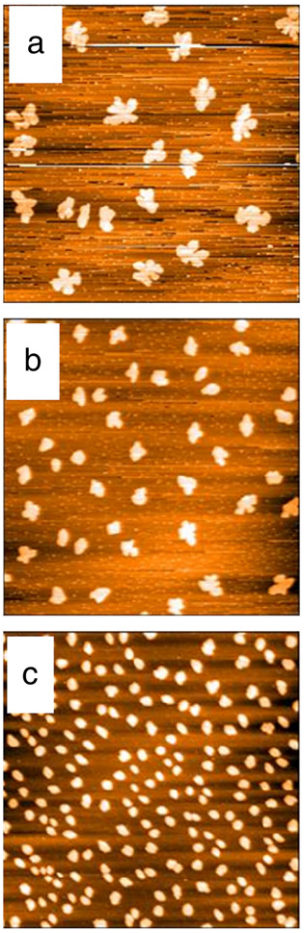

Fig. 1. AFM images (8 μm×8 μm) of 6P grown on sputter-modified mica(001) surfaces at T = 300 K, with various sputter time: (a) 3 min (b) 10 min (c) 60 min, sputter voltage: 500 V, Ar pressure: 5×10^{-5} mbar; 6P deposition rate: 0.1 ML/min, coverage: 0.1 ML.

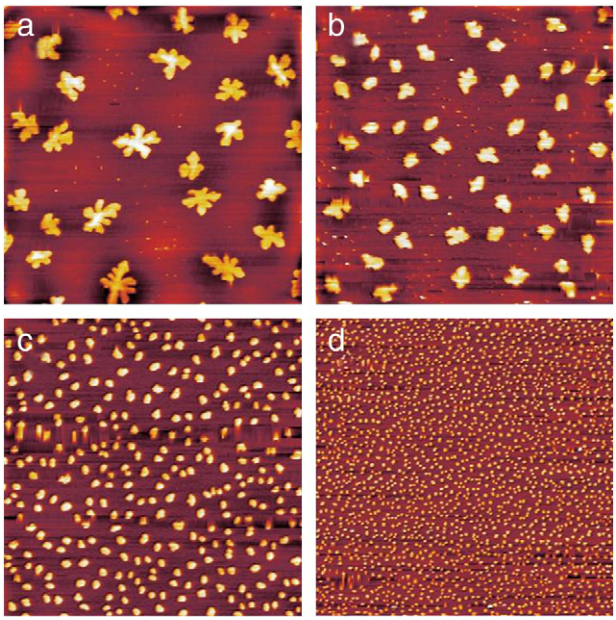

Fig. 2. AFM images (8 μm x 8 μm) of 6P grown on sputter modified mica(001) at 200 K with different deposition rates: (a) 0.14 ML at 0.037 ML/min (b) 0.13 ML at 0.097 ML/min, (c) 0.18 ML at 0.30 ML/min, (d) 0.26 ML at 0.80 ML/min.

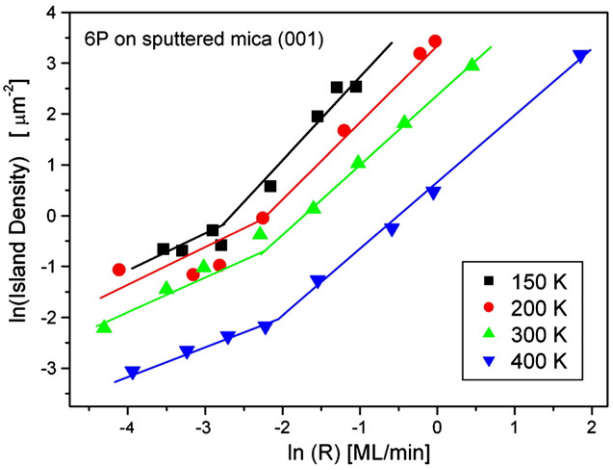

Fig. 3. Deposition rate dependence of the island density in the aggregation regime for 6P on sputter modified mica (001) at different temperatures. The lines are drawn to guide the eye for the two different regimes. The slopes α are 0.7 and 1.4 in the low and high deposition rate regime, respectively.

coverage Θ and the critical island size *i*, with η is ~0.2–0.3 [3], ν_0 the attempt frequency for surface diffusion, E_d the activation energy for monomer diffusion, E_i the binding energy of the critical cluster, and k the Boltzmann constant. In this model it is assumed that condensation is complete, i.e. no desorption of the monomers is allowed, and the attachment probability at the island edge is unity. According to Eq. (1) the critical island size can be determined from the deposition rate dependence of the island density. The value $\alpha = i/(i+2)$ can only vary between 1/3 (for $i=1$) and 1 (for large i). In Fig. 3 $\ln(N_x)$ versus $\ln(R)$ is compiled for four different series of deposition, performed at substrate temperatures of 150 K, 200 K, 300 K, and 400 K, respectively. One can see that two regimes with different slopes α exist, but within the regimes the slopes are nearly the same for all substrate temperatures. The surprising result is, however, that the average values of $\alpha \approx 1.4 \pm 0.1$ for higher deposition rates and $\alpha \approx 0.7 \pm 0.1$ for lower deposition rates. Apparently, the experimental data compiled in Fig. 3 for the high deposition rate regime cannot be explained by diffusion limited aggregation, where the slope α should be smaller than unity.

Kandel [17] and more recently Venables and Brune [18] have considered a scenario where the incorporation of the approaching monomers at the island edge is hindered. Such island edge barriers can exist in surfactant mediated growth, where the island edge atoms have first to be removed in order to attach further approaching atoms [19]. A physically different, but phenomenologically equivalent scenario can be visualized for the incorporation of the approaching flat lying 6P molecules at the edge of the islands, which are either composed of lying molecules for cluster size smaller than about 15 molecules or of standing molecules in larger islands [7]. Here the attachment probability will depend on the relative orientation between the approaching (lying) molecules and the molecule arrangement at the rim of the island, leading to an effective barrier for attachment. The overall capture number σ of an island depends on both, the diffusion barrier and the attachment barrier. Venables and Brune [18] have shown that the capture numbers add inversely ($1/\sigma = 1/\sigma_D + 1/\sigma_B$). If the attachment barrier capture number σ_B is negligible compared to the diffusion barrier capture number σ_D, the nucleation and growth are diffusion limited and Eq. (1) describes the nucleation process. For the reverse situation, $\sigma_B >> \sigma_D$, however, the following relationship was derived by Kandel [17]:

$$\frac{N_x}{N_0} = \eta^*(\Theta, i)\left(\frac{4R}{\nu_0 N_0}\right)^{\frac{2i}{i+3}} \exp\left(\frac{2[i(E_d+E_b)+E_i]}{(i+3)kT}\right). \quad (2)$$

Here, E_b is the attachment barrier and η^* again a weak function of the coverage Θ and the critical island size i [18]. One can see that for such a scenario the slope $\alpha = 2i/(i+3)$ can vary between 0.5 (for $i=1$) and 2 (for large i). For the above mentioned slope of $\alpha = 1.4 \pm 0.1$ we derive a critical island size of 7 ± 2 for 6P nucleation on moderately sputtered mica. For very low deposition rates the relative importance of the diffusion limitation increases. We assume that this is the reason for the decreased slope in Fig. 3. The evaluation of this regime according to Eq. (1) would yield a critical island size of 5 ± 2. However, one has to be cautious in the interpretation of the data points at very low deposition rate, because partial desorption and/or preferred nucleation at some surface inhomogeneity (heteronucleation) might also play a role in this case. Of course, it would be desirable to identify the critical island size directly by high-resolution AFM. However, since nucleation is a dynamic process it would be very difficult to unambiguously determine the critical island size by this method during deposition.

From the comprehensive data set in Fig. 3 one can also extract the island density as a function of temperature at constant deposition rate. The slope of the straight line in the plot $\ln N_x$ vs $1/T$ yields the energy term $\hat{E} = 2[i(E_d + E_b) + E_i]/(i+3)k$. The evaluation for deposition rates between 0.1 and 1 ML/min yields $\hat{E} \approx 0.2$ eV. Unfortunately, from this evaluation the contribution of the individual energy terms cannot be identified.

4. Conclusions

In conclusion, we have shown that the nucleation of rod-like organic molecules (6P) on a moderately sputtered mica(001) surface is attachment limited. The reason for this behavior is most likely that the attachment probability of the elongated 6P molecules depends on the relative orientation between the approaching (lying) molecules and the molecules at the rim of the islands (either lying in small clusters or standing in larger islands). There exist many unfavorable configurations for molecule incorporation, leading to an effective attachment barrier and hence to an integral attachment probability smaller than unity. A critical size of $i = 7 \pm 2$ molecules was determined from the deposition rate dependent island densities, using Kandel's formalism for attachment limited nucleation. Furthermore, we have shown that the surface roughness, and hence the diffusion probability on the surface, plays a crucial role for the nucleation and aggregation mode. With increasing surface roughness and/or by decreasing the deposition rate, the nucleation process can change from attachment limited to diffusion limited. The scenario of attachment limitation has not been considered so far in organic film growth, but it may play an important role for many practical cases in organic electronics, e.g. for pentacene film formation on silicon oxide.

Acknowledgments

This work was financially supported by the Austrian Science Fund (FWF), Project No. P 23530.

References

[1] H. Brune, Surf. Sci. Rep. 31 (1998) 121.
[2] T. Michely, J. Krug, Islands, mounds and atoms, Vol. 42, Springer Verlag, Berlin Heidelberg, 2004 Springer Series in Surface Sciences.
[3] J.A. Venables, G.D.T. Spiller, M. Hanbücken, Rep. Prog. Phys. 47 (1984) 399.
[4] R. Ruiz, B. Nickel, N. Koch, L.C. Feldman, R.F. Haglund Jr., A. Kahn, F. Family, G. Scoles, Phys. Rev. Lett. 91 (2003) 136102.
[5] B. Stadlober, U. Haas, H. Maresch, A. Haase, Phys. Rev. B 74 (2006) 165302.
[6] M. Campione, S. Caprioli, M. Moret, A. Sassella, J. Phys. Chem. C 111 (2007) 12741.
[7] G. Hlawacek, P. Puschnig, P. Frank, A. Winkler, C. Ambrosch-Draxl, C. Teichert, Science 321 (2008) 108.
[8] J. Yang, T. Wang, H. Wang, F. Zhu, G. Li, D. Yan, J. Phys. Chem. B 112 (2008) 7816.
[9] T. Potocar, S. Lorbek, D. Nabok, Q. Shen, L. Tumbek, G. Hlawacek, P. Puschnig, C. Ambrosch-Draxl, C. Teichert, A. Winkler, Phys. Rev. B 83 (2011) 075423.

[10] A. Andreev, G. Matt, C.J. Brabec, H. Sitter, D. Badt, H. Seyringer, N.S. Sariciftci, Adv. Mater. 12 (2000) 629.
[11] F. Balzer, H.-G. Rubahn, Appl. Phys. Lett. 79 (2001) 3860.
[12] P. Frank, G. Hlawacek, O. Lengyel, A. Satka, C. Teichert, R. Resel, A. Winkler, Surf. Sci. 601 (2007) 2152.
[13] K. Puntambekar, J. Dong, G. Haugstad, C.D. Frisbie, Adv. Funct. Mater. 16 (2006) 879.
[14] S. Pratontep, F. Nüesch, L. Zupprioli, M. Brinkmann, Phys. Rev. B 72 (2005) 085211.
[15] P. Pacher, A. Lex, V. Proschek, H. Etschmaier, E. Tchernychova, M. Sezen, U. Scherf, W. Grogger, G. Trimmel, C. Slugovc, E. Zojer, Adv. Mater. 20 (2008) 3143.
[16] T.A. Witten Jr., L.M. Sander, Phys. Rev. Lett. 47 (1981) 1400.
[17] D. Kandel, Phys. Rev. Lett. 78 (1997) 499.
[18] J.A. Venables, H. Brune, Phys. Rev. B 66 (2002) 195404.
[19] D. Kandel, E. Kaxiras, Phys. Rev. Lett. 75 (1995) 2742.

Paper II [P2]

“Origin of the bimodal island size distribution in ultra-thin films of para-hexaphenyl on mica”

L. Tumbek, C. Gleichweit, K. Zojer, A. Winkler

Phys. Rev. B 86 (2012) 085402

Origin of the bimodal island size distribution in ultrathin films of *para*-hexaphenyl on mica

L. Tumbek,[1] C. Gleichweit,[1] K. Zojer,[2] and A. Winkler[1,*]

[1]*Institute of Solid State Physics, Graz University of Technology, Petersgasse 16, A-8010 Graz, Austria*

[2]*Institute of Theoretical Physics, Graz University of Technology, Petersgasse 16, A-8010 Graz, Austria*

(Received 20 February 2012; revised manuscript received 11 May 2012; published 1 August 2012)

Ultrathin films of *para*-hexaphenyl ($6P$) were prepared on freshly cleaved and sputter-amorphized mica(001) by physical vapor deposition. *Ex situ* atomic force microscopy (AFM) revealed a bimodal island size distribution for the films on both surfaces. On freshly cleaved mica long needlelike islands exist, which are surrounded by small crystallites. On the sputter-amorphized substrates, large dendritic islands exist which are again surrounded by small, compact islands. We could prove by thermal desorption spectroscopy that the small islands are the result of adsorbate-induced subsequent nucleation, when the films were exposed to air. In case of the freshly cleaved mica, islands grow on a wetting layer in vacuum. This layer dewets and forms the small islands upon venting, due to the adsorption of water. In the case of the amorphous mica substrate an equilibrium exists between the islands and a two-dimensional gas phase in the sub-monolayer regime. Again, the latter phase nucleates after venting. In a particular coverage range, islands due to nucleation during deposition and subsequent nucleation coexist on the substrate, leading to the bimodal island size distribution. Kinetic Monte Carlo (KMC) simulations were performed to model the nucleation process after venting on the sputter-modified mica substrate. The density of the subsequently nucleated islands just depends on the initial coverage and the critical island size. A critical cluster size of $i = 7$ molecules was determined for $6P$ on amorphized mica, by comparing the KMC results with the AFM images in case of adsorbate-induced nucleation. Furthermore, the experimentally obtained island size distributions could be well reproduced by KMC simulations.

DOI: 10.1103/PhysRevB.86.085402 PACS number(s): 68.55.A−, 81.15.Aa, 68.37.Ps, 68.43.Vx

I. INTRODUCTION

Understanding the fundamental processes in the formation of organic thin films is of utmost importance for the application in organic electronic devices. In particular, the morphology of the organic films plays a crucial role for their electrical and electro-optical properties.[1,2] Frequently used organic molecules, like oligoacenes or oligophenylenes, are of rodlike shape; such molecules can be arranged in thin films either predominantly parallel or normal to the substrate surface. For the application as active layers in organic field effect transistors the films should be composed of standing molecules, because the charge carrier transport will mainly occur along the direction of the π-π bonds.[3] On the other hand, the fluorescence emission of rodlike organic molecules will be most intense normal to the long molecular axis, requiring molecule orientation parallel to the substrate for organic light-emitting diodes.[4] It has been shown that the preferred orientation of rodlike organic molecules in the film can be significantly influenced by a change of the chemical and/or geometrical composition of the substrate. Typically, on contaminated and/or rough surfaces films composed of upright-oriented molecules will be dominant, whereas on clean, reactive surfaces the molecules in the film will be forced to lie parallel to the surface, even for thicker films.[5] In particular, the molecule orientation in the first layer will usually determine the molecule orientation in the whole film.[6]

A frequently investigated model system for organic thin film growth is *para*-hexaphenyl ($6P$) on mica(001). The advantage of mica as a substrate is the easy production of very flat and clean single-crystal surfaces by simply cleaving a thin sheet of mica and installing it immediately into the evaporation chamber. The rodlike $6P$ molecules form extremely long needles on a freshly cleaved mica surface, which are composed of lying molecules. These needles could be used as optical nanofibers.[7] On the other hand, it has been shown that sputter amorphization of a mica surface, or the contamination of the surface with a sub-monolayer of carbon, leads to a totally different film formation, where dendritic islands appear which are composed of standing molecules.[8]

A special feature of very thin $6P$ films on mica, in the case of needle formation on the freshly cleaved mica,[8–11] as well as of dendritic island formation on sputter-amorphized mica,[12] is the frequent appearance of an extremely bimodal island size distribution. A similar bimodal distribution was also observed for $6P$ on titanium oxide.[13] Between the large islands many small islands (clusters) are distributed. Moreover, around the large islands a zone exists which is denuded of small clusters. It has been suggested that for the needle/cluster bimodal distribution on the freshly cleaved mica the needle growth is governed by the agglomeration of pre-existing clusters. An elastic strain-induced process has been proposed as the driving force.[9] Clusters of the size of up to 140 000 molecules were assumed to have sufficient mobility to agglomerate into the needlelike islands. This assumption was supported by the observation that the needles were indeed not uniform, but actually composed of individual clusters.[9,14]

In this work we reexamine the initial $6P$ growth of needlelike islands on freshly cleaved mica and compare the data with the bimodal island size distribution, as obtained

on the sputter-modified mica surface, using *ex situ* atomic force microscopy (AFM). In addition to that, we apply thermal desorption spectroscopy (TDS), which allows us to identify a possible wetting layer and its influence on the film formation. It turns out, that the small 6*P* islands (clusters) on both, the freshly cleaved and the sputter-modified mica surface, are the result of subsequent nucleation, when the 6*P*-covered mica surface is exposed to air for *ex situ* AFM investigations. Thus, the frequently observed bimodal island size distribution is the combined result of nucleation and growth during deposition and subsequent nucleation caused most probably by water adsorption after venting the vacuum chamber, which we call adsorbate-induced nucleation. For the modeling of the latter type of nucleation process we have carried out kinetic Monte Carlo (KMC) simulations.

II. EXPERIMENTAL DETAILS

Ultrathin films of 6*P* were deposited on muscovite mica(001) samples in an ultrahigh vacuum (UHV) chamber by physical vapor deposition (PVD) from a glass Knudsen cell. The mica(001) samples ($10 \times 10 \times \sim 0.01$ mm^3) were prepared by cleaving a mica sheet with the help of adhesive tape in air and immediately installed into the UHV chamber. The base pressure of the vacuum chamber after bake-out was 1×10^{-10} mbar, but typically the experiments were performed without baking the system, resulting in a working pressure of about 2×10^{-8} mbar. We have experimentally verified that the film growth was, within experimental error, the same in both vacuum regimes. The mica sheets were attached to a steel plate via tantalum wires, which was heated resistively. The temperature was controlled by a Ni-NiCr thermocouple spot welded to the back of the steel plate. This allowed a controlled heating of the steel plate and hence of the mica sample for TDS, typically with heating rates of 1 K/s. With additional LN_2 cooling, the temperature of the steel plate could be varied between 100 K and 1000 K. Unfortunately, a considerable temperature difference existed between the front mica surface and the heating plate, due to the low heat conductivity of mica normal to the (001) plane.[15] However, a calibration of the temperature can be performed by comparing the multilayer peak maximum of desorbing 6*P* from mica with that from the tantalum wires, as described in more detail elsewhere.[8] For TDS a multiplexed quadrupole mass spectrometer (QMS) (0–500 amu) was used. In addition to the mass of the 6*P* molecules ($m = 458.6$ amu), typically the mass $m = 61$ amu was measured, because this showed the largest signal of the cracking pattern in the QMS. Furthermore, it was verified that no cracking of the 6*P* molecules occurred at the surface.

For the quantitative determination of the 6*P* film thickness a quartz microbalance was used which was positioned next to the sample. The reliability of this device was checked in two ways: (a) by comparing with corresponding AFM images of sub-monolayer films of standing molecules and (b) by TDS, as outlined in more detail elsewhere.[8] For the modification of the mica surface to obtain exclusively layers with standing 6*P* molecules, the surface was sputtered for about 10 min by Ar^+ ions with 500 eV at an argon partial pressure of 5×10^{-5} mbar. Auger electron spectroscopy (AES) and x-ray photoelectron spectroscopy (XPS) were applied to check the chemical composition of the mica substrate. After the *in situ* preparation and characterization of the 6*P* films on mica, the samples were investigated *ex situ* by AFM in the tapping mode (Nanosurf, EasyScan2).

III. KINETIC MONTE CARLO SIMULATION

Kinetic Monte Carlo simulations are frequently applied to study various aspects of epitaxial film growth. In nearly all known studies the particles, which are assumed to be pointlike, can occupy specific lattice sites and move between these sites with specific hopping rates. Although in our case the particles are rodlike entities, we chose to apply the well-established computational techniques of pointlike particles. We justify our choice of pointlike entities for the KMC simulations as follows: First, the elongated molecules are oriented upright in the condensed islands and therefore occupy single adsorption sites in the 6*P*(001) plane. Second, the distance between the islands, which is on the order of micrometers, is much larger than the size of the (anisotropic) molecules. Third, the isotropic island distribution (on the sputter-modified substrate) and the irregular dendritic shape of the islands show that the diffusion behavior of the anisotropic, lying molecules can be sufficiently well approximated by the diffusion of pointlike particles. We are only aware of one KMC study where dimer particles were allowed to occupy lattice sites in lying and standing configurations.[16] However, the consideration of all possible conformations in the nucleation process of extended oligomers and the (unknown) energy barriers involved would make KMC simulations exceedingly time consuming and most probably of little physical significance.

Our simulations are based on the approach of Bales and Chrzan,[17] which we extended by considering also reversible aggregation by including the critical island size i as a parameter of the simulations, in the spirit of Li and Evans.[18] The simulations were performed on a square lattice, where each lattice site can contain one molecule.[19] Because we investigate the system in the sub-monolayer regime, we do not regard molecules hopping into a second layer. Monomers can diffuse at a rate $h_1 = \nu \exp(-\frac{Q}{kT})$, where Q is the energy barrier for surface diffusion, ν is the hopping frequency, k the Boltzmann constant, and T the substrate temperature. This rate also applies for particles having neighbors in the nearest-neighbor cells, as long as the size of the island does not exceed the critical nucleus size i. As soon as an island reaches this size, aggregation is irreversible, meaning that the particles cannot detach anymore from the island, but may diffuse along the edge. In the classical solid-on-solid model the edge hopping rate is described by $h_n = \nu \exp(-\frac{Q+nE}{kT})$, where n is the number of in-plane nearest neighbors ($n = 1$–4) and E is the nearest-neighbor binding energy. In our simulations we do not consider the binding of the molecules to the substrate when they diffuse along the island rim. This is justified because the bonding of the standing molecules to the mica substrate via one H atom is negligible, compared to the bonding between the many C atoms between parallel arranged 6*P* molecules. It is, of course, not known how exactly diffusion along the island rim proceeds, but for the final stability of the incorporated molecules only the bonds between the molecules will be of

relevance. Thus, we describe the hopping rate along the rim of the islands by $h_n = v \exp(-\frac{nE}{kT})$. Furthermore, a flux F of impinging particles can be applied which corresponds to adsorption. We do not allow for desorption.

When referring to KMC, the so-called BKL algorithm of Bortz, Kalos, and Lebowitz,[20] originally proposed for simulating the Ising spin system, is commonly applied. Their way of keeping track of the possible event types that exist in a system (the so-called n-fold way) can be applied in our simple model. Namely, there are only a small number of different classes of sites a particle can belong to, depending on the number of neighbor particles. Each particle belonging to the class j hops at a rate Γ_j. By choosing a random number, first an event class is selected and then one event of that class is executed, meaning that the particle is moved. A time-saving algorithm for updating the event list is essential. In short, this is done by recalculating the events of the neighboring particles only, using an inverse list that keeps track of where to find the events of a specific particle in the event lists.[21] The time is then incremented by a stochastic variable $\Delta t = -\frac{\ln(r)}{\Gamma_{\text{tot}}}$, where $r \in (0,1)$ is a random number, $\Gamma_{\text{tot}} = \sum_j n_j \Gamma_j$ is the total rate, and n_j is the number of events of class j.

Our partially reversible approach leads to the well-known problem of stiffness (Ref. 22 and references therein), which in our case refers to the separation of time scales between monomer diffusion processes and edge hopping. Most of the computational time is used for calculating the diffusion processes of particles that may be far away from any nucleation site. The monomer density in our case can be quite high, while still only very few islands form. This is because the local nucleation probability scales with $dN_{\text{isl}}/dt \sim N_1^{i+1}$,[23] where N_{isl} denotes the number of islands and N_1 is the monomer density.

Although our KMC formalism is constructed to simulate nucleation processes during the impingement of monomers, in this work we mainly apply the formalism to simulate the adsorbate-induced subsequent nucleation process. In this case we assume that initially a specific amount of immobile monomers exists on the surface (in the sub-monolayer coverage range), which are randomly distributed. With the start of the KMC simulation the monomers are allowed to become mobile with a specific diffusion probability and the number of monomers and islands is computed as a function of time and critical island size, until all monomers are incorporated in the islands. We could show that in this case the actual values of E and Q just influence the shape of the formed islands and only effect the simulation time. It turns out that only the critical island size and the monomer density determine the final island density.

IV. RESULTS AND DISCUSSION

In Fig. 1 typical AFM images are shown for $6P$ films grown under appropriate growth conditions on freshly cleaved mica(001) [Fig. 1(a)] and on sputter-modified mica [Fig. 1(b)]. Figures 1(c) and 1(d) show selected cross sections as indicated in Figs. 1(a) and 1(b). In both cases a clear bimodal island size distribution can be observed. However, this film morphology can only be seen in a special coverage range, when deposited at a particular surface temperature. For the freshly cleaved mica surface this phenomenon was investigated in detail by Kankate *et al.*,[10] but it was also observed by others.[8,9,11] Generally, at low coverage only small clusters exist; in a medium coverage range clusters and needles coexist, whereas at higher coverage, when the needle density is already quite high, the density of the small clusters vanishes. With respect to the substrate temperature, the needle length, width, and height increase with temperature. Due to the overlapping of the denuded zones with increasing number density of the long needles, the total number density of the small clusters decreases with increasing coverage.

While the needlelike island formation on the freshly cleaved (anisotropic) mica surface could be rationalized by a strain-induced agglomeration of the small crystallites, where the wetting layer should play an important role,[9] this scenario cannot explain the quite similar bimodal island size distribution on the sputter-modified mica surface [Fig. 1(b)]. In this case, no wetting layer exists and the irregular, dendritic shape of the large and small islands demonstrates that the sputtered mica surface is isotropic. This is also supported by the lack of a regular LEED pattern in case of the sputtered surface.[8]

A. $6P$ on freshly cleaved mica

Before we focus on the $6P$ layer growth on the sputter-modified surface we present some illustrative experimental results for the initial growth of $6P$ on the freshly cleaved mica. As outlined previously,[24] TDS is a powerful method to get insight into the energetics of organic thin films. In particular, one can distinguish between molecules in a strongly bound wetting layer and the more weakly bound molecules in the three-dimensional (3D) islands. In Fig. 2(a) (curve a) a $6P$ desorption spectrum from the freshly cleaved mica surface is shown, obtained after deposition of an amount equivalent to 10-Hz frequency change at the quartz microbalance. The high-temperature peak at about 535 K can be attributed to the wetting layer, whereas the large peak at 490 K corresponds to desorption from the needlelike islands.[8] At a lower deposited amount, equivalent to a quartz frequency change of 2 Hz, only the wetting layer is observed [Fig. 2(a), curve b]. We have calibrated our experimental setup for $6P$ deposition with AFM, where we could attribute a quartz frequency change of 16 Hz to a saturated monolayer of standing molecules on the sputter-modified mica surface. Assuming that the molecule packing in this layer is close to that in the $6P(001)$ crystal plane, 1 ML of standing molecules equals 4.4×10^{14} $6P$ molecules/cm^2, equivalent to a mean height of 2.6 nm. Correspondingly, the coverage of a densely packed layer of flat-lying molecules (wetting layer) corresponds to 5.8×10^{13} $6P$ molecules/cm^2, or a mean height of 0.35 nm. This fits quite well to the 2 Hz needed to saturate the wetting layer (0.32 nm mean thickness) [Fig. 2(a), curve b].

Interestingly, the *ex situ* AFM image of the 2-Hz film did not show a uniform, unstructured film, as one would expect for a wetting layer, but showed instead many small, slightly elongated islands, with a mean diameter of about 50 nm and a mean height of about 5 nm [Fig. 2(b)]. The size of these islands is similar to that as frequently observed for the small clusters in the bimodal films obtained at higher total coverage.[9–11] From

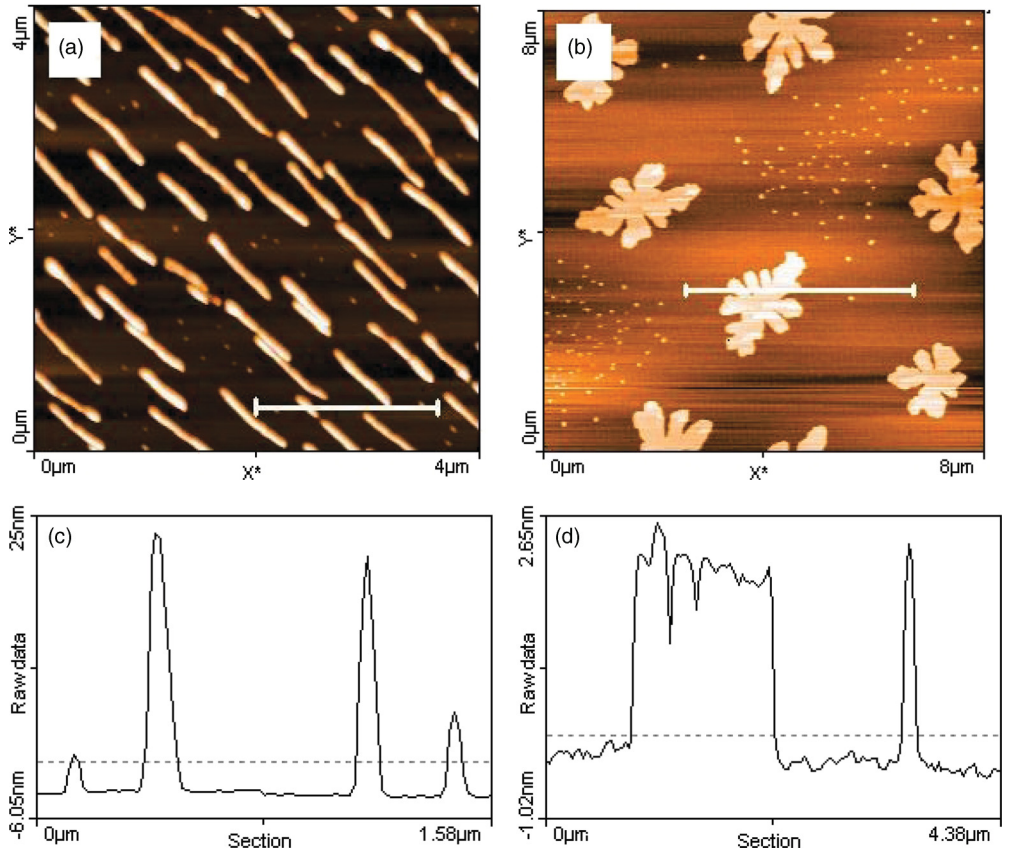

FIG. 1. (Color online) (a) AFM image (4×4 μm) for 6P on a freshly cleaved mica(001) surface. Deposition temperature, 400 K; deposition rate, 0.06 ML/min; deposited amount, 0.62 ML (standing monolayer equivalents). (b) AFM image (8×8 μm) for 6P on a sputtered mica(001) surface. Deposition temperature, 400 K; deposition rate, 0.07 ML/min; deposited amount, 0.18 ML. (c) Cross section along the line as indicated in (a), demonstrating different heights of the needles and clusters. (d) Cross section along the line as indicated in (b), demonstrating the same heights for the large and small islands, consisting of one layer of standing molecules.

the height and height distribution we can reason that in this case the islands are again composed of flat-lying molecules. The evaluation of Fig. 2(b) with respect to the total coverage by integrating over all islands gives a mean height of 0.4 $\pm$ 0.1 nm, in good agreement with the expected saturated wetting layer. (Actually, the somewhat too high value for the mean height can be rationalized, because no tip deconvolution for the AFM image was made). The answer to this puzzling result was found, when after the AFM measurement the sample was again installed into the vacuum chamber and a TDS was

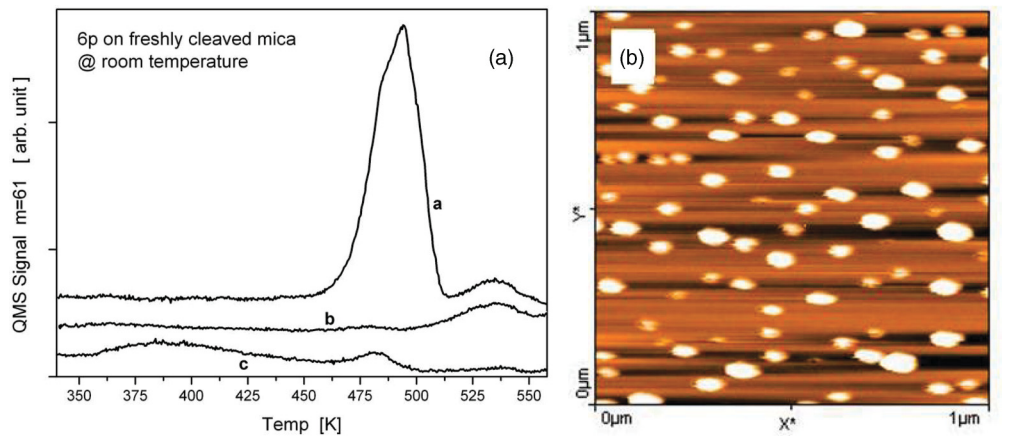

FIG. 2. (Color online) (a) Thermal desorption spectra of 6P (mass 61 amu) on freshly cleaved mica(001), deposited at room temperature. Curve a: deposited amount, 10 Hz (1.6 nm mean thickness); curve b: deposited amount, 2 Hz (0.32 nm mean thickness); curve c: deposited amount, 2 Hz, but afterwards exposed to air and evacuated again before desorption. (b) AFM image (1×1 μm) of 6P on freshly cleaved mica. Deposition temperature, 400 K; deposition rate, 0.05 nm/min; deposited amount, 2 Hz; equivalent to 0.32 nm mean thickness.

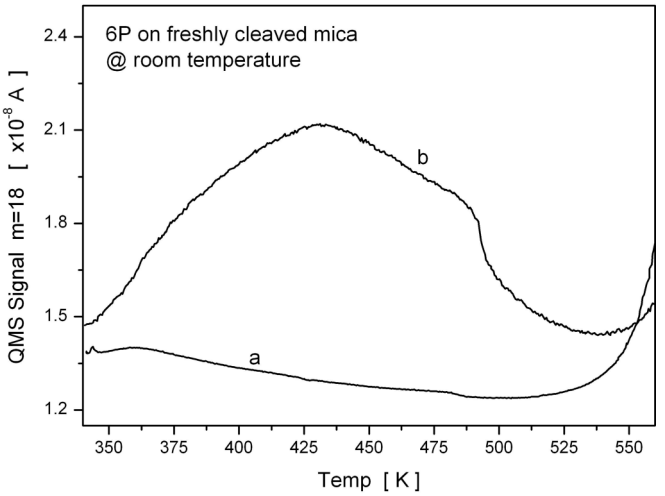

FIG. 3. Multiplexed thermal desorption spectra of water (m = 18 amu) after the deposition of 2-Hz equivalents of 6P on the freshly cleaved mica, prior to venting the vacuum chamber (a) and after venting and reevacuation (b).

performed after a proper vacuum was achieved [Fig. 2(a), curve c]. The desorption spectrum is now significantly changed in comparison to curve b. There is nearly no material desorbing in the temperature regime of the wetting layer, but a considerable amount desorbs in a temperature range which is characteristic for desorption from 3D islands. In addition, quite some 6P desorbs already at low temperature between 350 K and 430 K. However, the total amount of desorbing 6P molecules before and after venting the vacuum system is nearly the same. From this result we have to draw the conclusion that the energetics, and hence the morphology of the wetting layer, have changed dramatically upon venting the vacuum system. The reason for this behavior is most probably the adsorption of water. Indeed, multiplexed mass spectrometry clearly shows increased water desorption in case of the reinstalled sample, compared to that prior to venting, as shown in Fig. 3, but no significant desorption of oxygen was observed. Thus, we have to assume that adsorbed water weakens the bonding between the flat-lying 6P molecules in the wetting layer and the mica substrate, which increases the mobility of the molecules and allows the nucleation of islands by dewetting. Consequently, at higher coverage, where already needlelike islands have formed above the wetting layer in vacuum, again after venting the remaining molecules in the wetting layer will postnucleate and thus lead to the bimodal island size distribution. The molecules which exist in the vicinity of the needles will be predominantly incorporated in the needles upon venting, thus leading to the denuded zone for the small clusters.

B. 6P on sputter-modified mica

Now we turn to the 6P layer growth on the sputter-modified mica surface in the sub-monolayer coverage regime. As shown in Fig. 1(b) and in our previous work,[12] also in this case a bimodal island size distribution can be observed in a certain coverage range, where both the large and small islands are composed of standing molecules, as verified by AFM [Fig. 1(d)]. The large islands exhibit a dendritic shape,

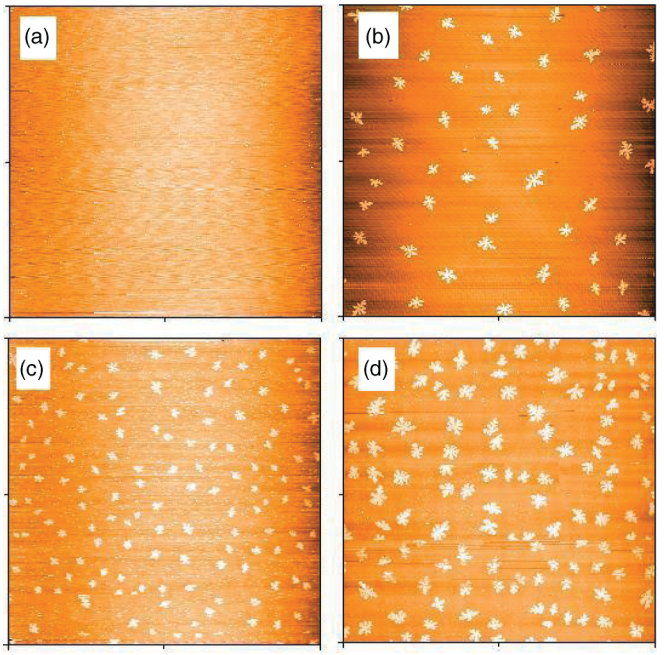

FIG. 4. (Color online) Large-scale AFM images (32 × 32 μm) for 6P on sputter-modified mica(001) surfaces. Deposition temperature, 400 K; deposition rate, 0.08 ML/min; deposited amount: (a) 0.036 ML, (b) 0.04 ML, (c) 0.077 ML, (d) 0.147 ML. The small islands are hardly visible in this representation.

whereas the small islands are more compact. In Figs. 4(a)–4(d) and Figs. 5(a)–5(d) we present large-scale (32 × 32 μm) and smaller-scale (8 × 8 μm, 2 × 2 μm) AFM images of such films, respectively, for different total coverage in the sub-monolayer regime, in order to figure out the coverage-dependent development of the large and small islands. The

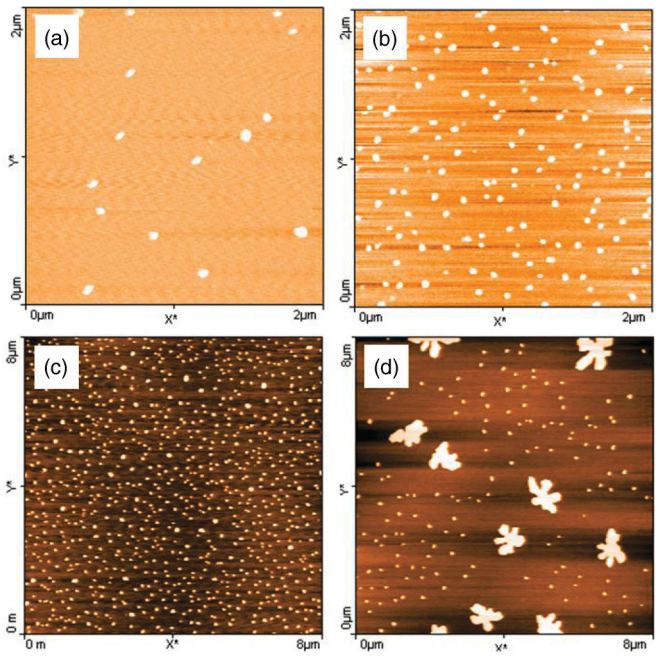

FIG. 5. (Color online) Small-scale AFM images for 6P on sputter-modified mica (001) surfaces. Deposition temperature, 400 K; deposition rate, 0.08 ML/min; deposited amount: (a) 0.014 ML, (b) 0.03 ML, (c) 0.036 ML, (d) 0.04 ML.

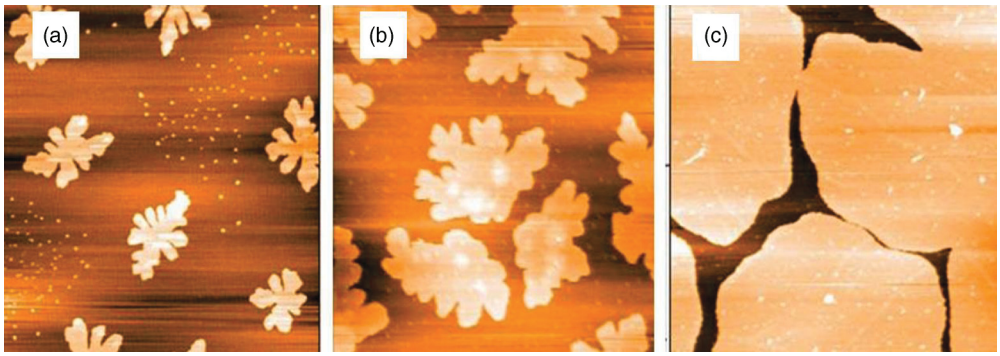

FIG. 6. (Color online) AFM images (8 × 8 μm) for different coverages of 6P grown on sputter-modified mica(001) at 400 K, with a deposition rate of 0. 1 ML/min: (a) 0.18 ML, (b) 0.47 ML, (c) 0.94 ML.

large-scale AFM images [Figs. 4(a)–4(d)], in which the small islands are rarely visible, show a continuous increase of the large island density between 0.04 and 0.15 ML, demonstrating that in this coverage range the system is in the nucleation regime. Below 0.04 ML no large islands exist. Between about 0.1 and 0.6 ML the system is in the aggregation regime, where the island density remains nearly constant and only the island size increases [Figs. 6(a) and 6(b)], before coalescence starts above 0.7 ML [Fig. 6(c)].

AFM images with higher resolution (2 × 2 μm) show the small islands too, which can be observed already before the large islands develop [Figs. 5(a) and 5(b)]. For larger coverage, small and large islands coexist, showing a denuded zone next to the large islands [Figs. 5(d) and 6(a)]. In Fig. 5(c) we can just see the onset of the formation of some large islands. As long as no large islands exist, the density of the small islands increases with the evaporated amount. However, as soon as large islands start to nucleate, the local density of the small islands between the large islands (and outside the denuded zones) decreases again. The number density of the small and large islands as a function of the total coverage is plotted in Fig. 7. This behavior resembles the general coverage dependence of island and monomer densities for diffusion-limited aggregation (DLA).[25] Thus, we again speculate that the small islands are not formed during deposition, but are rather the result of nucleation of the monomers in the 2D gas phase when the sample is exposed to air. This assumption is again corroborated by TDS performed before and after venting the vacuum chamber. While before venting only a single desorption peak around 480 K is observed for a 2-Hz film (Fig. 8), after venting and reevacuation again a broad desorption peak appears between 350 K and 450 K, which is accompanied by water desorption, in addition to a peak at 500 K. Why the main desorption peak has even moved to somewhat higher temperature upon venting is not clear at the moment.

Finally, we had a closer look at the TDS for very low coverage with respect to a possible strongly bound wetting layer on the sputter-modified surface. However, down to the coverage of 0.01 ML we observed only a single desorption peak around 480 K (Fig. 9). This single peak also shows up for higher sub-monolayer coverage, when already the bimodal island size distribution exists, and also for multilayer coverage. Thus, we have to assume that the desorption process is the same in the whole coverage range, that is, for desorption from the monomer phase and desorption from condensed islands.

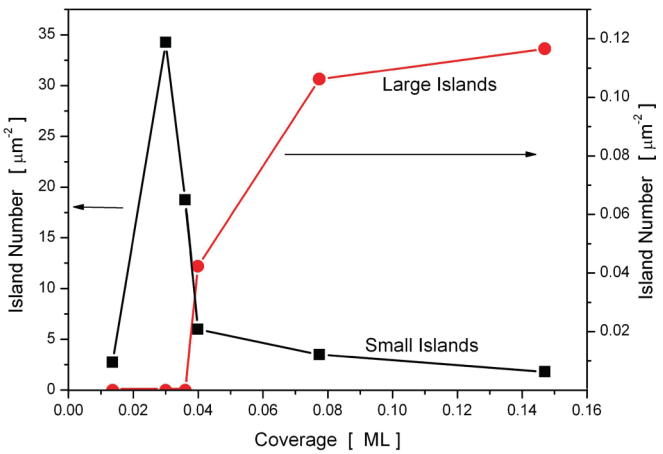

FIG. 7. (Color online) Coverage dependence of the small and large island density for 6P on sputter-modified mica. The lines are to guide the eye.

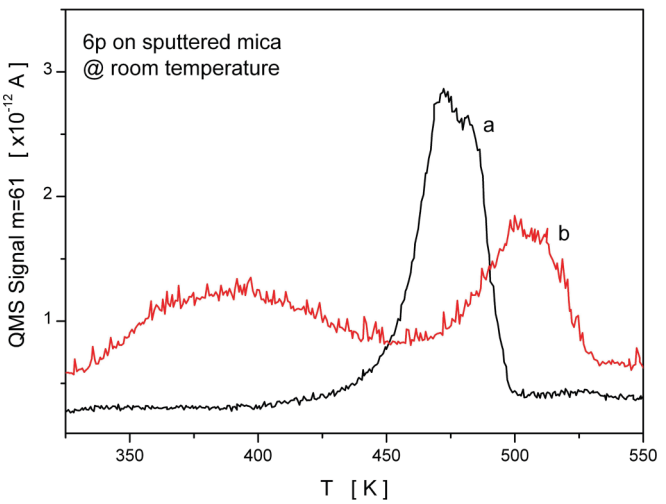

FIG. 8. (Color online) Thermal desorption spectra of 6P (mass 61 amu) on sputter-modified mica(001), deposited at room temperature. (a) Deposited amount, 2 Hz (0.32 nm mean thickness); (b) deposited amount, 2 Hz, but afterwards exposed to air and evacuated again before desorption.

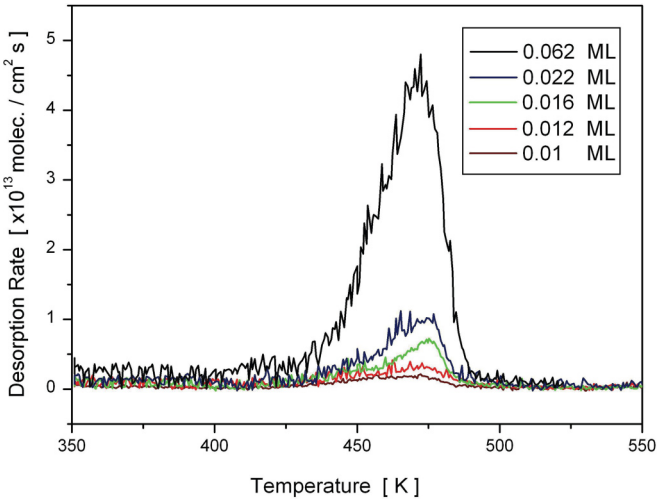

FIG. 9. (Color online) Series of TDS for very small $6P$ coverage on sputter-modified mica. The deposited amount in monolayers is given in the inset.

Based on these findings we explain the AFM images and TD spectra of sub-monolayer $6P$ films, deposited on sputtered mica at and below 400 K as follows: At very low coverage (<0.04 ML) the molecule density is too small to form nuclei during deposition. Thus, the molecules exist most likely as flat-lying monomers on the surface, forming a 2D gas phase. When heating the surface during TDS the molecules become more mobile and start to form nuclei of standing molecules. With further temperature increase the standing molecules then desorb from the rim of these islands. Such a desorption mechanism has to be assumed; otherwise the desorption peak would not be at the same temperature as for the multilayer. This is the case for $6P$ on the freshly cleaved mica, where the flat-lying molecules at low coverage desorb at a higher temperature.

However, if the sputtered mica surface, when covered with <0.04 ML $6P$, is exposed to air, the adsorption of water apparently initiates nucleation of the molecules in the 2D gas phase. This could be accomplished either by a lowering of the adsorption and/or diffusion energy, and/or by a decrease of the activation energy for nucleation (smaller critical island size, lower attachment barrier). For higher coverage ($\Theta > 0.04$ ML) the nucleation already starts during deposition under vacuum conditions, leading to a quasiequilibrium between the islands and the 2D gas phase. The latter will again nucleate upon venting, resulting in the bimodal island size distribution. At even higher $6P$ coverage the distance between the islands becomes so small that most of the monomers are already incorporated in the existing islands either during deposition or at the latest after venting (see Fig. 6). Actually, we have shown in a recent paper that for the nucleation of $6P$ on mica, the attachment limitation indeed plays an even larger role than the diffusion limitation.[26]

To corroborate the above-made assumptions we compare the number density, morphology, island size, and capture zone distribution of the large $6P$ islands in the aggregation regime with that of the small $6P$ islands in the low coverage regime. From Fig. 4(d) ($\Theta = 0.147$ ML) we obtain a density of the large islands, which are clearly dendritic, of $N = 0.12\ \mu\text{m}^{-2}$,

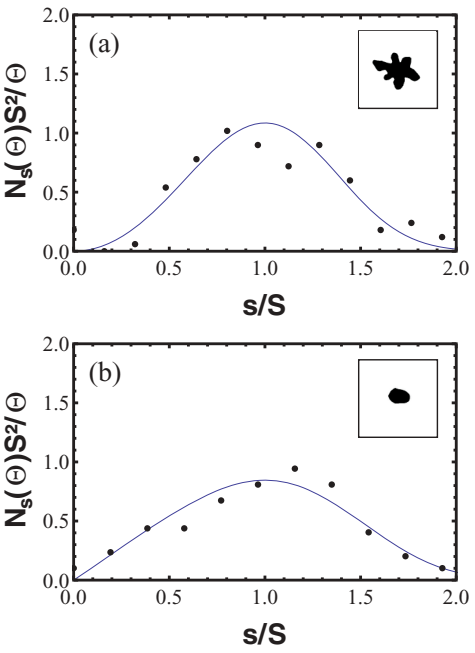

FIG. 10. (Color online) (a) Size distribution of the large $6P$ islands on sputter-modified mica (001) after deposition of 0.147 ML at 400 K, as measured with *ex situ* AFM at room temperature. The curve is a fit according to the function as proposed by Amar and Family[27] for ISD, with $p = 2$. A typical island morphology is shown in the inset. (b) Size distribution of the small $6P$ islands on sputter-modified mica (001) after deposition of 0.03 ML at 400 K, as measured with *ex situ* AFM at room temperature. The curve is a fit according to the function as proposed by Amar and Family[27] for ISD, with $p = 1$. A typical island morphology is shown in the inset.

equivalent to a mean island separation of 2.9 μm. In contrast, the small islands [Fig. 5(b)] are of compact shape and exhibit a maximum island density of 34 μm^{-2} at $\Theta \approx 0.03$ ML, just before nucleation starts, equivalent to a mean island separation of 0.17 μm. From the very different features of the small and large islands in terms of density and morphology, one can safely assume that their physical origin is quite different. We have also measured the island size distributions (ISDs) for the large [Fig. 10(a)] and small islands [Fig. 10(b)]. In order to describe the distributions we have fitted the data by a function as used for ISD in case of DLA, proposed by Amar and Family,[27]

$$f_p(u) = C_p u^p \exp\left(-p a_p u^{\frac{1}{a_p}}\right), \qquad (1)$$

with $u = s/S$, where s is the island size and S the average island size. C_p and a_p are p-dependent constants.[12] The value p, which stands for the critical island size in DLA, is, however, a mere fitting parameter in the case of adsorbate-induced subsequent nucleation. Unfortunately, the statistics is very poor, due to the limited number of islands and the errors which are made in processing the AFM images. Nevertheless, there seems to be a significant difference between the ISD for the large islands, with $p \approx 2$, and the small islands with $p \approx 1$. The value of $p = 2$ agrees reasonably well with our previously obtained value of $i = 3 \pm 1$.[12]

Furthermore, we have evaluated the same AFM images [Figs. 4(d) and 5(b)] with respect to their capture zone

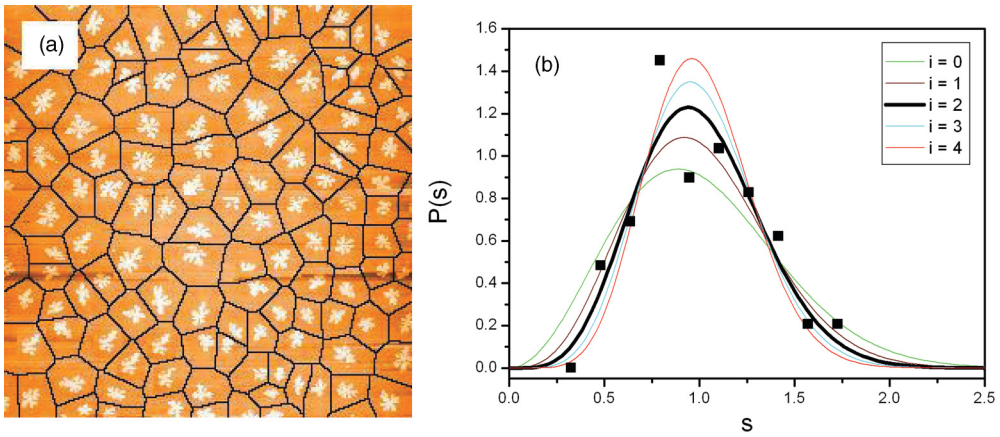

FIG. 11. (Color online) (a) Voronoi tesselation for the island distribution of Fig. 4(d) (large islands). (b) Capture zone distribution obtained by averaging over four AFM images of the film corresponding to Fig. 4(d). The curves are the scaling functions of Eq. (2) with parameter $i =$ 0 through 4. The best fit yields $i \approx 2$.

distributions (CZDs). Pimpinelli and Einstein[28] proposed an expression for the CZD in the following form:

$$P_{ß}(s) = a_{ß} s^{ß} \exp(-b_{ß} s^2), \tag{2}$$

with $s = v/V$, with v the Voronoi polygon size, V the mean value of v, $a_{ß}$ and $b_{ß}$ are constants fixed by normalization and unit-mean conditions, respectively, and $ß = i + 2$.[29,30] Again, only for nucleation during deposition the value i stand for the critical island size, but should be seen as a mere parameter for the adsorbate-induced subsequent nucleation. The Voronoi tessellation and the CZD are shown in Figs. 11(a) and 11(b) for the large islands and in Figs. 12(a) and 12(b) for the small islands. The best fit of Eq. (2) to the CZD yields $i \approx 2$ for the large islands and $i \approx 1$ for the small islands, in good agreement with the result obtained from the ISD.

C. KMC simulations of adsorbate-induced subsequent nucleation

KMC simulations were applied for adsorbate-induced subsequent nucleation, in order to understand this process in more detail and to get information on the critical island size involved. As outlined above, at the beginning a specific amount of particles is randomly deposited on a square lattice with 1000 × 1000 lattice sites, which should be immobile for $t < 0$, but should become mobile for $t \geqslant 0$. Proper surface diffusion energies Q and edge diffusion energies E were assumed, and the same ν was taken for surface and edge diffusion. If the edge diffusion energy is set to a high value, rim diffusion is suppressed and the islands grow with a fractal-like shape according to the hit-and-stick mechanism. Figure 13 shows the results for adsorbate-induced subsequent nucleation of a monomer film with initial coverage $\Theta = 0.03$ ML and a critical island size $i = 7$, for vanishing edge hopping ($E \gg$) [Fig. 13(a)] and with edge hopping, by taking $E = Q = 0.05$ eV and $\nu = 10^{13}$ s^{-1} [Fig. 13(b)]. The used value for Q was inspired by MD calculation.[31] In the latter case the islands were already quite compact at the end of the simulation, that is, when the last monomers were incorporated in the islands. The important result is, however, that the island density depends only weakly on the shape of the islands (fractal vs compact). A comparison of several simulations with and without island edge hopping

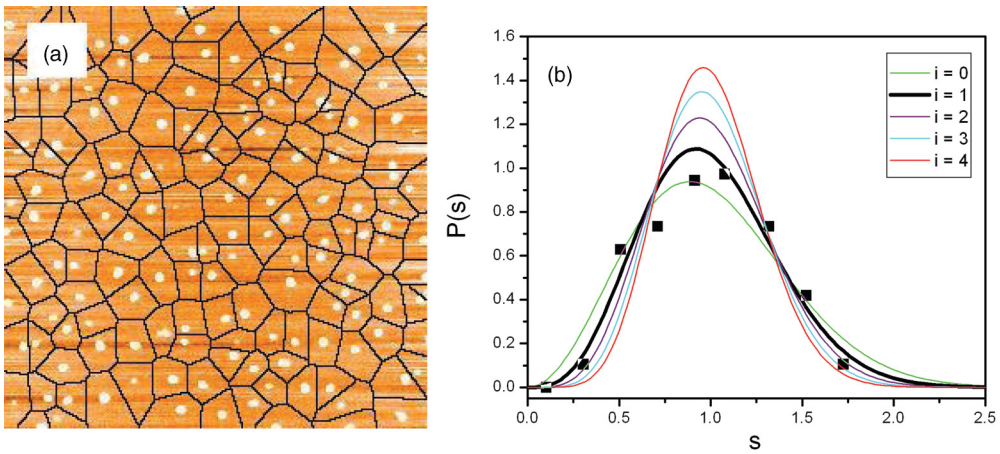

FIG. 12. (Color online) (a) Voronoi tesselation for the island distribution of Fig. 5(b) (small islands). (b) Capture zone distribution obtained by averaging over four AFM images of the film corresponding to Fig. 5(b). The curves are the scaling functions of Eq. (2) with parameter $i =$ 0 through 4. The best fit yields $i \approx 1$.

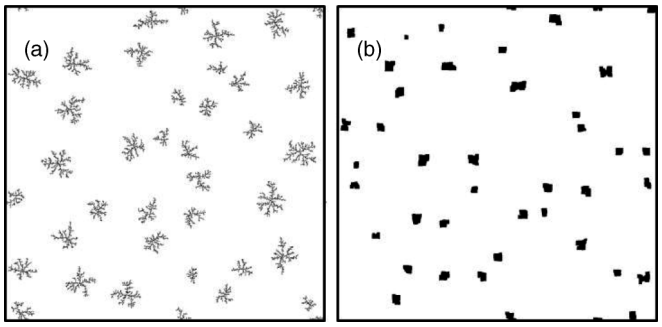

FIG. 13. Comparison of KMC simulations for adsorbate-induced subsequent nucleation without edge hopping (a) and with edge hopping, where $E = Q = 0.05$ eV (b). Lattice sites, 1000 × 1000; initial coverage, 0.03 ML.

yields that the island density is only about 10% larger in the case of compact islands. These findings are similar to the results by Bales and Chrzan[17] on the influence of the island morphology on the island density. Similarly, the influence of the island morphology on the scaling of the ISD[25] and CZD[32] was found to be of minor importance. Since the KMC simulations including edge diffusion need about 50 times more computer time, compared to that for the hit-and-stick scenario, most simulations were done without edge diffusion, if not stated otherwise.

However, the island density depends strongly on the critical island size. In Fig. 14 KMC simulations are presented for $\Theta = 0.03$ ML, taking into account island compacting by edge diffusion, with $i = 6$ [Fig. 14(a)] and $i = 7$ [Fig. 14(b)] and compared with the AFM image (1 × 1 μm) of a 6P film with 0.03 ML coverage [Fig. 14(c)]. Assuming a lattice constant of 1 nm for our simulations, which is a reasonable compromise for the distance between 6P molecules in the 2D gas phase (Van der Waals dimensions: 0.65 × 2.6 nm) and in the condensed phase of the standing molecules [lattice vectors 0.6 × 0.8 nm of the herringbone structure in the 6P(001) plane], the KMC simulation and the AFM images can be quantitatively compared. According to AFM an island density of $N = 35 \pm 5$ μm^{-2} can be determined, the KMC simulations yield an island density of $N = 36 \pm 4$ μm^{-2} for $i = 7$, whereas $i = 6$ would yield $N = 114 \pm 10$ μm^{-2} and $i = 8$ yields only $N = 12 \pm 3$ μm^{-2}. This shows that a critical island size of $i = 7$ describes the experimental results best. The

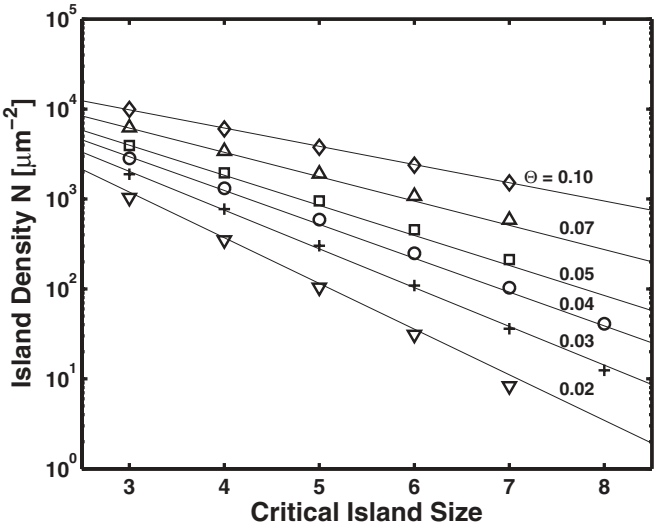

FIG. 15. Island density as a function of the critical island size, for different initial coverages (0.02–0.1 ML), obtained by KMC for adsorbate-induced subsequent nucleation. No edge diffusion was considered.

island densities as a function of the critical island size in the range of $i = 3$–8 are compiled in Fig. 15, for initial monomer coverages between 0.02 and 0.1 ML. For these simulations no edge diffusion was considered. In Fig. 16 the same data set is plotted versus the initial monomer coverage, which shows a linear dependence between ln$N$ and lnΘ. By using a trial function in the form

$$N(i,\Theta) = c \cdot \Theta^{\alpha(i)} e^{ß(i)} \tag{3}$$

we could successfully fit the obtained island densities in the range of $i = 3$–8 and $\Theta = 0.02$–0.1 ML with the parameters $c = 4 \times 10^4$, $\alpha(i) = 0.436i$ and $ß(i) = 0.538i$.

In addition, we have also determined the evolution of the island density and the change of the monomer density with time. An example is presented in Fig. 17 for an initial coverage of 0.03 ML and various critical island sizes i. For these calculations we have again assumed an attempt frequency $\nu = 10^{13}$ s^{-1}, a diffusion energy $Q = 0.05$ eV and $T = 300$ K. As expected, the time increases for adsorbate-induced subsequent nucleation with increasing i, but it is in all cases much faster

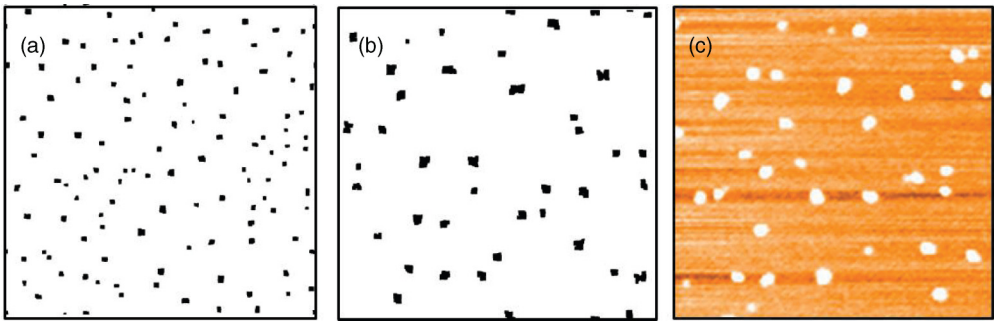

FIG. 14. (Color online) Comparison of KMC simulations for island densities as a result of adsorbate-induced subsequent nucleation (initial coverage, 0.03 ML; 1000 × 1000 lattice sites) with an AFM image of 6P on amorphous mica. (a) KMC, critical island size $i = 6$; (b) KMC, critical island size $i = 7$; (c) AFM image (1 × 1 μm); coverage, 0.03 ML.

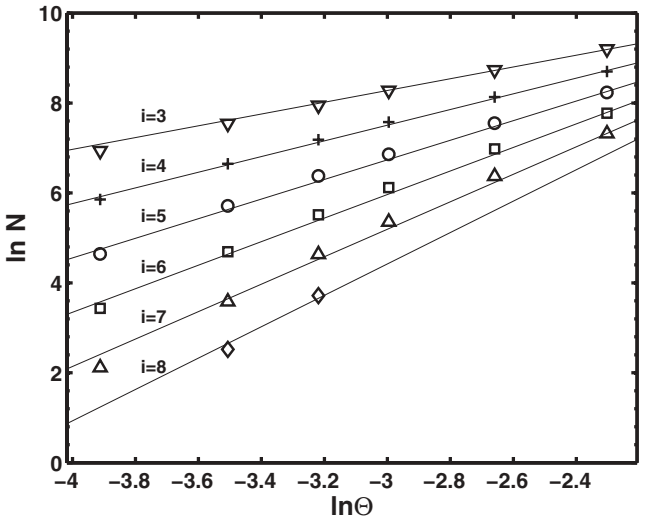

FIG. 16. Logarithm of the island density, $\ln N$, versus the logarithm of the coverage, $\ln\Theta$, for various critical island size ($i = 3$–8), obtained by KMC for adsorbate-induced subsequent nucleation. No edge diffusion was considered.

than the time elapsed in the experiments between venting the vacuum chamber and the AFM measurements.

Finally, ISDs for simulated island films were determined for various critical island sizes. Two exemplary distributions are shown in Fig. 18(a) for $i = 5$ and in Fig. 18(b) for $i = 7$. It turns out that the distributions depend only weakly on the critical island size, and can be roughly described according to Eq. (1) with $p = 1.5 \pm 0.5$. Thus, the calculated ISD is close to that as experimentally determined for adsorbate-induced subsequent nucleation, with $p \approx 1$. It is clear that the meaning of the fit parameter p in Eq. (1) for adsorbate-induced subsequent nucleation is quite different to that for "normal" nucleation during particle deposition, where p directly represents the

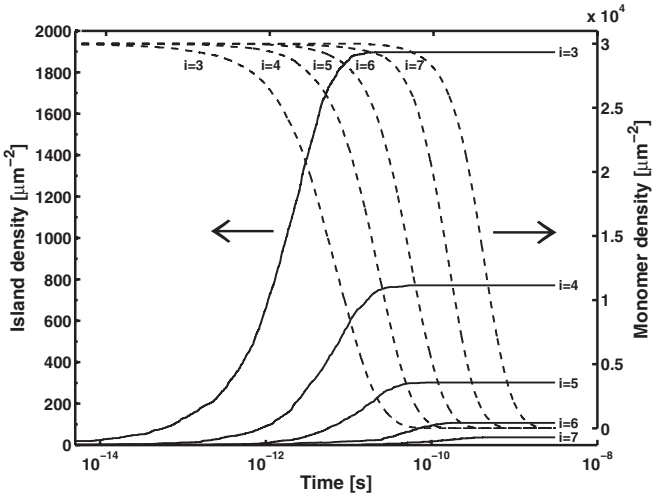

FIG. 17. Time development of the monomer (dashed lines) and island density (solid lines) for adsorbate-induced subsequent nucleation as a function of the critical island size i. Initial coverage, 0.03 ML; attempt frequency, $\nu = 10^{13}$ s^{-1}; diffusion energy, $Q = 0.05$ eV.

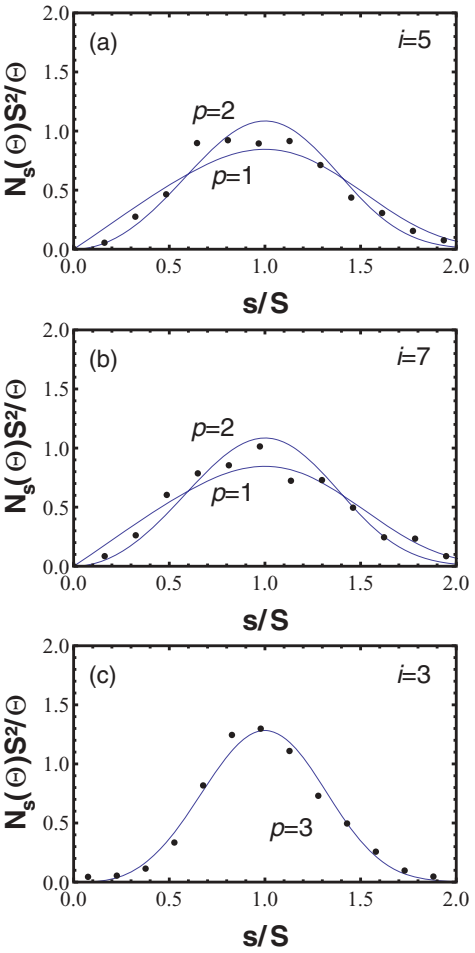

FIG. 18. (Color online) Island size distribution for KMC-simulated island films resulting from adsorbate-induced subsequent nucleation, with $i = 5$ (a) and $i = 7$ (b); initial coverage, 0.03 ML. Fit curves according to the function by Amar and Family,[27] with fit parameters $p = 1$, 2. For comparison an ISD from KMC-simulated nucleation during deposition is shown (c), assuming $i = 3$. This demonstrates the very good agreement with the function of Amar and Family with fit parameter $p = 3$.

critical island size i. Actually, we could show for comparison, that our simulations for nucleation *during particle deposition*, by assuming a particular critical island size i, indeed lead to ISDs which could be well described by Eq. (1), as depicted in Fig. 18(c). For this simulation we assumed, as in the paper by Li and Evans,[33] a critical island size $i = 3$, a ratio of the edge hopping rate h_1 to the deposition rate F, $h_1/F = 10^6$, and a coverage of 0.1 ML.

V. SUMMARY AND CONCLUSIONS

The bimodal ISD, which is frequently observed when a sub-monolayer of $6P$ is deposited on muscovite mica, has been investigated in detail. On the freshly cleaved mica(001) surface the films are composed of needlelike islands, which are surrounded by small crystallites, exhibiting a denuded zone around the needles. Both, the large islands and the small crystallites are composed of lying molecules. On a sputter-

amorphized mica surface the island formation is drastically changed. In this case dendritic islands are formed, which are again surrounded by small islands, also exhibiting a denuded zone. However, the small and large islands are now composed of standing molecules. Nevertheless, we could demonstrate, by combining AFM and TDS, that in both cases the small islands do not exist after deposition in vacuum. They are rather the result of adsorbate-induced nucleation after venting the vacuum system. In the case of the freshly cleaved mica surface a wetting layer dewets, and in the case of the sputtered mica surface a 2D gas phase nucleates after venting. Most probably the adsorption of water on the mica surface is responsible for the subsequent nucleation process. Due to this coadsorption the molecule/substrate bond energy is reduced, leading to decreased barriers for surface diffusion and/or for the attachment of the monomers at the rim of the islands. In addition, also a change of the critical island size, due to the adsorption of water, might be responsible for the subsequent nucleation. Thus, if for a particular coverage already some islands have developed during deposition under vacuum conditions, either above a wetting layer or in quasiequilibrium with a 2D gas phase, a second type of island will appear after venting due to adsorbate-induced subsequent nucleation, leading to the bimodal ISD.

We have applied kinetic Monte Carlo simulations; in particular to simulate the adsorbate-induced subsequent nucleation process, by assuming that an initially immobile monomer phase becomes mobile at the moment of venting. It turns out that the island density, due to subsequent nucleation, is just a function of the critical island size and the initial monomer coverage. A comparison of KMC simulations with AFM images for $6P$ on amorphized mica resulted in a critical island size of $i = 7$ molecules. Furthermore, the ISD as determined from AFM images could be well reproduced by the KMC simulations.

ACKNOWLEDGMENT

This work was financially supported by the Austrian Science Fund (FWF), Project No. 23530.

*Corresponding author: a.winkler@tugraz.at

[1] H. Klauk (editor), *Organic Electronics: Materials, Manufacturing and Applications* (Wiley-VHC Verlag, Weinheim, 2006).
[2] C. Wöll (editor), *Physical and Chemical Aspects of Organic Electronics* (Wiley-VHC Verlag, Weinheim, 2009).
[3] D. Braga and G. Horowitz, Adv. Mater. **21**, 1473 (2009).
[4] H. Yanagi and S. Okamoto, Appl. Phys. Lett. **71**, 2563 (1997).
[5] T. Haber, S. Muellegger, A. Winkler, and R. Resel, Phys. Rev. B **74**, 045419 (2006).
[6] R. Resel, Thin Solid Films **433**, 1 (2003).
[7] F. Balzer, V. G. Bordo, A. C. Simonsen, and H.-G. Rubahn, Phys. Rev. B **67**, 115408 (2003).
[8] P. Frank, G. Hlawacek, O. Lengyel, A. Satka, C. Teichert, R. Resel, and A. Winkler, Surf. Sci. **601**, 2152 (2007).
[9] C. Teichert, G. Hlawacek, A. Y. Andreev, H. Sitter, P. Frank, A. Winkler, and N. S. Sariciftci, App. Phys. A. **82**, 665 (2006).
[10] L. Kankate, F. Balzer, H. Niehus, and H. G. Rubahn, J. Chem. Phys. **128**, 084709 (2008).
[11] A. Andreev, C. Teichert, G. Hlawacek, H. Hope, R. Resel, D. M. Smilgies, H. Sitter, and N. S. Sariciftci, Org. Electron. **5**, 23 (2004).
[12] T. Potocar, S. Lorbek, D. Nabok, Q. Shen, L. Tumbek, G. Hlawacek, P. Puschnig, C. Ambrosch-Draxl, C. Teichert, and A. Winkler, Phys. Rev. B **83**, 075423 (2011).
[13] S. Berkebile, G. Koller, G. Hlawacek, C. Teichert, F. P. Netzer, and M. G. Ramsey, Surf. Sci. Lett. **600**, 313 (2006).
[14] H. Plank, R. Resel, H. Sitter, A. Andreev, N. S. Sariciftci, G. Hlawacek, C. Teichert, A. Thierry, and B. Lotz, Thin Solid Films **443**, 108 (2003).
[15] A. S. Gray and C. Uher, J. Mater. Sci. **12**, 959 (1977).
[16] D. Choudhary, P. Clancy, R. Shetty, and F. Escobedo, Adv. Funct. Mater. **16**, 1768 (2006).
[17] G. S. Bales and D. C. Chrzan, Phys. Rev. B **50**, 6057 (1994).
[18] M. Li and J. W. Evans, Surf. Sci. **546**, 127 (2003).
[19] C. Ratsch and J. A. Venables, J. Vac. Sci. Technol. A **21**, S96 (2003).
[20] A. B. Bortz, M. H. Kalos, and J. L. Lebowitz, J. Comp. Phys. **17**, 10 (1975).
[21] T. P. Schulze, Phys. Rev. E **65**, 036704 (2002).
[22] A. Chatterjee and D. Vlachos, J. Comput.-Aided Mater. Des. **14**, 253 (2007).
[23] J. A. Venables and H. Brune, Phys. Rev. B **66**, 195404 (2002).
[24] A. Winkler, Springer Proc. Phys. **129**, 29 (2009).
[25] J.G. Amar, F. Family, and P.-M. Lam, Phys. Rev. B **50**, 8781 (1994).
[26] L. Tumbek and A. Winkler, Surf. Sci. **606**, L55 (2012).
[27] J.G. Amar and F. Family, Phys. Rev. Lett. **74**, 2066 (1995).
[28] A. Pimpinelli and T. L. Einstein, Phys. Rev. Lett. **99**, 226102 (2007).
[29] M. Li, Y. Han, and J. W. Evans, Phys. Rev. Lett. **104**, 149601 (2010).
[30] A. Pimpinelli and T. L. Einstein, Phys. Rev. Lett. **104**, 149602 (2010).
[31] G. Hlawacek, P. Puschnig, P. Frank, A. Winkler, C. Ambrosch-Draxl, and C. Teichert, Science **321**, 108 (2008).
[32] P. A. Mulheran and J. A. Blackman, Phys. Rev. B **53**, 10261 (1996).
[33] M. Li and J. W. Evans, Multiscale Model. Simul. **3**, 629 (2005).

Paper III [P3]

“Nucleation of organic molecules via a hot-precursor state: Pentacene on amorphous mica”

A. Winkler, L. Tumbek

J. Phys. Chem. Lett. 4 (2013) 4080

THE JOURNAL OF PHYSICAL CHEMISTRY Letters

Letter

pubs.acs.org/JPCL

Nucleation of Organic Molecules via a Hot Precursor State: Pentacene on Amorphous Mica

Adolf Winkler* and Levent Tumbek

Institute of Solid State Physics, Graz University of Technology, Petersgasse 16, A-8010 Graz, Austria

ABSTRACT: Organic thin films have attracted considerable interest due to their applicability in organic electronics. The classical scenario for thin film nucleation is the diffusion-limited aggregation (DLA). Recently, it has been shown that organic thin film growth is better described by attachment-limited aggregation (ALA). However, in both cases, an unusual relationship between the island density and the substrate temperature was observed. Here, we present an aggregation model that goes beyond the classical DLA or ALA models to explain this behavior. We propose that the (hot) molecules impinging on the surface cannot immediately equilibrate to the substrate temperature but remain in a hot precursor state. In this state, the molecules can migrate considerable distances before attaching to a stable or unstable island. This results in a significantly smaller island density than expected by assuming fast equilibration and random diffusion. We have applied our model to pentacene film growth on amorphous Muscovite mica.

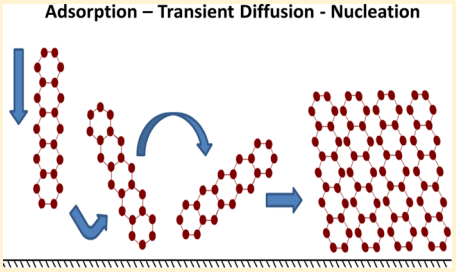

SECTION: Surfaces, Interfaces, Porous Materials, and Catalysis

In recent years, considerable progress has been made in the understanding of organic film growth. In particular, the initial steps of film formation, nucleation, and aggregation have been at the center of interest because they essentially define the final morphology and hence the physical properties of thin organic films. The driving force for this interest is the potential applicability of organic layers in electronic devices, such as organic field-effect transistors, solar cells, light-emitting devices, sensors, and so forth.[1,2] So far, it has been assumed that the nucleation and growth of organic films, in particular, of those consisting of rod-like molecules such as pentacene, thiophen, or hexaphenyl, can be described along the existing nucleation models for point-like monomers, such as metal atoms.[3,4] Recently, however, various experimental results pointed to a somewhat more complex nucleation mechanism for such organic molecules.[5]

The most relevant experimental observables of submonolayer films are the island density and the island size distribution. These quantities depend on the experimental parameters, such as deposition rate and substrate temperature, as well as on system parameters, such as the critical island size, the monomer diffusion energy, and the binding energy of the critical island. By critical island, one understands the largest cluster that is not yet stable. The incorporation of one more monomer results in a stable island that can further grow by the attachment of monomers. Although it is known that this is a simplified scenario,[6,7] the assumption of a critical island size is nearly exclusively made to characterize the initial layer formation. Furthermore, it is assumed that nucleation and growth are governed by diffusion-limited aggregation (DLA).[8] On the basis of these assumptions, Venables et al.[9] have developed a relationship between the island density N and the experimental and system-specific parameters

$$N \propto R^{\alpha} \exp\left(\frac{iE_d + E_i}{(i+2)kT}\right) \quad (1)$$

where R is the deposition rate, E_d is the activation energy for surface diffusion of the monomers, E_i is the binding energy of the critical island, T is the substrate temperature, k is Boltzmann's constant, i is the critical island size, and the exponent α is $i/(i+2)$. The deposition rate dependence of the island density has been frequently applied to evaluate the critical island size for rod-like organic molecules. Stadlober et al.[10] determined a critical island size i between 3 and 4 for pentacene on various organic and inorganic substrates. A similar result was obtained by Ribič et al.[11] for pentacene on polymeric substrates. In our research group, we also determined a critical island size of $i = 2$ and/or 3 for *para*-hexaphenyl on a heavily sputter-amorphized mica surface, depending on the special arrangement of the molecules in the cluster.[12]

Nevertheless, some recent experimental results on the nucleation of *p*-hexaphenyl (6P)[5] and pentacene (5A) (unpublished results) on sputter-amorphized mica have shown that the concept of DLA is of limited applicability. As pointed out above, the power law scaling of the island density with respect to deposition rate should allow the determination of the critical island size, according to $\ln N \approx \alpha \ln R$, with $\alpha = i/(i+2)$. Accordingly, in this case, the value of α has to be between 1/3 and 1. While this has been found to be applicable for 6P deposited on heavily sputtered mica,[12] for 6P deposited on gently sputtered mica, the slope α turned out to be 1.4, at least in a certain range of the deposition rate.[5] It was proposed

Received: October 24, 2013
Accepted: November 18, 2013
Published: November 18, 2013

that in this case, the nucleation can be better described by attachment-limited aggregation (ALA), as put forward first by Kandel[13] and worked out later in more detail by Venables and Brune[14]

$$N \propto R^{\alpha} \exp\left(\frac{2[i(E_d + E_b) + E_i]}{(i+3)kT}\right) \quad (2)$$

In this case, an activation barrier E_b for monomer attachment at the rim of the islands hinders nucleation. Moreover, the meaning of the exponent α is changed to $\alpha = 2i/(i+3)$; thus, α can vary between 0.5 and 2. This resulted in a critical island size of $i = 7$ for 6P nucleation on gently sputtered mica.[5] A similar result has recently been obtained for pentacene on the same substrate, where $\alpha = 1.3$ and consequently $i = 6$ (unpublished results). The difference between the nucleation behavior of 6P on heavily sputtered mica in comparison to that for the gently sputtered mica was explained by the increased importance of diffusion limitation on the increasingly roughened mica surface.

Apart from the peculiar island density dependence of the deposition rate, which clearly showed that for rod-like organic molecules, the nucleation process cannot be described by the classical DLA model, another striking feature is frequently observed with respect to the temperature dependence of the island density. According to eqs 1 and 2, for both DLA and ALA, a plot of $\ln N$ versus $1/T$ should yield a straight line; the slope of this line is determined by the activation energies involved. However, there exist several examples in the literature where a clear bend in the relationship $\ln N$ versus $1/T$ was observed. Sassella et al.[15,16] observed a straight line for the growth of quaterthiophene on silica for substrate temperatures $T > 200$ K but a strong leveling off for lower temperatures. The authors explained this as being due to postdeposition nucleation and growth at low temperatures. Similarly, for α-hexathiophene (6T) grown on a (001) surface of a 6T single crystal, they also reported a leveling off at low substrate temperatures.[17] Ribič et al.[11] observed a bend in the $\ln N$ versus $1/T$ representation for pentacene on various substrates at around 330 K. The authors described this phenomenon as being due to possible desorption at higher substrate temperatures. Finally, Yang et al.[18] have studied the thin film growth of *para*-sexiphenyl (6P) on silica, and they also reported a bend at around 330 K in their representation of the mean island area versus $1/T$. The authors ascribed this to a change in the growth mechanism. At low substrate temperature, the impinging molecules should immediately freeze and form a disordered layer. Subsequently, this film should rearrange into an island film; this suggestion is similar to the idea of postdeposition nucleation.[15] While all of the mentioned examples refer to organic molecules, a similar behavior has also been described for metal film growth, copper on Ni(110), showing even two bends in the $\ln N$ versus $1/T$ representation.[19] In that detailed study, the authors describe the first bend as being due to a change from postnucleation at low temperatures (no temperature dependence) to nucleation with a critical island size of $i = 1$ and the second bend to a change of the critical island size from $i = 1$ to 3.

We do not want to evaluate the proposed mechanisms and ponder the pros and cons of the various propositions. Nevertheless, deviations from a straight line in plots of $\ln N$ versus $1/T$ seem to be a quite frequent behavior in organic thin film growth. Indeed, we have also observed such a behavior in our laboratory for *para*-hexaphenyl (6P) on heavily sputtered mica, where nucleation could be described by DLA,[12] as well as on weakly sputtered mica, where nucleation had to be described by ALA.[5] Recently, we found a similar behavior for pentacene (5A) on weakly sputtered mica, as depicted in Figure 1. Data from previous work for 6P on mica are included as well.[5,12]

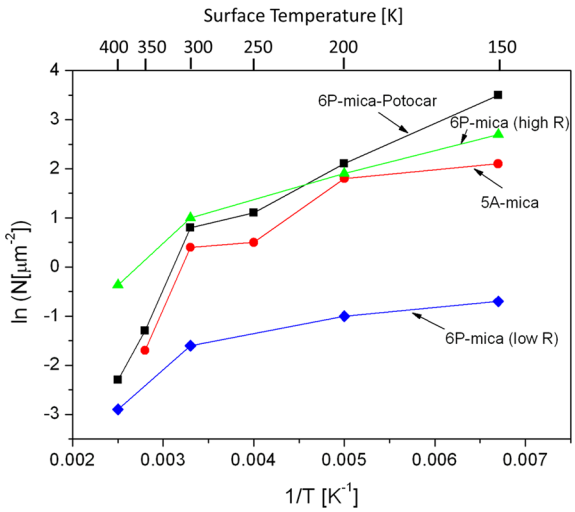

Figure 1. Substrate temperature dependence of the island density for various film/substrate systems. The data "6P-mica-Potocar" were taken from ref 12, and the data "6P-mica (high R)" and "6P-mica (low R)" were deduced from ref 5.

It is obvious that all of the data strongly deviate from linear relationships. We have experimentally verified by thermal desorption spectroscopy that up to 400 K for 6P and up to 350 K for 5A, no significant desorption exists, thus excluding one of the above given explanations for this behavior. We also exclude postdeposition nucleation to be responsible for the decrease of the slope below the rather high temperature of 300 K. In the case of Cu on Ni(100), where an activation energy for diffusion of 0.35 eV was determined, postdeposition nucleation appeared only below 160 K. Because the diffusion energy of large organic molecules on inert substrates is significantly smaller (e.g., 0.02 eV for 6P on 6P(001)),[20] postdeposition nucleation could only appear at very low substrate temperatures. A possible reason for the change of the slope could of course be a change of the critical island size with surface temperature. However, for 6P on gently sputtered mica, we have obtained a critical island size of $i = 7 \pm 2$ for substrate temperatures between 150 and 400 K.[5] No trend to a lower critical island size for lower temperature could be observed. Moreover, the dramatic change of the slope by more than a factor of 7 cannot be explained by a change in the critical island size. Even if it changed from $i = 7$ at 400 K to $i = 1$ at 150 K, this would only lead to a change by less than a factor of 3. The most surprising fact, however, is that the slope in the low-temperature regime of Figure 1 yields unrealistically small activation energies. According to eq 2, the slope β in the plot of $\ln N$ versus $1/T$ for ALA is given by $2[i(E_d + E_b) + E_i]/(i+3)k$. From Figure 1, we can deduce an average asymptotic slope of $\beta \approx 3600$ K in the high-temperature regime and ~500 K in the low-temperature regime. Assuming a simple bond-breaking model for the binding energy of the critical cluster ($E_i = (i-1)E_c$, with E_c being the binding energy between two 6P molecules) and by making a further simplification of $7(E_d + E_b) + 6E_c \approx 6(E_d + E_b + Ec) = 6\bar{E}$ (because E_c is much larger than E_d and possibly E_b), we can estimate the sum of all energies

dx.doi.org/10.1021/jz402301v | J. Phys. Chem. Lett. 2013, 4, 4080−4084

involved, $\bar{E}$, from the slope β. For the large slope, we obtain $\bar{E} \approx 0.26$ eV, and for the small slope, $\bar{E} \approx 0.036$ eV. In particular, the latter value is ridiculously small, considering the fact that the binding energy E_c between two 6P molecules in a cluster, consisting of seven molecules lying on a 6P(001) plane, has been calculated by molecular dynamics to be about 0.6 eV.[12]

In this Letter, we propose a quite different nucleation scenario that can account for the observed unusual phenomena. We suggest that the impinging organic molecules, which initially possess a kinetic energy according to the Knudsen cell temperature (typically 500 K), cannot immediately dissipate their kinetic energy upon impact on the substrate. Furthermore, excited rotational and vibrational states have to equilibrate. This may lead to a so-called hot precursor state in which the molecules are confined to the surface but have some transient mobility along the surface until they fully accommodate.[21] This idea was inspired by experimentally[22,23] and theoretically[24,25] well-founded similar adsorption processes, for example, for the dissociative adsorption of small molecules or the adsorption of hydrogen atoms.[26] An instructive example is the adsorption of Xe on Pt(111),[27] where most of the adsorbed Xe atoms were found at step edge sites, even at a surface temperature of 4 K, indicating a transient mobility over several 100 Å at this temperature. Some other examples for adsorption via a hot precursor are oxygen adsorption on Ag(110)[28] and water adsorption on Rh(111).[29] Furthermore, when the scenario of a hot precursor holds, varying the kinetic energy of the impinging molecules should allow modification of the nucleation and growth. This has indeed been shown by several groups where the kinetic energy of pentacene has been varied by seeding in supersonic molecular beams. An influence on both the film morphology[30,31] as well as the electronic properties of the pentacene films has been observed.[32] Although the existence and importance of transient mobility in precursor states has frequently been questioned in the past, nowadays, this scenario is generally accepted. A comprehensive reference list to this subject can be found in a recent paper by Gao et al.[33]

It is quite difficult to describe the microscopic details of the formation and duration of a hot precursor state and the subsequent processes that lead to nucleation. When an impinging molecule encounters the substrate surface, part of its initial kinetic energy (about 86 meV at 500 K) and internal energy (rotation, vibration) will be dissipated, but some part can also be converted into parallel kinetic energy and frustrated rotational motion. Furthermore, the molecule will be accelerated in the attractive potential, and this energy can then also be partially converted into lateral motion. The rotational to lateral kinetic energy conversion will strongly depend on the orientation of the impinging molecule. When the molecule is finally trapped on the surface, it will travel along the surface in a ballistic-like motion, where it can continuously lose energy by inelastic scatting with surface phonons until it fully equilibrates, and the further motion can be described by random hopping. During this hyperthermal sojourn, the molecules can hit other molecules to form unstable or stable clusters or become incorporated into an existing cluster. The clusters may even not be in equilibrium with the surface. Hot molecules hitting the islands may transfer enough energy to break them apart or at least detach some monomers again. A comprehensive description of the processes for molecules in a hot precursor and their contribution in aggregation would require detailed molecular dynamics and kinetic Monte Carlo simulations, which is beyond the scope of this work and has not been performed on large organic molecules so far, to the best of our knowledge.

For a semiquantitative description of our experimental data, we mimic the increased mobility in the hot precursor state by random diffusion of molecules with an effective temperature larger than the surface temperature. We define an effective temperature

$$T_{\mathrm{eff}}(T_i, T_s, \kappa) = T_i - \kappa\cdot(T_i - T_s) \tag{3}$$

with T_i as the temperature of the impinging molecules (i.e., the Knudsen cell temperature), T_s as the surface temperature, and κ as a coefficient that is related to the energy dissipation during the molecule impact at the surface and the sojourn in the hot precursor. The special ansatz (eq 3) was inspired by the well-known energy accommodation coefficient α^*, which can be measured by molecular beam scattering, $\alpha^* = (T_i - T_{\mathrm{out}})/(T_i - T_s)$.[34] In that case, the outgoing (nonaccommodated) scattered molecules can be described by a temperature $T_{\mathrm{out}} = T_i - \alpha^*(T_i - T_s)$. If we now assume that these nonaccommodated molecules cannot leave the surface because their normal component of the momentum is not high enough to overcome the adsorption potential well due to an efficient normal-to-parallel momentum transfer, the molecules my travel temporarily along the surface as hot molecules. We describe the ensemble of hot and thermalized molecules, including the stable and unstable clusters on the surface, by the effective temperature T_{eff}.

In Figure 2, we plot the qualitative relationship between the island density $\ln N$ as a function of $1/T_s$ for various coefficients

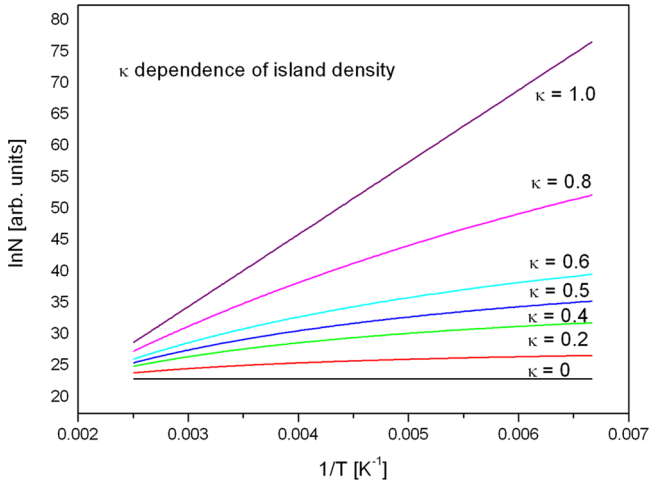

Figure 2. Qualitative dependence of the island density on the surface temperature for various energy dissipation coefficients κ according to eqs 2 and 3. For the calculation, an energy $\hat{E} = 1$ eV and $T_i = 500$ K were used.

κ, according to eqs 2 and 3, $\ln N \approx \hat{E}/kT_{\mathrm{eff}}(T_i,T_s,\kappa)$, with $\hat{E} = 2[i(E_d + E_b) + E_i]/(i + 3)$. One clearly recognizes the curved shape of these relationships, which is most pronounced for an energy dissipation coefficient of about 0.5. Furthermore, one can observe the significant decrease in slope with decreasing κ for the same constant activation energies involved.

In Figure 3, we show quantitative fits to the experimental data for pentacene on the sputter-amorphized mica surface by using the following equation, assuming the ALA nucleation scenario

dx.doi.org/10.1021/jz402301v | J. Phys. Chem. Lett. 2013, 4, 4080−4084

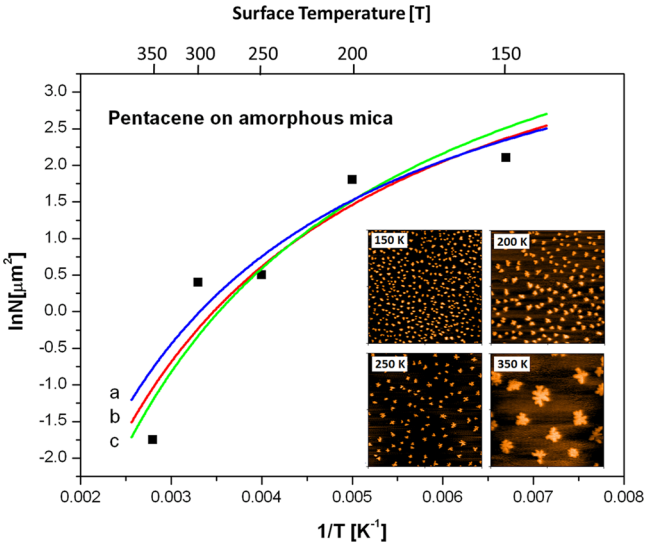

Figure 3. Experimental data points (black squares) for the island density as a function of the surface temperature for pentacene on sputter amorphized mica, together with three fit curves a–c. (a) $\bar{E}$ = 1.01 eV, κ = 0.23; (b) $\bar{E}$ = 0.99 eV, κ = 0.25; (c) $\bar{E}$ = 0.98 eV, κ = 0.27. The inset shows some of the AFM images used for the determination of the island density, 8 × 8 μm^2 for 150, 250, and 350 K and 4 × 4 μm^2 for 200 K.

$$N[\mu m^{-2}] = 10^{-8} \cdot N_0 \left(\frac{4R}{\nu_0 N_0}\right)^{2i/i+3} \exp\left(\frac{2[i(E_d + E_b) + (i-1)E_c]}{(i+3)k(T_i - \kappa(T_i - T_s))}\right) \quad (4)$$

with $N_0 = 4 \times 10^{14}$ cm^{-2} (density of pentacene molecules in the islands composed of standing molecules, roughly equivalent to the density in a 5A (001) layer), R = 1 ML/min (7×10^{12} cm^{-2} s^{-1}), T_i = 500 K (Knudsen cell temperature), and i = 6 (this value was obtained from the deposition rate dependence of the island density, unpublished results). Furthermore, we make use of the before-mentioned simplification $i(E_d + E_b) + (i-1)E_c \approx (i-1)(E_d + E_b + E_c) = (i-1)\bar{E}$. The curvature of the fit is mainly determined by the accommodation coefficient κ. Only values of $\kappa \approx 0.15–0.3$ lead to a proper curvature. For a quantitative fit, the parameters are not independent from each other. The classical hopping frequencies for surface diffusion are on the order of 10^{13} s^{-1}. Using this frequency, we obtain a best fit with $\bar{E}$ = 0.99 eV and κ = 0.25 (Figure 3). However, because, according to transition-state theory, the rate constant is the product of kT/h and the ratio of the partition functions in the transition state and the adsorbed state, this value can be much larger for large organic molecules. This has not only been shown for desorption[35] but also for diffusion of organic molecules. For 6P on sputtered mica, we obtained $\nu_0 = 2 \times 10^{17}$ s^{-1}.[12] Using such a diffusion frequency, we obtain a best fit with $\bar{E}$ = 1.49 eV and κ = 0.19. Despite the rather broad range of possible energy and frequency factors, the obtained values are much more realistic than those deduced by the classical evaluation, where diffusion of equilibrated molecules is assumed.

In summary, we have described a possible scenario for the unusual temperature dependence of the nucleation of organic molecules. We propose that the impinging molecules, which possess a translational energy according to the evaporation source temperature, enter a transient hot precursor state before equilibrating to the surface temperature. This enables the molecules to migrate over larger distances along the surface than in the equilibrated state, thus influencing the nucleation and growth considerably. Specifically, for the system pentacene on sputtered Muscovite mica, which has been shown to obey ALA, we observe a strong deviation from a straight line in the ln N versus $1/T$ plot, indicating the effect of transient mobility in nucleation and aggregation. In particular, for low surface temperatures, the island density is much smaller than expected from classical nucleation theory. It turns out that for a proper description of the experimental results, an energy dissipation coefficient of $\kappa \approx 0.19–0.25$ has to be assumed. Although several unknown parameters enter the modified Venables equation (diffusion constants and various activation energies), a reasonable value for the sum of all energies involved of about 1–1.5 eV could be obtained, whereas the application of the classical nucleation models dramatically failed.

EXPERIMENTAL METHODS

Pentacene was deposited on a Muscovite mica surface by physical vapor deposition from a Knudsen cell in an ultrahigh vacuum chamber. The cell temperature was about 500 K to realize a deposition rate of 1 monolayer/min. The mica samples (10 × 10 × 0.01 mm^3) were attached to a steel plate via tantalum wires. The steel plate was heated resistively, and its temperature was controlled by a Ni–NiCr thermocouple spot-welded to the back of the plate. This allowed controlled heating of the mica sample. With additional LN_2 cooling, the temperature of the mica sample could be varied between 100 and 1000 K. For a quantitative determination of the deposited material, a quartz microbalance was used, which was located next to the mica substrate. The mica substrate was cleaved with adhesive tape prior to installation into the vacuum chamber and subsequently gently sputtered by argon ions. Ten minutes of sputtering with 500 eV Ar^+ ions at an argon pressure of 5 × 10^{-5} mbar was sufficient to change the 5A film morphology from needle-like islands, composed of lying molecules, to compact islands composed of standing molecules.[5] The surface chemical composition was analyzed by Auger electron spectroscopy and X-ray photoelectron spectroscopy. Thermal desorption spectroscopy was applied to determine the thermal stability of the pentacene film and the sticking coefficient. Ex situ atomic force microscopy (Nanosurf, EasyScan2) was used to analyze the film morphology.

AUTHOR INFORMATION

Corresponding Author

*E-mail: a.winkler@tugraz.at.

Notes

The authors declare no competing financial interest.

ACKNOWLEDGMENTS

This work was financially supported by the Austrian Science Fund (FWF), Project No. P 23530. The authors appreciate helpful discussions with Alberto Pimpinelli, Rice University.

REFERENCES

(1) Dimitrakopoulos, C.; Malenfant, P. Organic Thin Film Transistors for Large Area Electronics. *Adv. Mater.* **2002**, *14*, 99–117.
(2) Braga, D.; Horowitz, G. High-Performance Organic Field-Effect Transistors. *Adv. Mater.* **2009**, *21*, 1473–1486.
(3) Ruiz, R.; Choudhary, D.; Nickel, B.; Toccoli, T.; Chang, K.-C.; Mayer, A. C.; Clancy, P.; Blakely, J. M.; Headrick, R. L.; Iannotta, S.;

Malliaras, G. G. Pentacene Thin Film Growth. *Chem. Mater.* **2004**, *16*, 4497−4508.
(4) Wu, Y.; Toccoli, T.; Koch, N.; Iacob, E.; Pallaoro, A.; Rudolf, P.; Iannotta, S. Controlling the Early Stages of Pentacene Growth by Supersonic Molecular Beam Deposition. *Phys. Rev. Lett.* **2007**, *98*, 076601.
(5) Tumbek, L.; Winkler, A. Attachment Limited versus Diffusion Limited Nucleation of Organic Molecules: Hexaphenyl on Sputter Modified Mica. *Surf. Sci.* **2012**, *606*, L55−L58.
(6) Frankl, D. R.; Venables, J. A. Nucleation on Substrates from Vapour Phase. *Adv. Phys.* **1970**, *19*, 409−456.
(7) Ratsch, C.; Šmilauer, P.; Zangwill, A.; Vvedensky, D. D. Submonolayer Epitaxy without a Critical Nucleus. *Surf. Sci. Lett.* **1995**, *329*, L599−L604.
(8) Witten, T. A.; Sander, L. M. Diffusion-Limited Aggregation, a Kinetic Critical Phenomenon. *Phys. Rev. Lett.* **1981**, *47*, 1400−1403.
(9) Venables, J. A.; Spiller, G. D. T.; Hanbücken, M. Nucleation and Growth of Thin Films. *Rep. Prog. Phys.* **1984**, *4*, 399−459.
(10) Stadlober, B.; Haas, U.; Maresch, H.; Haase, A. Growth Model of Pentacene on Inorganic and Organic Dielectrics Based on Scaling and Rate-Equation Theory. *Phys. Rev. B* **2006**, *74*, 165302.
(11) Ribič, P. R.; Kalihari, V.; Frisbie, C. D.; Bratina, G. Growth of Ultrathin Pentacene Films on Polymeric Substrates. *Phys. Rev. B* **2009**, *80*, 115307.
(12) Potocar, T.; Lorbek, S.; Nabok, D.; Shen, Q.; Tumbek, L.; Hlawacek, G.; Puschnig, P.; Ambrosch-Draxl, C.; Teichert, C.; Winkler, A. Initial Stages of *para*-Hexaphenyl Film Growth on Amorphous Mica. *Phys. Rev. B* **2011**, *83*, 075423.
(13) Kandel, D. Initial Stages of Thin Film Growth in the Presence of Island-Edge Barriers. *Phys. Rev. Lett.* **1997**, *78*, 499.
(14) Venables, J. A.; Brune, H. Capture Numbers in the Presence of Repulsive Adsorbate Interactions. *Phys. Rev. B* **2002**, *66*, 195404.
(15) Berlanda, G.; Campione, M.; Moret, M.; Sassella, A.; Borghesi, A. Evidence of Postdeposition Nucleation in Organic Molecular Thin Films. *Phys. Rev. B* **2004**, *69*, 085409.
(16) Sassella, A.; Campione, M.; Papagni, A.; Goletti, C.; Bussetti, G.; Chiaradia, P.; Marcon, V.; Raos, G. Strategies for Two-Dimensional Growth of Organic Molecular Films. *Chem. Phys.* **2006**, *325*, 193−206.
(17) Campione, M.; Caprioli, S.; Moret, M.; Sassella, A. Homoepitaxial Growth of α-Hexathiophene. *J. Phys. Chem. C* **2007**, *111*, 12741−12746.
(18) Yang, J.; Wang, T.; Wang, H.; Zhu, F.; Li, G.; Yan, D. Ultrathin-Film Growth of *para*-Sexiphenyl (I): Submonolayer Thin-Film Growth as a Function of the Substrate Temperature. *J. Phys. Chem. B* **2008**, *112*, 7816−7820.
(19) Müller, B.; Nedelmann, B.; Brune, H.; Kern, K. Initial Stages of Cu Epitaxy on Ni(100): Postnucleation and a Well-Defined Transition in Critical Island Size. *Phys. Rev. B* **1996**, *54*, 17858−17865.
(20) Hlawacek, G.; Puschnig, P.; Frank, P.; Winkler, A.; Ambrosch-Draxl, C.; Teichert, C. Characterization of Step-Edge Barriers in Organic Thin-Film Growth. *Science* **2008**, *321*, 108−111.
(21) Barth, J. V. Transport of Adsorbates at Metal Surfaces: From Thermal Migration to Hot Precursors. *Surf. Sci. Rep.* **2000**, *40*, 75−149.
(22) Barker, J. A.; Auerbach, D. J. Gas−Surface Interactions and Dynamics: Thermal Energy Atomic and Molecular Beam Studies. *Surf. Sci. Rep.* **1984**, *4*, 1−99.
(23) Rendulic, K. D.; Winkler, A. Adsorption and Desorption Dynamics As Seen through Molecular Beam Techniques. *Surf. Sci.* **1994**, *299*, 261−276.
(24) Gross, A. Reactions at Surfaces Studied by Ab-Initio Dynamics Calculations. *Surf. Sci. Rep.* **1998**, *32*, 291−340.
(25) Tully, J. C. Dynamics of Chemical Processes at Surfaces. *Acc. Chem. Res.* **1981**, *14*, 188−194.
(26) Harris, J.; Kasemo, B. On Precursor Mechanisms for Surface Reactions. *Surf. Sci.* **1981**, *105*, L281−L287.
(27) Weiss, P. S.; Eigler, D. M. Adsorption and Accommodation of Xe on Pt(111). *Phys. Rev. Lett.* **1992**, *69*, 2240−2243.
(28) Barth, J. V.; Zambelli, T.; Winnterlin, J.; Ertl, G. Hot Precursors in the Adsorption of Molecular Oxygen on Ag(110). *Chem. Phys. Lett.* **1997**, *270*, 152−156.
(29) Beniya, A.; Mukai, K.; Yamashita, Y.; Yoshinobu, J. Transient Diffusion and Cluster Formation of Water Molecules on Rh(111) at 20 K. *J. Chem. Phys.* **2007**, *126*, 141102.
(30) Wu, Y.; Toccoli, T.; Zhang, J.; Koch, N.; Iacob, E.; Pallaoro, A.; Ianotta, S.; Rudolf, P. Key Role of the Molecular Kinetic Energy in Early Stages of Pentacene Island Growth. *Appl. Phys. A: Mater. Sci. Process.* **2009**, *95*, 21−27.
(31) Casalis, L.; Danisman, M. F.; Nickel, B.; Bracco, G.; Toccoli, T.; Ianotta, S.; Scoles, G. Hyperthermal Molecular Beam Deposition of Highly Ordered Organic Thin Films. *Phys. Rev. Lett.* **2003**, *90*, 206101.
(32) Toccoli, T.; Pallaoro, A.; Coppedè, N.; Ianotta, S.; De Angelis, F.; Mariucci, L.; Fortunato, G. Controlling Field-Effect Mobility in Pentacene-Based Transistors by Supersonic Molecular-Beam Deposition. *Appl. Phys. Lett.* **2006**, *88*, 132106.
(33) Gao, D. Z.; Watkins, M. B.; Shluger, A. L. Transient Mobility Mechanisms of Deposited Metal Atoms on Insulating Surfaces: Pd on MgO(001). *J. Phys. Chem. C* **2012**, *116*, 14471−14479.
(34) Goodman, F. O. Thermal Accommodation. *Prog. Surf. Sci.* **1974**, *5*, 261−375.
(35) Winkler, A. Thermal Desorption of Organic Molecules. *Springer Proc. Phys.* **2009**, *129*, 29−36.

Paper IV [P4]

“Scaling and exponent equalities in island nucleation: Novel results and application to organic films ”

A. Pimpinelli, L. Tumbek, A. Winkler

J. Phys. Chem. Lett. 5 (2014) 995-998

.

THE JOURNAL OF PHYSICAL CHEMISTRY Letters

Letter

pubs.acs.org/JPCL

Scaling and Exponent Equalities in Island Nucleation: Novel Results and Application to Organic Films

Alberto Pimpinelli,*[,†] Levent Tumbek,[‡] and Adolf Winkler*[,‡]

[†]Rice Quantum Institute, Rice University, Houston, Texas 77005, United States

[‡]Institute of Solid State Physics, Graz University of Technology, 8010 Graz, Austria

ABSTRACT: It is known in thin-film deposition that the density of nucleated clusters N varies with the deposition rate F as a power law, $N \sim F^{\alpha}$. The exponent α is a function of the critical nucleus size i in a way that changes with the aggregation limiting process. We extend here the derivation of the analytical capture-zone distribution function $P_{\beta}(s) = a_{\beta} \cdot s^{\beta} \cdot \exp(-b_{\beta} s^2)$ of Pimpinelli and Einstein to generic aggregation-limiting processes. We show that the parameter β is generally related to the critical nucleus size i and to the exponent α by the equality $\alpha \cdot \beta = i$, in the case of compact islands. This remarkable result allows one to measure i with no *a priori* knowledge of the actual aggregation mechanism. We apply this equality to measuring the critical nucleus size for pentacene deposition on mica. This system shows a crossover from diffusion-limited to attachment-limited aggregation with increasing deposition rates.

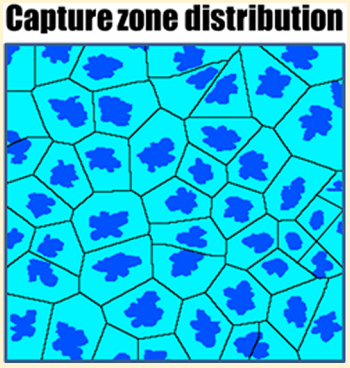

SECTION: Surfaces, Interfaces, Porous Materials, and Catalysis

When growing a thin film by depositing atoms or molecules on a substrate, one of the most easily accessible pieces of information is the surface density of clusters—also called islands—after a given deposition time. As Venables and co-workers[1] showed many years ago, the island density N is a function of the substrate temperature T and of the deposition rate F, and it depends on a material parameter, the size of the critical nucleus, i. The latter is the number of atoms that are part of the largest unstable cluster: a cluster of size i+1 can only grow—through capture of diffusing monomers—while smaller clusters can both grow and dissolve. The critical nucleus size itself is in reality a function of T and F, but simulations and actual experiments show that a real—or realistic—system behaves in some range of values of the external parameters as though a given value of i were selected. In particular, Venables and co-workers showed that the island density at fixed substrate temperature behaves as a power-law function of the deposition rate, $N \sim F^{\alpha}$, where the exponent α depends on i. Measuring the island density as a function of the deposition rate thus allows one to obtain the value of i for given experimental conditions.

Measuring N was made possible by observation techniques such as transmission electron microscopy (TEM), scanning electron microscopy (SEM), scanning tunneling microscopy (STM) or atomic force microscopy (AFM). The same techniques allow one to measure the size of each cluster and thus obtain the island size distribution (ISD) for given T and F. Simulations have shown[2] that the ISD can be quantitatively described by an *ad hoc* analytic expression which contains a single parameter, the critical cluster size i. Therefore, that expression has been widely used to extract i from STM or AFM images.

More recently, Pimpinelli and Einstein (PE)[3] have proposed an alternative analytic approach for extracting values of i based on the capture zone distribution (CZD). A capture zone, as the name suggests, is the region of the substrate around an island that collects monomers that are most likely to be captured by that island. Capture zones are approximated (see the inset in Figure 2 below) by the more manageable Voronoi polygons—regions of the plane whose points are closest to the center of mass of the islands than to any other point. The CZD is then the statistical distribution of the sizes (areas) of the capture zones. The idea of using CZD in connection with island nucleation dates back to the 90s[4] and has been reviewed and discussed more frequently by several authors.[5−7] The novel feature of PE's proposal was to provide a prescription for computing the analytical—though approximate—form of the CZD depending on a single parameter, which turned out to be precisely i, the size of the critical nucleus. The analytical form coincides with the so-called generalized Wigner distribution (GWD) previously used for describing, among other things, fluctuations of crystal steps.[8,9] The agreement between the GWD and CZD has been checked against results from kinetic Monte Carlo (kMC) simulations by several authors.[10−13] A thorough discussion of kMC simulations can also be found in refs 14−16, which concludes that the GWD is indeed an excellent quantitative approximation to the CZD.

The original PE derivation was made for nucleation—or aggregation—limited by surface diffusion, which is called

Received: February 10, 2014
Accepted: March 3, 2014
Published: March 3, 2014

diffusion-limited aggregation (DLA). This is also the only aggregation mechanism for which an analytical approximation to the ISD exists.[2] We will show here that PE's approach can be generalized to any kind of aggregation mechanism, which makes it a much more powerful tool than the ISD. In fact, we will show that coupling the measurements of the island density as a function of the deposition rate with measurement of the CZD allows one to extract the critical nucleus size i without the need of any assumptions concerning the nucleation mechanism.

We will apply these novel results to deposition, diffusion and aggregation of pentacene molecules on sputter amorphized mica surfaces. This system exhibits a crossover between different nucleation regimes. We will show how PE's approach allows one to determine i without *a priori* assumptions about the aggregation process.

One of the most interesting aspects of PE's approach is the connection between the form of the CZD and nucleation: the small-area behavior of the distribution is directly dictated by creation of new CZs when new islands are nucleated. PE conjectured a proportionality relation between the probability $P(s)$ of finding a given value of the dimensionless area $s = A/\langle A\rangle$ of a CZ (at small s), and the probability of nucleating a new island. The latter is in turn proportional to $\int \mathrm{d}r\, r\, [n(r)]^{i+1}$, n being the density of diffusing monomers, and the integral being computed over half the average distance between islands, L.[17] The precise functional form of the CZD depends therefore on the monomer density inside the CZ or, more precisely, on the way the monomer density scales with the area of the CZ. This is in turn determined by the characteristics of the diffusion and aggregation process involved. For instance, if aggregation is limited by diffusion (DLA) as in ref 3, so that attachment of monomers at the rim of the islands is fast compared to diffusion, the monomer density n must vanish at the island edge. The average monomer density can be then shown to scale as the area $A = L^2$ of the capture zone, within logarithmic corrections.[17] The nucleation probability scales thus as $\int \mathrm{d}r\, r\, [n(r)]^{i+1} \sim L^{2(i+2)} = A^{(i+2)}$. The corresponding CZD has therefore the form of a GWD, $P_\beta(s) = a_\beta \cdot s^\beta \cdot \exp(-b_\beta s^2)$, where the parameter β reads $\beta_{\mathrm{DLA}} = i + 2$.[18] The GWD arises as the stationary solution of a Fokker−Planck equation describing the fluctuation of a single CZ in an external potential due to neighboring CZs.[3] A quadratic term hinders the CZ from growing much larger than average, and originates the Gaussian decay.

However, different types of aggregation regimes are observed: besides diffusion, nucleation can be limited by attachment barriers, reactions, blocking impurities, and desorption, just to name a few. Anisotropies in diffusion and/or attachment can also lead to different nucleation regimes. Such differences manifest themselves in the power-law relation $N \sim F^\alpha$: the way the exponent α depends on i changes with the various limiting processes. This happens because, in the steady state where most islands have formed, the monomer density is fixed by the balance between deposition and capture by islands—at least, when monomer desorption is negligible. Assuming that just a single aggregation mechanism is at work the monomer density n will scale as a power of the island density N, $n \sim (F/D)N^{-\gamma}$,[19] where γ is characteristic of the limiting process: $\gamma = 1$ for isotropic diffusion, $\gamma = 2$ for strongly anisotropic (1D) diffusion, $\gamma = 1/a$ for restricted monomer diffusion, where a is an *a priori* unknown function of the concentration of blocking impurities.[19] In the case of attachment-limited aggregation (ALA), as shown by Kandel,[20] the monomer density scales as the distance between islands, so that $\gamma = 1/2$. The scaling of the island density with deposition rate in the saturation regime—where the island density has its maximum—is then found balancing the nucleation rate $(D/F)nn^i$ against island coalescence (see ref 19 for details):

$$N/\theta_c \approx (D/F)nn^i \tag{1}$$

where θ_c is the surface coverage when islands come into contact, D the monomer diffusion coefficient, and n^i is a mean-field approximation to the density of critical nuclei of size i (Walton relation).[21] A temperature-dependent coefficient has been omitted from eq 1. As shown in ref 19, θ_c is in special situations (e.g., when clusters are fractal) a function of the island density itself. Assuming that $\theta_c \sim N^\delta$ (for instance, eq 23 of ref 19 implies $\theta_c \sim N^\delta$ with $\delta = 1 - d_f/2$; more details are given below) and substituting $n \sim (F/D)N^{-\gamma}$ into eq 1 yields $N \sim F^\alpha$, with $\alpha = i/(\gamma i+1+\gamma-\delta)$. In the case of DLA and isotropic diffusion ($\gamma = 1$) this leads to the well-known relationship $\alpha = i/(i+2)$, with $\delta = 0$. For attachment-limited aggregation ($\gamma = 1/2$ and $\delta = 0$) one finds $\alpha = 2i/(i+3)$.[20,22]

Consider PE's prescription for the small-s behavior of $P(s)$: it must follow from equating $P(s)$ and $\int \mathrm{d}r\, r\, [n(r)]^{i+1}$. Substituting $n \sim (F/D)N^{-\gamma}$ and $N \sim L^{-2} \sim A^{-1}$ yields $P(s) \sim s^{[1+\gamma(i+1)]}$ at small s. Factoring in the Gaussian decay[3] at large s yields a GWD $P_\beta(s) = a_\beta \cdot s^\beta \cdot \exp(-b_\beta s^2)$ where

$$\beta = \gamma i + 1 + \gamma \tag{2}$$

As a consequence, the equality

$$\alpha(\beta - \delta) = i \tag{3}$$

holds.

Therefore, when $\delta = 0$, eq 3 reduces to

$$\alpha\beta = i \tag{4}$$

Equation 4 also holds as an approximate identity valid when $\delta \ll \beta$, which is true in most situations of practical interest. As an example, consider a (possibly) fractal island growing in diffusion-limited conditions (DLA). The "mass" M (number of monomers) of an island at time t obeys the equation $M = j_{\mathrm{DLA}}\, t$, where $j_{\mathrm{DLA}} = Dn$ is the monomer current to the island edge. For 2D growth, the island mass M and its radius r is related by $M = (t/a)^{d_f}$ where d_f is the—possibly fractal—dimensionality of the island, and a a molecular length scale. The surface coverage at which two islands come into contact, $\theta_c = Ft_c$ is found by letting $r = 1/N^{1/2}$ at $t = t_c$. Therefore, $Dn \sim FN^{-1}$ ($\gamma = 1$ for DLA in 2D), so that $Ft_c \sim N^{1-d_f/2}$ and $\delta = 1 - d_f/2$. Hence, for compact islands ($d_f = 2$), $\delta = 0$, while $\delta = 0.15$ for fractal islands with $d_f = 1.7$.

The same result is found for islands growing in attachment-limited conditions (attachment-limited aggregation, or ALA). In this case, $M = j_{\mathrm{ALA}}\, t$, where $j_{\mathrm{ALA}} = 2\pi rkn$, and k is an attachment kinetic coefficient. As shown by Kandel,[20] the monomer density scales as the distance between islands, $kn \sim FN^{-1/2}$ ($\gamma = 1/2$) so that $Ft_c \sim N^{1-df/2}$ and again $\delta = 1 - d_f/2$. We can therefore generalize eq 3 to fractal islands:

$$\alpha(2\beta + d_f - 2)/2 = i \tag{5}$$

As a byproduct of eq 4 the exponent β_{ALA} of the corresponding GWD can be computed for compact islands:

$$\beta_{\mathrm{ALA}} = (i+3)/2 \tag{6}$$

dx.doi.org/10.1021/jz500282t | J. Phys. Chem. Lett. 2014, 5, 995−998

Equations 2−6 are the main theoretical results of the present Letter. They are indeed remarkable, because they imply that measuring α and β (and possibly the fractal dimensionality of the clusters) allows one to measure the critical nucleus size, *without any knowledge of the aggregation mechanism*. However, of course, the knowledge of the aggregation mechanism is still a crucial point to fully understand the film morphology.

In order to show how this theoretical approach can be useful for interpreting experiments, we have investigated island nucleation in a typical organic system: pentacene deposited on amorphized mica. The growth behavior is similar to that for the system p-hexaphenyl (6P) on sputtered mica.[23−25] That system was shown not to conform to standard reversible DLA.[26] As stated above, (reversible) DLA is characterized by an island density N that, in the submonolayer regime, depends on the deposition rate F as $N \sim F^{\alpha}$, with $\alpha = i/(i+2)$. It is readily seen that α can only take values between 0.33 and 1 in DLA. However, deposition experiments of 6P molecules on mica resulted in exponents α larger than one,[26] inconsistent with DLA. The growth kinetics of pentacene (5A) cannot be described simply by reversible DLA either, as shown in Figure 1. In particular, a crossover is observed in the ln N versus ln F plot between a value of the exponent $\alpha = 0.8 \pm 0.1$ at low, and $\alpha = 1.3 \pm 0.1$ at high deposition rate. We have then measured the CZD in both the low (Figure 2a) and high F range (Figure 2b), and determined $\beta = 5.0 \pm 0.5$ for the low and $\beta = 4.0 \pm 0.5$ for the high F range, respectively. This allows us to estimate the critical nucleus size using eq 4, assuming that δ is either vanishing or small. We find $i = 4.0 \pm 0.9$ in the low F regime, and $i = 5.2 \pm 0.9$ in the high F one.

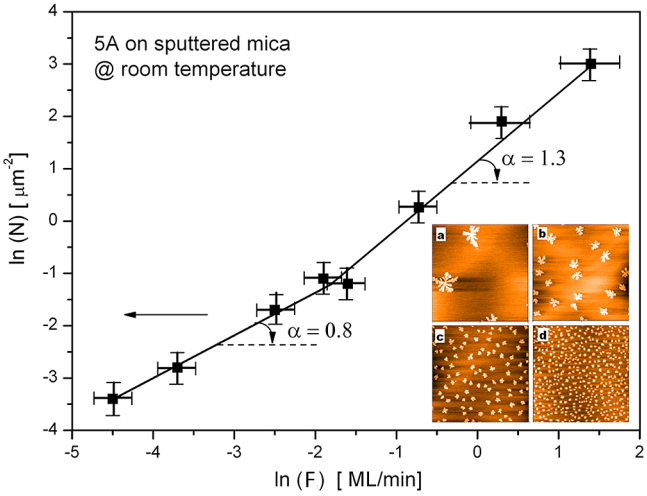

Figure 1. Island density N as a function of deposition rate F at 300 K. The slope at low rate is $\alpha = 0.8 \pm 0.1$, at high rate $\alpha = 1.3 \pm 0.1$. The inset shows exemplary AFM images (8 μm × 8 μm) for different deposition rates. (a) 0.01 ML/min, (b) 0.15 ML/min, (c) 0.48 ML/min, (d) 1.37 ML/min. The mean coverage is in all cases 0.1 ± 0.01 ML.

The traditional approach would be to use the measured value of α and to *surmise* the aggregation regime, and then compute i from the theoretical expressions for α and β. Thus, the value measured at high deposition rate is inconsistent with DLA, and possibly consistent with ALA. Using now $\alpha = 2i/(i+3)$ and the experimental value $\alpha = 1.3 \pm 0.1$ yield $i = 5.6 \pm 1.4$. Using $\beta = (i + 3)/2$, ($\beta = 4.0 \pm 0.5$) yields $i = 5.0 \pm 1.0$. The value from

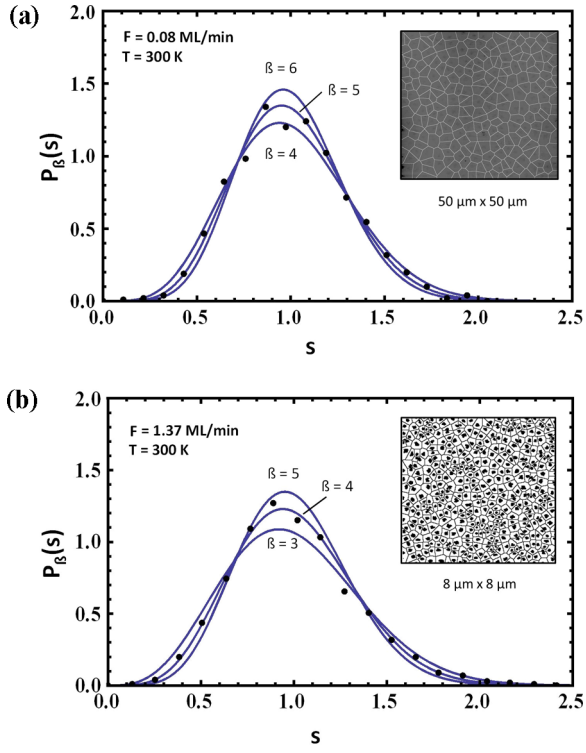

Figure 2. (a) Capture zone distribution (black dots) obtained by summing over 5 different AFM images of a 5A film deposited on sputtered mica with a low deposition rate $F = 0.08$ ML/min at room temperature. The curves were calculated using the fit function $P_\beta(s)$ from PE[3]. The best fit yields $\beta = 5.0 \pm 0.5$. The inset shows a representative Voronoi tessellation (50 μm × 50 μm). (b) Capture zone distribution (black dots) obtained by summing over 5 different AFM images of a 5A film deposited on sputtered mica with a high deposition rate $F = 1.37$ ML/min at room temperature. The curves are calculated using the fit function $P_\beta(s)$ from PE[3]. The best fit yields $\beta = 4.0 \pm 0.5$. The inset shows a representative Voronoi tessellation (8 μm × 8 μm).

eq 4 ($\alpha \cdot \beta = i$, $i = 5.2 \pm 1.0$) is right in between, and consistent with both values within error bars.

At low deposition rate, the measured $\alpha = 0.8 \pm 0.1$ is (possibly) consistent with both DLA and ALA. Assuming that DLA holds, $\alpha = i/(i + 2)$ yields an estimate for i that varies between 4.7 and 18, while $\beta = i + 2$ gives $i = 3 \pm 0.5$. Assuming ALA, $\alpha = 2i/(i + 3)$ yields $i = 2.0 \pm 0.4$, while $\beta = 5.0 \pm 0.5$ and $\beta = (i + 3)/2$ gives $i = 7 \pm 1.0$. The value $i = 4.0 \pm 0.9$ as obtained by eq 4 is roughly consistent with nucleation being in a DLA regime at small deposition rates. We stress, however, that the values obtained from eq 4 do not assume any given aggregation mechanism, and are unbiased measures of the size of the critical nucleus size.

In summary, we have presented a general relationship between the exponents α, describing the rate dependence of the island density and the exponent β, as used to describe the capture zone distribution (CZD) in form of the Wigner surmise: $\alpha \cdot \beta = i$, i being the critical island size. The PE proposal[3] that the generalized Wigner distribution (GWD) be used to describe the CZD in the submonolayer regime shows here all its strength; it has the merit of deriving from a formal mathematical argument that allows it to be extended to any aggregation-limiting process. For the scenario of attachment-limited aggregation we obtain $\beta = (i+3)/2$. Such an extension is not possible for the island size distribution (ISD), whose

dx.doi.org/10.1021/jz500282t | J. Phys. Chem. Lett. 2014, 5, 995−998

analytic form was derived from fits to Monte Carlo simulations of reversible diffusion-limited aggregation (DLA). Nothing is known to what the ISD should be in other instances, e.g., for attachment-limited aggregation (ALA). We have applied the CZD to the system pentacene on sputter amorphized mica. This system showed a crossover from DLA for low deposition rates to ALA for high deposition rates. A critical island size of about 5 molecules was determined.

EXPERIMENTAL METHODS

Pentacene was deposited on a Muscovite mica surface by physical vapor deposition from a Knudsen cell in an ultrahigh vacuum chamber. The cell temperatures were adjusted between 450 and 490 K, in order to realize deposition rates between 0.01 ML/min and 4.5 ML/min, respectively. The mica samples ($10 \times 10 \times 0.01$ mm^3) were attached to a steel plate via tantalum wires. The steel plate was heated resistively, and its temperature was controlled by a Ni−NiCr thermocouple spot-welded to the back of the plate. This allowed controlled heating of the mica sample. With additional LN_2 cooling, the temperature of the mica sample could be varied between 100 and 1000 K. Typically, the sample holder was cooled during the experiments for a better residual gas pressure, but the sample was hold at 300 K during deposition by proper sample heating. For a quantitative determination of the deposited material a quartz microbalance was used, which was located next to the mica substrate. The mica substrate was cleaved with adhesive tape prior to installation into the vacuum chamber and subsequently gently sputtered by argon ions. Ten minutes of sputtering with 500 eV Ar+ ions at an argon pressure of 5×10^{-5} mbar were sufficient to change the 5A film morphology from needle like islands, composed of lying molecules, to compact islands composed of standing molecules. The surface chemical composition was analyzed by Auger electron spectroscopy and X-ray photoelectron spectroscopy. Thermal desorption spectroscopy was applied to determine the thermal stability of the pentacene film and the sticking coefficient. Ex-situ atomic force microscopy (Nanosurf, EasyScan2) was used to analyze the film morphology.

AUTHOR INFORMATION

Corresponding Authors

*E-mail: ap19@rice.edu (A.P.).
*E-mail: a.winkler@tugraz.at (A.W.).

Notes

The authors declare no competing financial interest.

ACKNOWLEDGMENTS

L.T. and A.W. were supported by the Austrian Science Fund, FWF, Proj. No. P23530.

REFERENCES

(1) Venables, J. A.; Spiller, G. D. T.; Hanbücken, M. Nucleation and Growth of Thin Films. *Rep. Prog. Phys.* **1984**, *47*, 399−459.
(2) Amar, J. G.; Family, F. Critical Cluster Size: Island Morphology and Size Distribution in Submonolayer Epitaxial Growth. *Phys. Rev. Lett.* **1995**, *74*, 2066.
(3) Pimpinelli, A.; Einstein, T. L. Capture-Zone Scaling in Island Nucleation: Universal Fluctuation Behavior. *Phys. Rev. Lett.* **2007**, *99*, 226102.
(4) Mulheran, P. A.; Blackman, J. A. Capture Zones and Scaling in Homogeneous Thin-Film Growth. *Phys. Rev. B* **1996**, *53*, 10261−10267.
(5) Mulheran, P. A.; ÒNeill, K. P.; Grinfeld, M.; Lamb, W. Distributional Fixed-Point Equations for Island Nucleation in One Dimension: A Retrospective Approach for Capture-Zone Scaling. *Phys. Rev. B* **2012**, *86*, 151606.
(6) Körner, M.; Einax, M.; Maass, P. Capture Numbers and Island Size Distribution in Models of Submonolayer Surface Growth. *Phys. Rev. B* **2012**, *86*, 085403.
(7) Einstein, T. L.; Pimpinelli, A.; Gonzáles, D. L. Analyzing Capture Zone Distributions (CZD) in Growth: Theory and Applications. *J. Cryst. Growth* **2014**, DOI: 10.1016/j.jcrysgro.2014.01.053.
(8) Pimpinelli, A.; Gebremariam, H.; Einstein, T. L. Evolution of Terrace-Width Distributions on Vicinal Surfaces: Fokker-Planck Derivation of the Generalized Wigner Surmise. *Phys. Rev. Lett.* **2005**, *95*, 246101.
(9) Einstein, T. L. Using the Wigner-Ibach Surmise to Analyze Terrace-Width Distributions: History, User's Guide, and Advances. *Appl. Phys. A: Mater. Sci. Process.* **2007**, *87*, 375−384.
(10) Amar, J. G.; Family, F.; Popescu, M. N. Kinetics of Submonolayer Epitaxial Growth. *Comput. Phys. Commun.* **2002**, *146*, 1−8.
(11) Evans, J. W.; Bartelt, M. C. Island Size and Capture Zone Areas in Submonolayer Depositions: Scaling and Factorization of the Joint Probability Function. *Phys. Rev. B.* **2002**, *66*, 235410.
(12) Bashan, M.; Montalenti, F.; Mulheran, P. A. Multiscale Modeling of Island Nucleation and Growth During Cu(100) Homoepitaxy. *Phys. Rev. B.* **2006**, *73*, 045422.
(13) Körner, M.; Einax, M.; Maass, P. Island Size Distribution in Submonolayer Growth: Prediction by Mean Field Theory with Coverage Dependent Capture Numbers. *Phys. Rev. B.* **2010**, *82*, 201401(R).
(14) Oliveira, T. J.; Aarão Reis, F. D. A. Scaling of Island Size and Capture Zone Distributions in Submonolayer Growth. *Phys. Rev. B* **2011**, *83*, 201405(R).
(15) Oliveira, T. J.; Aarão Reis, F. D. A. Crossover in the Scaling of Island Size and Capture Zone Distribution. *Phys. Rev. B* **2012**, *86*, 115402.
(16) Oliveira, T. J.; Aarão Reis, F. D. A. Scaling in Reversible Submonolayer Deposition. *Phys. Rev. B* **2013**, *87*, 235430.
(17) Routledge, K. J.; Stowell, M. J. Nucleation Kinetics in Thin Film Growth. I. Computer Simulation of Nucleation and Growth Behavior. *Thin Solid Films* **1970**, *6*, 407−421.
(18) Pimpinelli, A.; Einstein, T. L. Comment on "Capture-Zone Scaling in Island Nucleation: Universal Fluctuation Behavior" Reply. *Phys. Rev. Lett.* **2010**, *104*, 149602.
(19) Pimpinelli, A.; Jensen, P.; Larralde, H.; Peyla, P. Scaling and Crossovers in Models for Thin Film Growth. In *Morphological Organization in Epitaxial Growth and Removal*; Series on Directions in Condensed Matter Physics; Zheng, Z., Lagally, M. G., Eds.; World Scientific: Singapore, 1998; Vol. *14*, pp 121−148.
(20) Kandel, D. Initial Stages of Thin Film Growth in the Presence of Island-Edge Barriers. *Phys. Rev. Lett.* **1997**, *78*, 499−502.
(21) Walton, D. Nucleation of Vapor Deposits. *J. Chem. Phys.* **1962**, *37*, 2182−2188.
(22) Venables, J. A.; Brune, H. Capture Numbers in the Presence of Repulsive Adsorbate Interactions. *Phys. Rev. B* **2002**, *66*, 195404.
(23) Frank, P.; Hlawacek, G.; Lengyel, O.; Satka, A.; Teichert, C.; Resel, R.; Winkler, A. Influence of Surface Temperature and Surface Modifications on the Initial Layer Growth of Para-Hexaphenyl on Mica(001). *Surf. Sci.* **2007**, *601*, 2152−2160.
(24) Hlawacek, G.; Puschnig, P.; Frank, P.; Winkler, A.; Ambrosch-Draxl, C.; Teichert, C. Characterization of Step-Edge Barriers in Organic Thin-Film Growth. *Science* **2008**, *321*, 108−111.
(25) Potocar, T.; Lorbek, S.; Nabok, D.; Shen, Q.; Tumbek, L.; Hlawacek, G.; Puschnig, P.; Ambrosch-Draxl, C.; Teichert, C.; Winkler, A. Initial Stages of a *para*-Hexaphenyl Film Growth on Amorphous Mica. *Phys. Rev. B* **2011**, *83*, 075423.
(26) Tumbek, L.; Winkler, A. Attachment Limited versus Diffusion Limited Nucleation of Organic Molecules: Hexaphenyl on Sputter Modified Mica. *Surf. Sci. Lett.* **2012**, *606*, L55−L58.

Paper V [P5]

“The influence of potassium on the growth of ultra-thin films of para-hexaphenyl on muscovite mica(001)”

B. Putsche, L. Tumbek and A. Winkler

J. Chem. Phys., 137 (2012) 134701

The influence of potassium on the growth of ultra-thin films of para-hexaphenyl on muscovite mica(001)

Bernhard Putsche, Levent Tumbek, and Adolf Winkler[a)]
Institute of Solid State Physics, Graz University of Technology, Petersgasse 16, A-8010 Graz, Austria

(Received 13 July 2012; accepted 12 September 2012; published online 2 October 2012)

The interaction of potassium with mica(001) and its influence on the subsequent film growth of para-hexaphenyl (6P) was studied by Auger electron spectroscopy, thermal desorption spectroscopy, and atomic force microscopy (AFM). Freshly cleaved mica is covered with 0.5 monolayer (ML) of potassium. By intentional potassium deposition in ultra-high vacuum a saturation of 1 ML can be achieved, which is stable up to 1000 K. Additional potassium desorbs at around 350 K. The film morphology of 6P on mica(001) is significantly influenced by the potassium monolayer. On the freshly cleaved mica surface, which contains 1/2 ML of K, 6P forms needle-like islands which are composed of lying molecules. On the fully potassium covered mica surface 6P grows in form of dendritic islands, composed of standing molecules. The reason for this change is attributed to the removal of lateral electric fields which exist on the freshly cleaved mica surface, due to the specific arrangements of the atoms in the surface near region of mica. © *2012 American Institute of Physics*. [http://dx.doi.org/10.1063/1.4754833]

I. INTRODUCTION

Muscovite mica is a frequently used substrate for epitaxial film growth. Due to the sheet-like structure of this material one can easily prepare atomically smooth surfaces just by cleaving. Such freshly cleaved mica substrates have been particularly used to study the film growth of rod-like organic molecules, e.g., oligo-phenylenes,[1–4] oligo-acenes,[5] and oligo-thiophenes.[6,7] In most of these cases the ultra-thin films consist of needle-like islands, which are composed of molecules with their long axis parallel to the substrate surface. It is assumed that this particular film growth is stabilized by lateral electric fields existing on the surface of the freshly cleaved mica substrate.[2]

Muscovite mica is a layered aluminosilicate with the formula $KAl_2(AlSi_3O_{10})(OH)_2$. Each layer is composed of a sub-layer of octahedrally coordinated Al^{3+} ions, which is sandwiched between two tetrahedral silicate layers with vertices pointing toward the octahedral layer, and a layer of potassium.[8] In the silicate layers some of the Si^{4+} ions are replaced by Al^{3+} ions (with a ratio of 3:1), creating negatively charged areas. These negative charges are compensated by the K^+ counterions. Cleavage is known to take place along the potassium layers. After the cleavage, half of the potassium ions are assumed to be left on each surface. Between the K^+ ions and the negatively charged sites of the Al^{3+} substituent dipoles are generated, leading to dipole fields with components parallel to the surface.[9,10]

Recently, it has been shown that a modification of the freshly cleaved mica surface in vacuum, either by carbon deposition or by argon sputtering, changes the layer growth of para-hexaphenyl (6P) dramatically.[11–13] Instead of forming needle-like islands, which are composed of lying molecules, the film morphology changes to dendritic islands, which are composed of standing molecules. It was argued that the surface modifications destroy the lateral dipole fields and thus weaken the attractive forces between the 6P molecules and the substrate.

In this work, we focus on the role of surface potassium on the layer growth of 6P on muscovite mica. It is assumed that after cleavage in air half a monolayer of potassium remains on the surface. However, since no superstructure can be observed in low energy electron diffraction (LEED), potassium is apparently randomly distributed. In recent atomic force microscopy (AFM) investigations it was found that actually domains with and without potassium exist on the mica surface, resulting in positively and negatively charged areas.[14] Furthermore, carbon was observed on air cleaved mica. It was argued that this is the result of the adsorption of carbonaceous gases, CO, CO_2, CH_4, and their reactions with H_2O.[15–18] Nevertheless, this type of surface leads to the pronounced needle-like island growth of rod-like molecules, as long as the mica substrate is immediately installed into the vacuum chamber after cleaving. Here we will demonstrate that by evaporation of potassium under ultra-high vacuum (UHV) conditions a full monolayer of potassium can be created on the mica surface, which is stable up to 1000 K. On such a surface, the layer growth of 6P again changes from needle-like islands, composed of lying molecules, to weakly dendritic islands composed of standing molecules.

II. EXPERIMENTAL

The experiments were performed in an ultra-high vacuum chamber with a base pressure of 1×10^{-10} mbar. The chamber was equipped with an Auger electron spectrometer, a mass spectrometer, an Ar^+ ion gun, facilities for the evaporation of 6P and potassium, and a quartz microbalance. The mica(001) samples ($10 \times 10 \times \sim 0.01$ mm^3) were prepared by cleaving a

a)Electronic mail: a.winkler@tugraz.at.

mica sheet with the help of adhesive tape in air. The mica samples were attached to a steel plate via tantalum clamps, which could be heated resistively, and immediately installed into the UHV chamber. The temperature was controlled by a Ni–NiCr thermocouple spot-welded to the back of the steel plate. This allowed a controlled heating of the steel plate and hence of the mica sample for thermal desorption spectroscopy, typically with heating rates of 1 K/s. With additional LN_2 cooling, the temperature of the steel plate could be varied between 100 K and 1000 K.[11] Unfortunately, a considerable temperature difference existed between the front mica surface and the heating plate, due to the low heat conductivity of mica normal to the (001) plane.[19] A calibration of the temperature can be performed by comparing the multilayer peak maximum of desorbing 6P and potassium from mica with that for desorption from the steel plate (see below). 6P was evaporated from a stainless steel Knudsen cell, whereas potassium was evaporated from an SAES getters alkali metal dispenser.[20] For thermal desorption spectroscopy a multiplexed quadrupole mass spectrometer (QMS) (0–200 amu) was used. Instead of the mass of the 6P molecules (m = 458.6 amu) the mass m = 61 amu was measured, because it was shown that this is the largest signal of the cracking pattern in the QMS.[21] For potassium desorption the mass spectrometer was tuned to m = 39 amu.

For the quantitative determination of the 6P film thickness a quartz microbalance was used, which was positioned next to the sample. The reliability of this device was checked in two ways: (a) by comparing with corresponding AFM images of sub-monolayer films of standing molecules and (b) by thermal desorption spectroscopy, as outlined in more detail elsewhere.[11] After the *in situ* preparation and characterization of the 6P films on the potassium modified mica, the samples were investigated *ex situ* by AFM in the tapping mode (Nanosurf, EasyScan2).

III. RESULTS AND DISCUSSION

A. Potassium adsorption and desorption from mica

Freshly air cleaved mica, when immediately installed into the UHV chamber, always contains some carbon on the surface. The amount of adsorbed carbon differs somewhat for different samples, apparently due to changing environmental conditions during air cleavage. It was argued that the carbon contamination is due to adsorption and decomposition of carbonaceous gases, depending on the humidity.[15–18] Heating of the sample to 1000 K decreases the carbon signal slightly, but it cannot be removed completely. The amount of potassium and the other constituents in the surface near region (oxygen, silicon, and aluminum) do not change significantly upon heating. In particular, the potassium amount on the surface was found to be quite reproducible, showing an Auger ratio of K252/O510 $\approx$ 1.0 $\pm$ 0.1 (Fig. 1). This is an indication that indeed always about the same amount, i.e., half of a potassium layer, remains on both sides of the freshly exposed mica surfaces after cleaving. The carbon contamination can be removed easily by Ar^+ ion sputtering (800 V, 10 min, 5×10^{-6} mbar Ar). However, we abstained from removing

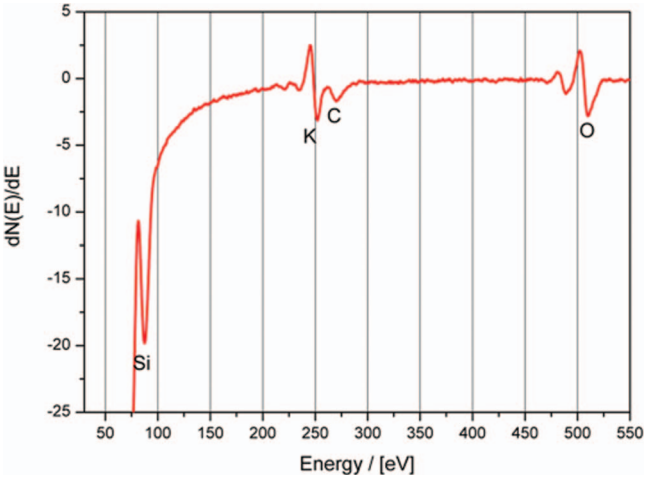

FIG. 1. Auger spectrum of the freshly cleaved and immediately installed muscovite mica, after heating to 1000 K in UHV, taken at 300 K. In addition to the expected elements Si, O, K, still some carbon contamination is observed. The ratio of K252/O510 is always about the same, 1.0 $\pm$ 0.1, indicating that about 1/2 ML remains on each freshly cleaved mica surface.

the residual carbon by sputtering, because it is known that this procedure already influences the 6P layer growth on mica (001) dramatically,[11] and hence would blur the effect of potassium adsorption.

The aim of this work was to elucidate the influence of potassium on mica on the 6P layer growth. For this purpose first the adsorption/desorption behavior of K on mica was studied. On a freshly cleaved mica surface several monolayers of potassium were deposited at a substrate temperature of 110 K. Subsequent heating of the sample leads to desorption of potassium, however, some part of the deposited potassium remains on the surface after the first adsorption/desorption cycle, leading to a saturation potassium coverage which is stable up to 1000 K. This can be seen in Fig. 2 where three subsequent desorption spectra are depicted. The first spectrum is

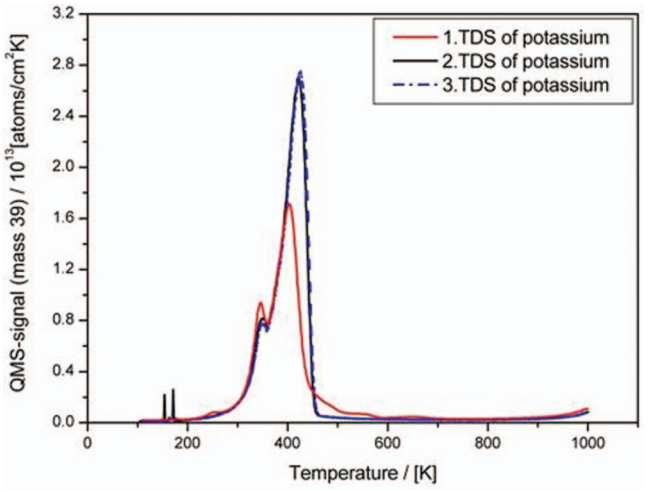

FIG. 2. Three subsequent thermal desorption spectra of potassium, starting with a freshly cleaved mica surface. In all cases the same amount of potassium (about 2 ML) was deposited at 110 K. The first spectrum (red) is significantly smaller than the subsequent spectra (black, dashed blue) demonstrating that some potassium deposited on freshly cleaved mica remains on the surface after heating to 1000 K.

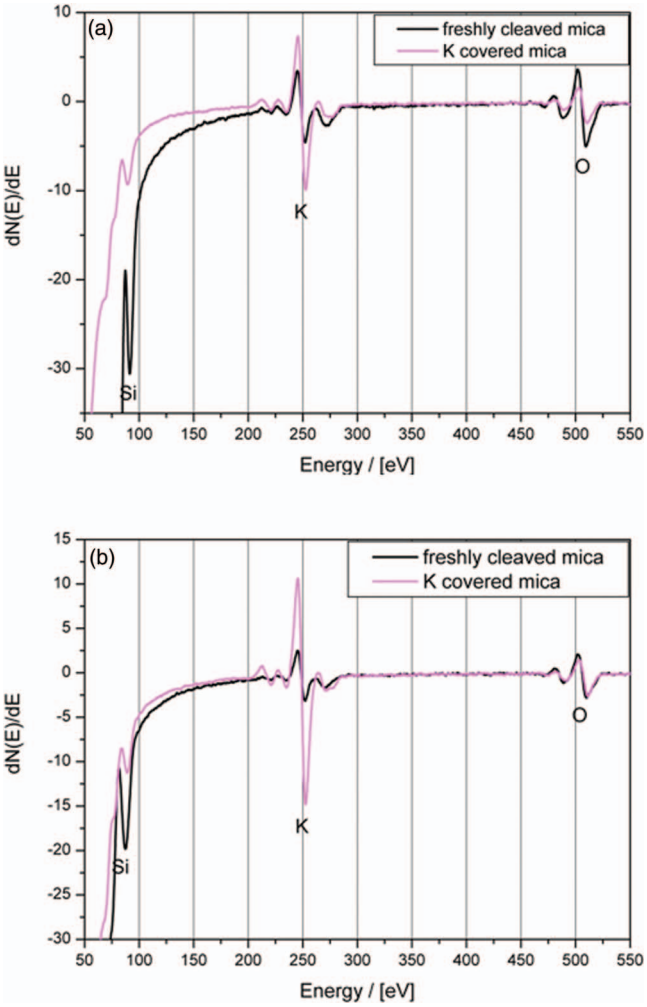

FIG. 3. Auger spectra after several potassium adsorption/desorption cycles on mica and heating to 1000 K (magenta), in comparison to that of the freshly cleaved mica (black). (a) Potassium layer prepared at 2×10^{-10} mbar. (b) Potassium layer prepared at 1×10^{-9} mbar.

significantly smaller than the subsequent spectra, demonstrating that some potassium remains on the freshly cleaved mica. All following spectra are identical within the experimental error, indicating that all adsorbed potassium (besides the stable monolayer) can be desorbed again.

The Auger spectrum of the K covered mica surface after several adsorption/desorption cycles, and heating to 1000 K, is shown in Fig. 3(a), in comparison to the spectrum of the freshly cleaved mica surface. Within the experimental error the K-Auger signal has doubled after this procedure, indicating that indeed the saturation layer is a full monolayer of potassium. Due to the attenuation of the substrate signal the Auger ratio changes to K252/O510 $\approx 4.0 \pm 0.2$ in this case. From the difference of the desorption spectra area between the first and second adsorption/desorption cycle (which can be attributed to 1/2 monolayer (ML) of potassium) (Fig. 2), one can calibrate the thermal desorption spectra for potassium. From the known surface unit cell for mica (a = 5.2 Å, b = 9.0 Å), which contains 2 K atoms, one can attribute 1 ML of K on mica to 4.2×10^{14} K-atoms/cm^2. In this way we have a correlation between the thermal desorption

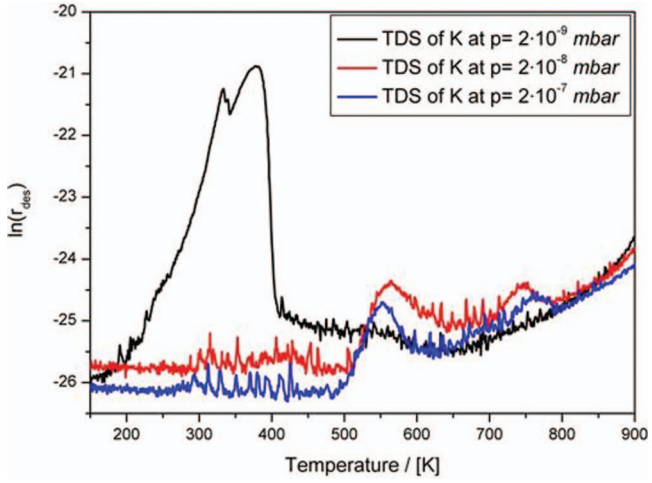

FIG. 4. TDS of potassium obtained after deposition of always the same amount of potassium at different base pressures. Note the logarithmic y-scale. The desorption peak at 350 K stems from metallic potassium, whereas the peaks at higher temperature are due to the decomposition of potassium compounds.

spectroscopy (TDS) area (difference) and the corresponding (1/2 ML adsorbed) K atoms. This correlation can be used to calibrate the desorbing amount of thicker (metallic) K films by TDS.

The formation of one stable monolayer of potassium by adsorption/desorption is only possible under good ultra-high vacuum conditions ($p \approx 10^{-10}$ mbar). At higher residual pressure ($p > 10^{-9}$ mbar) more potassium remains on the surface after several potassium adsorption/desorption cycles and heating to 1000 K (Auger ratio K252/O510 $\approx 6.5 \pm 0.2$) (Fig. 3(b)). This is most probably due to the reaction of potassium with residual oxygen or water, which may lead to highly stable K_xO_y[22] or KOH[23] species. We conclude this because no other species were observed in the Auger spectrum, and the oxygen signal did not decrease, in spite of the increased potassium signal.

This assumption is also supported by thermal desorption spectroscopy. Figure 4 shows desorption spectra of potassium after always the same potassium amount was deposited (2 ML equivalents), but at different base pressure. The various base pressures were adjusted by intentionally leaking air into the baked UHV chamber. Only in the 10^{-9} mbar pressure range and below, pure potassium desorption (from the metallic multilayer) can be observed, which is expected to take place at about 350 K.[24–26] However, at and above 2×10^{-8} mbar no potassium desorbs in the temperature range where desorption of pure potassium is expected. There exist only small desorption peaks (note the logarithmic y-scale) at higher temperature, which are most probably due to cracking products of more stable potassium containing compounds. Indeed, the desorption peak at 550 K (Fig. 4) has been identified by several authors[27,28] to be due to decomposition of KOH. With XPS and UPS it has also been shown that KOH on Pt(111) decomposes around 600 K.[23]

Figure 5 shows a set of desorption spectra for potassium with different amounts of K deposited on the mica surface at a residual pressure of 2×10^{-10} mbar at 110 K, containing 1 ML (non-desorbable) potassium. The appearance of two

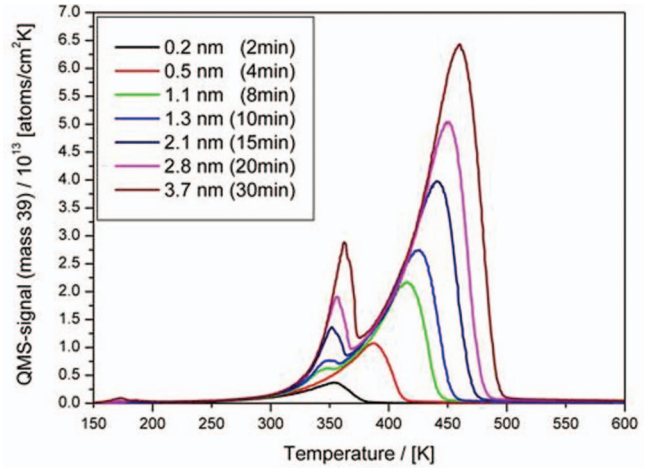

FIG. 5. Series of thermal desorption spectra of potassium from mica(001), for different adsorbed amounts (deposition times). Adsorption temperature: 110 K, heating rate: 1 K/s. The peaks at 350 K stem from desorption from the tantalum clamps, only the second, larger peaks are due to multilayer desorption from mica. No monolayer desorption can be observed.

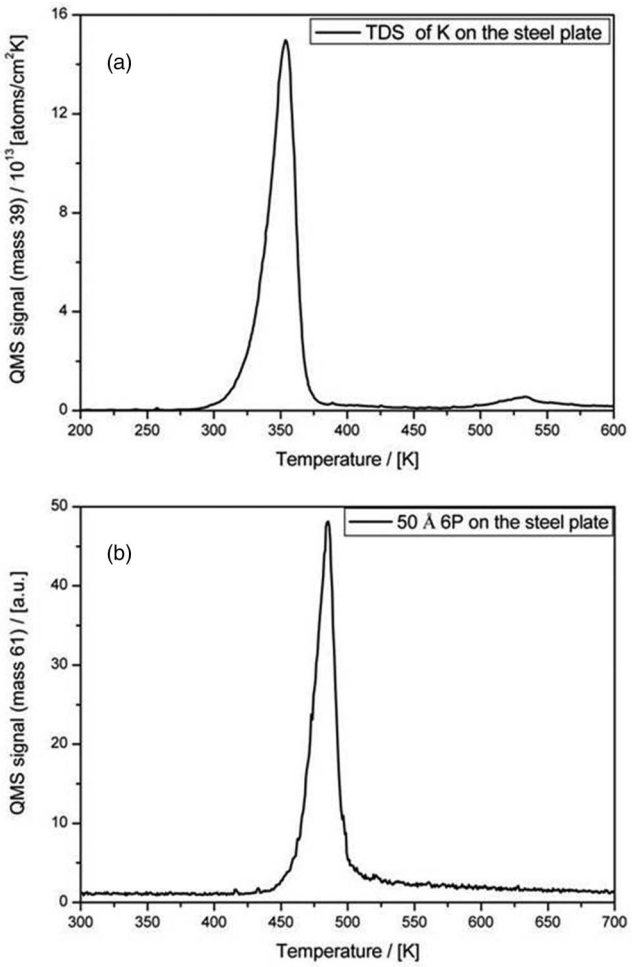

FIG. 6. (a) TDS of potassium from the steel plate sample holder. T_{ads}: 110 K, heating rate: 1 K/s, adsorbed amount: 2.9 nm mean thickness. (b) TDS of 6P from the steel plate sample holder. T_{ads}: 110 K, heating rate: 1 K/s, adsorbed amount: 5 nm mean thickness.

desorption peaks (as already observed in Fig. 2), is an experimental artifact: Due to the bad heat conductivity of mica normal to the (001) plane the actual temperature at the front mica surface lags behind the temperature of the steel plate, on which the thin mica sheet is clamped via tantalum foils. The first peak stems from potassium desorbing from the tantalum clamps, which can be assumed to have the same temperature as the steel plate. Only the second, larger peak stems from desorption from the mica surface. We have checked this behavior by thermal desorption spectroscopy of K multilayers (as well as 6P multilayers) which were directly deposited onto the steel plate. The corresponding desorption spectra are shown in Fig. 6(a) for potassium and in Fig. 6(b) for para-hexaphenyl, respectively. From these spectra, which show a clear zero order desorption behavior, as expected for multilayer desorption, one can derive the heat of evaporation E_d from the slope in the plot ln R vs. $1/T$, according to the Polanyi-Wigner equation.[29] We derive for potassium $E_d = 0.7 \pm 0.1$ eV and for 6P $E_d = 2.2 \pm 0.2$ eV. These values agree very well with literature data for K ($E_d = 0.8$ eV)[30] and 6P ($E_d = 2.4 \pm 0.1$ eV).[31] Furthermore, by comparing the desorption peaks for potassium from the tantalum clamps and the mica surface, the actual temperature of the mica surface can be calibrated. In this work, all TDS for potassium from mica are depicted in the uncorrected form. However, for 6P the TD spectra are temperature corrected, for better comparison with previous work.[11]

Unfortunately, with TDS we cannot determine if the metallic K-multilayer grows layer-by-layer or island like. Auger electron spectroscopy (AES) could in principle be used to discriminate between these two growth modes, but in the case of K on mica strong charging effects did not allow these measurements above the 1 ML limit. But there is general agreement in the literature that potassium tends to form islands on non-metallic substrates.[26,32]

With respect to the of potassium monolayer on mica one has to emphasize that the monolayer is so strongly bound that it cannot desorb (up to 1000 K), unlike for potassium desorption from metal surfaces, e.g., from nickel[24] or silver,[25] where monolayer desorption over a broad temperature range between 400 K and 1000 K is observed.

B. Adsorption/desorption of hexaphenyl on potassium covered mica(001)

The adsorption and film growth of 6P on freshly cleaved mica has been extensively investigated,[1–4] showing that needle-like islands form which consist of lying molecules. It has also been shown that a modification of the surface, either by sputtering or by contamination with carbon leads to a totally different layer growth: islands consisting of standing molecules are formed.[11] So far it was not clear to which extent the potassium coverage on the surface influences the layer growth of 6P. For this purpose we have prepared stable potassium coverages on the freshly cleaved and non-sputtered mica surface, as described above, and subsequently para-hexaphenyl was deposited at 110 K. We have previously shown that thermal desorption spectroscopy is a powerful tool to figure out whether or not a

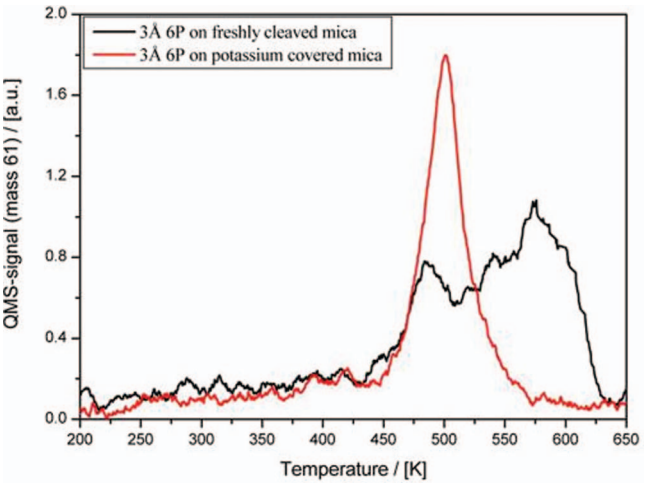

FIG. 7. TD spectra of 6P desorbing from freshly cleaved mica (black) and potassium covered mica (red). Adsorption temperature: 110 K, adsorbed amount: 3 Å mean thickness, heating rate: 1 K/s. While on freshly cleaved mica desorption from a strongly bound wetting layer (570 K) can be seen, no such desorption is observed on the potassium covered surface.

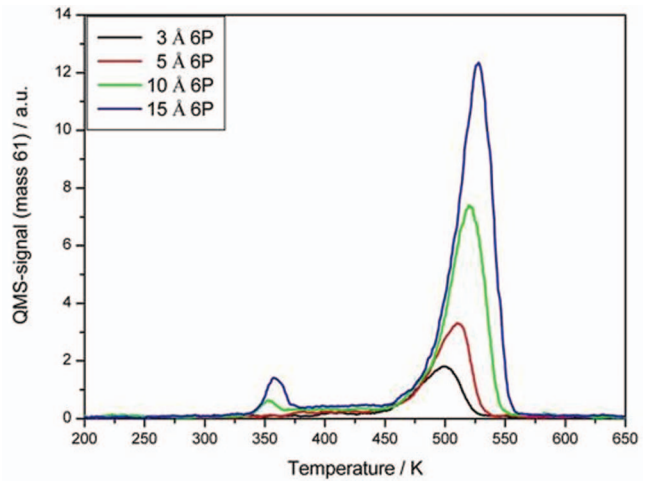

FIG. 9. Series of TD spectra for 6P from 1 ML potassium covered mica, deposited at 110 K. There exists no monolayer desorption peak, only a multilayer peak is observed. The peak at 350 K stems from desorption from the tantalum clamps. Heating rate: 1 K/s.

strongly bound wetting layer is formed before multilayer growth starts.[11,21,31] In Fig. 7 the (temperature corrected) thermal desorption spectrum of a 3 Å thick 6P layer on freshly cleaved mica is compared with that on a potassium covered mica surface. The desorption peak at 570 K for the freshly cleaved mica can be attributed to the wetting layer, and the peak at 490 K stems already from some multilayer islands. On the potassium covered surface, in contrast, no sign of a wetting layer is observed, similarly as on the sputtered or C contaminated mica surface.[11] A series of desorption spectra with different initial 6P coverages, between 3 Å and 15 Å, on the freshly cleaved and potassium covered surface are compiled in Figs. 8 and 9, respectively, supporting the above made statements. A closer look at the "multilayer" peak position in Figs. 8 and 9 reveals a shift of about 50 K. The reason for that is that a film with a mean coverage of 15 Å on the potassium covered surface is still a sub-monolayer

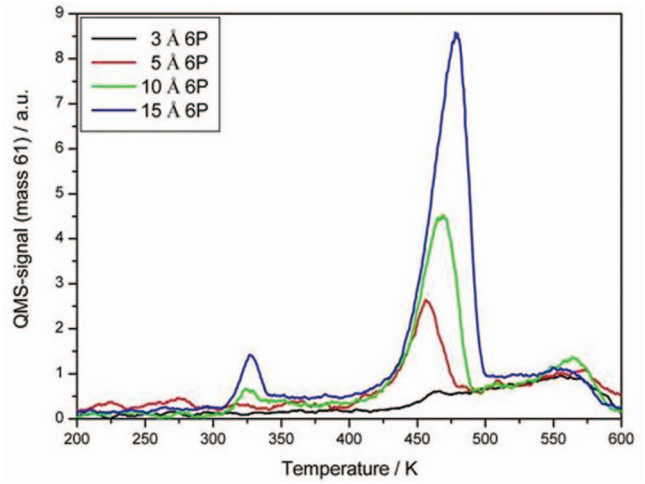

FIG. 8. Series of TD spectra for 6P from freshly cleaved mica(001), deposited at 110 K. Desorption from the monolayer (560 K) and the multilayer (470 K) can clearly be distinguished. The peak at 325 K stems from desorption from the tantalum clamps. Heating rate: 1 K/s.

film of standing molecules, considering the length of the 6P molecules of about 26 Å. Thus, the energy for removing 6P molecules from the rim of the monolayer islands, composed of standing molecules, is different to that from removing lying molecules from multilayer needle-like islands.

The conclusions drawn from TDS have been verified by AFM measurements. In Fig. 10(a) a 4 μm × 4 μm AFM image is shown, where a 6P film with 3 Å mean thickness was deposited on the potassium covered mica surface. In this image three different types of island morphologies can be observed. Islands #1 are slightly dendritic and have a height of about 26 Å, indicating islands of standing molecules. This can be seen in the cross section (along the line *a* in Fig. 10(a)) over several islands of the same type, as depicted in Fig. 11(a). Islands #2 have the shape of short needles with a width of about 50 nm and heights around 10 nm. A cross section along line *b* in Fig. 10(a), containing such islands, is shown in Fig. 11(b). These are apparently islands composed of lying molecules, because their width and height is similar to that for 6P on the freshly cleaved mica.[4,11] Apparently, there exist still some areas on the mica surface which are not sufficiently covered by potassium in order to induce the reorientation of the 6P molecules into the upright position. Finally, there exist some few islands (#3) which are nearly round shaped with diameters of about 180 nm and heights of about 30–50 nm (see cross section Fig. 11(c)). Since the total amount of material contained in these islands is not compatible with the mean thickness of 3 Å 6P, we believe that these hillocks represent K_xO_y or KOH compounds. Actually, for this experiment the stable potassium layer was prepared at a residual pressure of 1×10^{-9} mbar, a pressure which is already high enough to produce such potassium compounds, as described above. In this particular case the Auger signal ratio K252/O510 was about 5. The identification of these hillocks as being composed of potassium compounds is fostered by the observation of similar structures in AFM images of the mica surface after several potassium adsorption/desorption cycles, but without the deposition of 6P.

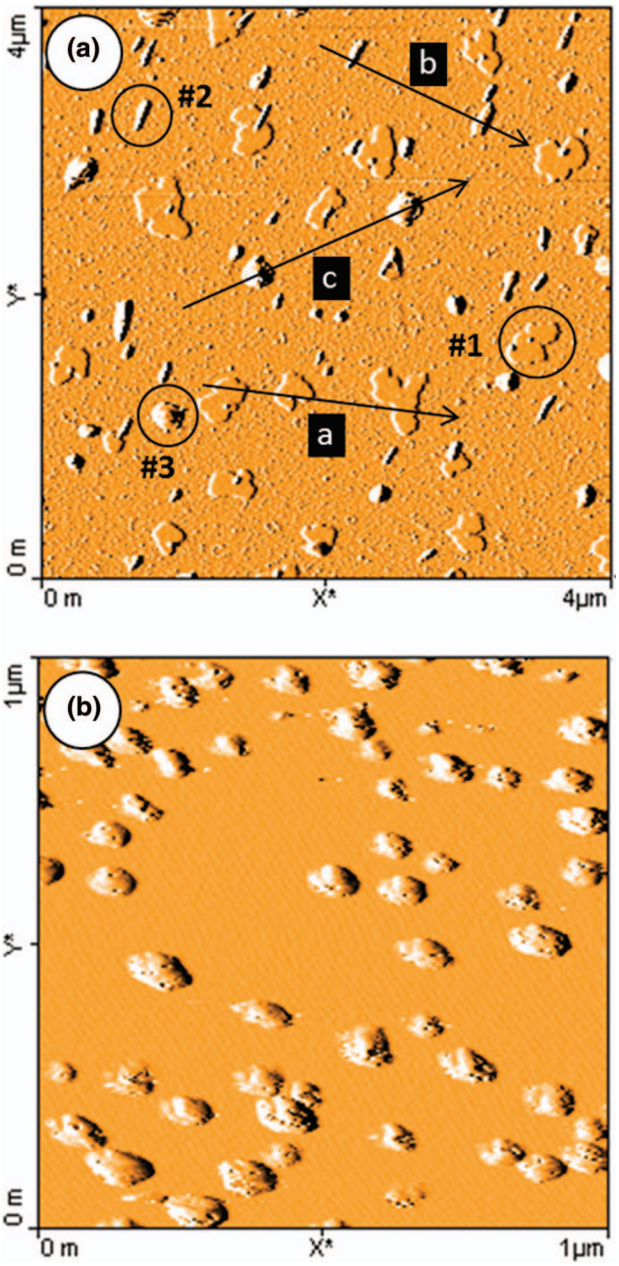

FIG. 10. (a) AFM image (4 μm × 4 μm) of a mica(001) substrate, covered with 1 ML of stable potassium and a 6P coverage with a mean thickness of 3 Å (derived mode). Islands #1 are composed of standing 6P molecules, with a height of 27 Å, islands #2 are composed of lying 6P molecules and islands #3 can be attributed to be composed of potassium compounds. The cross sections along *a*, *b*, and *c* are depicted in Figs. 11(a)–11(c). (b) AFM image (1 μm × 1 μm) of a freshly cleaved mica(001) substrate, covered with 6P of 3 Å mean thickness (derived mode).

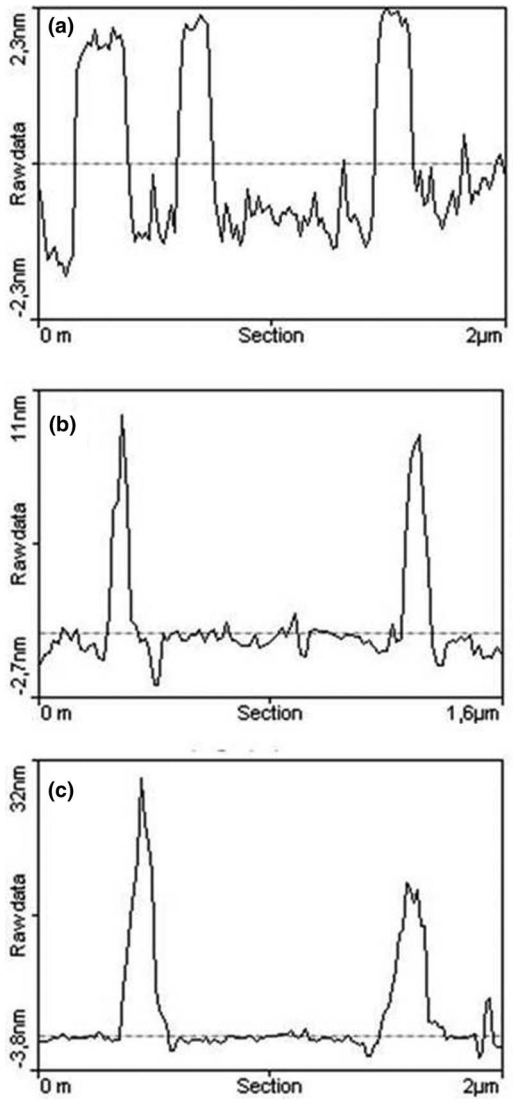

FIG. 11. Cross sections along the lines as depicted in Fig. 10(a).

In order to highlight the influence of potassium on the 6P layer growth we present a 1 μm × 1 μm AFM image of a 3 Å 6P film on freshly cleaved mica for comparison (Fig. 10(b)). This film is composed of small short needles composed of lying molecules, as can be deduced from cross sections, which show heights between 5 and 10 nm. There is no evidence of any round dendritic islands of monolayer height (2.6 nm). We have recently focused on this particular film and have shown that in this case the islands are the result of dewetting of the 3 Å thick wetting layer upon venting the system.[33]

Finally, we have also measured the surface roughness of the freshly cleaved mica surface and the 1 ML K covered mica surface. The line roughness R_a was determined along distances of 250 nm and the area roughness S_a on areas of 0.06 μm^2, which give similar results within the margin of error. On a freshly cleaved surface, the roughness is extremely small and varies between 0.5 Å and 3 Å, depending on the measured site on the surface. This is also true for the uncovered areas of the freshly cleaved substrate after 3 Å 6P deposition (Fig. 10(b)). On the 1 ML K covered surface (Fig. 10(a)) the roughness is 4–5 Å, demonstrating the increased roughness due to K adsorption. Interestingly, the roughness on top of the islands, composed of standing molecules, is even somewhat smaller, probably due to the softness of the 6P film (Fig. 11(a)).

IV. SUMMARY AND CONCLUSIONS

Freshly cleaved mica, which is frequently used as a substrate for thin film growth studies, contains half a monolayer of potassium on the surface. On such a surface, when

immediately installed into the deposition chamber, 6P forms needle-like islands which are composed of lying molecules. Deposition of additional potassium on the freshly cleaved mica surface under ultra-high vacuum condition (10^{-10} mbar) leads to a full monolayer of potassium, which is stable up to 1000 K. Additional potassium desorbs at around 350 K from the surface. Deposition of 6P on a mica surface containing 1 ML of stable potassium leads predominantly to islands composed of standing molecules. Only few needle-like islands can be observed, which demonstrate that the potassium monolayer is not uniform. The reason for the reorientation of the 6P molecules is a weakening of the interaction between the 6P molecules and the mica substrate. The potassium coverage acts in a similar way as the carbon contamination of mica or the amorphisation of the surface due to sputtering.[11] It has to be assumed that in all cases the existing dipole induced lateral electric fields, which stabilize the lying molecules on the freshly cleaved mica surface, are disturbed and hence the energetically more favorable vertical orientation of the molecules is preferred.

ACKNOWLEDGMENTS

This work was financially supported by the Austrian Science Fund FWF, Project No. P 23530.

[1]A. Andreev, G. Matt, C. J. Brabec, H. Sitter, D. Badt, H. Seyringer, and N. S. Sariciftci, Adv. Mater. **12**, 629 (2000).
[2]F. Balzer and H. G. Rubahn, Appl. Phys. Lett. **79**, 3860 (2001).
[3]C. Teichert, G. Hlawacek, A. Y. Andreev, H. Sitter, P. Frank, A. Winkler, and N. S. Sariciftci, App. Phys. A **82**, 665 (2006).
[4]L. Kankate, F. Balzer, H. Niehus, and H. G. Rubahn, J. Chem. Phys. **128**, 084709 (2008).
[5]M. Akai-Kasaya, C. Ohmori, T. Kawanishi, M. Nashiki, A. Saito, M. Aono, and Y. Kuwahara, Nanotechnology **21**, 365601 (2010).
[6]C. Simbrunner, G. Hernandez-Sosa, M. Oehzelt, T. Djuric, I. Salzmann, M. Brinkmann, G. Schwabegger, I. Watzinger, H. Sitter, and R. Resel, Phys. Rev. B **83**, 115443 (2011).
[7]L. Kankate, F. Balzer, H. Niehus, and H. G. Rubahn, Thin Solid Films **518**, 130 (2009).
[8]H. Plank, R. Resel, A. Y. Andreev, N. S. Sariciftci, and H. Sitter, J. Cryst. Growth **237–239**, 2076 (2002).
[9]K. Müller and C. C. Chang, Surf. Sci. **9**, 455 (1968).
[10]K. Müller and C. C. Chang, Surf. Sci. **14**, 39 (1969).
[11]P. Frank, G. Hlawacek, O. Lengyel, A. Satka, C. Teichert, R. Resel, and A. Winkler, Surf. Sci. **601**, 2152 (2007).
[12]T. Potocar, S. Lorbek, D. Nabok, Q. Shen, L. Tumbek, G. Hlawacek, P. Puschnig, C. Ambrosch-Draxl, C. Teichert, and A. Winkler, Phys. Rev. B **83**, 075423 (2011).
[13]G. Hlawacek, P. Puschnig, P. Frank, A. Winkler, C. Ambrosch-Draxl, and C. Teichert, Science **321**, 108 (2008).
[14]P. A. Campbell, L. J. Sinnamon, C. E. Thompson, and D. G. Walmsley, Surf. Sci. **410**, L768 (1998).
[15]H. Poppa and A. G. Elliot, Surf. Sci. **24**, 149 (1971).
[16]M. G. Dowsett, R. M. King, and E. H. C. Parker, J. Vac. Sci. Technol. **14**, 711 (1977).
[17]F. Ostendorf, C. Schmitz, S. Hirth, A. Kühnle, J. J. Kolodziej, and M. Reichling, Nanotechnology **19**, 305705 (2008).
[18]F. Ostendorf, C. Schmitz, S. Hirth, A. Kühnle, J. J. Kolodziej, and M. Reichling, Langmuir **25**, 10764 (2009).
[19]A. S. Gray and C. Uher, J. Mater. Sci. **12**, 959 (1977).
[20]See http://www.saesgetters.com for alkali metal dispensers.
[21]S. Müllegger and A. Winkler, Surf. Sci. **600**, 1290 (2006).
[22]B. Lamontagne, F. Semond, and D. Roy, Surf. Sci. **327**, 371 (1995).
[23]H. P. Bonzel, G. Pirug, and A. Winkler, Surf. Sci. **175**, 287 (1986).
[24]C. Resch, V. Zhukov, A. Lugstein, H. F. Berger, A. Winkler, and K. D. Rendulic, Chem. Phys. **177**, 421 (1993).
[25]V. Zhukov, K. D. Rendulic, and A. Winkler, Vacuum **47**, 5 (1996).
[26]W. Zhao, G. Kerner, M. Asscher, X. M. Wilde, K. Al-Shamery, H.-J. Freund, V. Staemmler, and M. Wieszbowska, Phys. Rev. B **62**, 7527 (2000).
[27]H. H. Huang, X. Jiang, H. L. Siew, W. S. Chin, and G. Q. Xu, Langmuir **14**, 7217 (1998).
[28]P. Sjövall and B. Kasemo, Surf. Sci. **290**, 55 (1993).
[29]P. A. Redhead, Vacuum **12**, 203 (1962).
[30]See http://www.webelements.com/potassium/thermochemistry.html for potassium heat of evaporation.
[31]A. Winkler, Springer Proc. Phys. **129**, 29 (2009).
[32]W. Hoheisel, M. Vollmer, and F. Träger, Phys. Rev. B **48**, 17463 (1993).
[33]L. Tumbek, C. Gleichweit, K. Zojer, and A. Winkler, Phys. Rev. B **86**, 085402 (2012).

Paper VI [P6]

“Initial stages of para-hexaphenyl film growth on amorphous mica”

T. Potocar, S. Lorbek, D. Nabok, Q. Shen, L. Tumbek, G. Hlawacek, P. Puschnig, C. Ambrosch-Draxl, C. Teichert, A. Winkler

Phys. Rev. B 83 (2011) 075423.

Initial stages of a *para*-hexaphenyl film growth on amorphous mica

T. Potocar,[1] S. Lorbek,[2] D. Nabok,[3] Q. Shen,[2] L. Tumbek,[1] G. Hlawacek,[4] P. Puschnig,[3] C. Ambrosch-Draxl,[3] C. Teichert,[2] and A. Winkler[1,*]

[1]*Institute of Solid State Physics, Graz University of Technology, Petersgasse 16, A-8010 Graz, Austria*

[2]*Institute of Physics, University of Leoben, Franz-Josef-Straße 18, A-8700 Leoben, Austria*

[3]*Chair of Atomic Modeling and Design of Materials, University of Leoben, Franz-Josef-Straße 18, A-8700 Leoben, Austria*

[4]*Physics of Interfaces and Nanomaterials, MESA+ Institute for Nanotechnology, University of Twente, P.O. Box 217, 7500AE Enschede, The Netherlands*

(Received 14 October 2010; published 22 February 2011)

Para-hexaphenyl (6P) molecules were deposited in the submonolayer range on a sputter- modified muscovite mica(001) surface by physical vapor deposition under ultrahigh vacuum conditions. The ultrathin films were investigated *in situ* by thermal desorption spectroscopy and *ex situ* by atomic force microscopy. On the sputter-modified amorphous mica surface the 6P molecules form two-dimensional islands of standing molecules. From the island size and capture zone distribution, as well as from the island density as a function of deposition rate and substrate temperature, all relevant parameters, characterizing the nucleation process, could be deduced. The critical island size was determined to be two and/or three molecules. The preexponential factor for surface diffusion of the monomers was determined to be 2×10^{17} s^{-1}. The binding energy of a critical nucleus with $i = 3$ was found to be 1.5 eV, using the calculated value of 0.02 eV for the diffusion energy barrier. This is in good agreement with our calculations of the binding energy for a critical cluster consisting of three lying molecules. Furthermore, the calculations show that the critical clusters are lying flat on the surface; they transform into islands of standing molecules only after the incorporation of further molecules. The shape of the islands is slightly dendritic at low surface temperature and becomes more dendritic with increasing temperature. This unusual behavior, which is the opposite of the frequently observed temperature dependence of metal islands, is also discussed in some detail.

DOI: 10.1103/PhysRevB.83.075423 PACS number(s): 68.55.A−, 68.37.Ps, 68.43.Jk, 81.15.Aa

I. INTRODUCTION

Organic thin films have attracted enormous interest in recent years due to their importance for organic electronics.[1–3] Electronic devices based on organic materials have already entered the market, for example, for displays, light-emitting diodes, transistors, solar cells, sensors, etc. Nevertheless, there is still a considerable lack in the basic understanding of film formation, in particular with respect to the initial stages of layer growth.[4] The question of whether the well-known models for inorganic film growth, mainly for metallic films,[5] can also be applied to the nucleation and growth of films consisting of large organic molecules arises. Although there is ample evidence that this might be the case,[6–8] experimental data that show a quite peculiar and different nucleation behavior for large organic molecules also exist.[9] The objective of this work is to shed some light on the initial stages of the layer growth of organic materials, using the example of *para*-hexaphenyl (6P) on muscovite mica(001) as a model system.

A large amount of literature exists on the fundamentals of nucleation and growth of inorganic thin films, and comprehensive overviews were given *inter alia* by Venables *et al.*,[5,10] Brune,[11] and Michely and Krug.[12] Rate equations for the individual processes during film formation—namely adsorption, diffusion, and desorption of the monomers, as well as the formation and disintegration of clusters—can be formulated, leading to relationships of the nucleation rate and island density as a function of the external parameters temperature and deposition flux. In this context, the critical island size is of importance, which is defined as the largest unstable island (cluster) that becomes stable upon the addition of just one more atom (molecule). The critical size depends on the interatomic (intermolecular) forces between the monomers of the film material and the substrate atoms. This quantity is critical for the further film growth and the final film structure and morphology. Thus, the evaluation and possibly the manipulation of the critical island size are of great importance. There also exists a strong correlation between the critical island size and the island-size distribution in the aggregation regime, which obeys a scaling law.[13,14] Island-size distributions can be determined rather easily with common experimental methods, for example, by atomic force microscopy (AFM) or scanning tunneling microscopy (STM), making such investigations indispensable to reveal the fundamentals of layer growth.

Most of the organic molecules frequently used for organic electronic devices can be categorized either as platelike (for example, phthalocyanines, porphyrins, etc.) or rodlike (for example, acenes, phenylenes, etc.) molecules. The film formation is naturally quite different for the individual groups of molecules. Here, we will focus on the rodlike 6P molecules because this material can be used *inter alia* for blue light-emitting diodes[15] and nano-optics devices.[16] There is only a small amount of literature available concerning the nucleation of such molecules on surfaces.[9,17] More frequently investigated is another group of rodlike molecules, namely pentacene (5A), mainly deposited on SiO_2.[4,7,18–27] This material is preferentially used for organic transistors because of its high electric mobility. A comparison of the existing literature shows that the morphology of ultrathin films of 6P and 5A molecules is quite similar. One puzzling result observed was the temperature dependence of the island shape of 6P[9] and 5A[7] molecules on SiO_2, and of hexathiophene (6T) on the

(100) surface of a 6T single crystal.[8] In all these cases the island shape changed from compact at low temperature to dendritic at higher temperature. This is the opposite of the frequently observed results for metal-atom deposition, where at low temperatures the islands are dendritic and only become compact with increasing temperature.[11,12] The reason for this is that at low temperature the atoms, which diffuse to an existing stable island, just hit and stick, without further diffusion along the rim of the island. This scenario is described by the classical diffusion-limited aggregation (DLA) model.[28] With increasing temperature, diffusion of the adatoms along the island edges and even crossing the corners of the islands becomes possible, leading to thermodynamically stable, compact island shapes. It seems that for large organic molecules this growth scenario cannot be applied. Another feature sometimes observed is a bend in the Arrhenius-type plot of the island density vs the inverse substrate temperature. This behavior has been interpreted in various ways. Some authors attributed this to a change of the critical island size,[24] others described it as being due to a change from complete condensation to initially incomplete condensation,[23] and others finally made a change of the nucleation mechanism responsible for this behavior.[9]

In this work, we focus on the nucleation and submonolayer growth of 6P on a modified mica(001) surface, which has been amorphized by Ar^+ ion sputtering. The 6P film formation on as-received mica(001) (typically produced by cleaving a mica sheet) has been intensively studied by several groups.[29–33] The main observation was that in this case the rodlike molecules first form a wetting layer of flat-lying molecules, and on top of this layer, needlelike islands that are also composed of flat-lying molecules grow (Stransky-Krastanov growth). Recently, we discovered that a modification of the mica surface by gentle sputtering or by covering the surface with a submonolayer of carbon results in a totally different growth behavior. On such a modified surface no wetting layer exists and the molecules start to form mounds consisting of standing molecules (Vollmer-Weber growth).[17,33] We use this system, which can be seen as a model system for organic film growth on a weakly interacting substrate, to investigate the fundamental parameters of nucleation in a comprehensive manner. We determine the island-number density as a function of the deposition rate and surface temperature over a wide range, as well as the island-size and capture zone distribution. This allows the evaluation of the critical island size, the frequency factor for surface diffusion, and the binding energy of the critical nuclei. These results are supported by molecular dynamics calculations of the energy and structure of the critical islands. In particular, we will figure out if the nucleation of large, rodlike organic molecules can be described in a similar way as the nucleation of single atoms.

II. EXPERIMENTAL DETAILS

Ultrathin films of 6P were deposited on muscovite mica(001) samples in an ultrahigh vacuum (UHV) chamber by physical vapor deposition (PVD) from a homemade glass Knudsen cell. The mica(001) samples ($10 \times 10 \times \sim 0.01$ mm^3) were prepared by cleaving a mica sheet with the help of adhesive tape and immediately installed into the UHV chamber. The base pressure of the vacuum chamber after bakeout was 1×10^{-10} mbar, but typically the experiments were performed without baking the system, resulting in a working pressure of about 2×10^{-8} mbar. It was verified experimentally that these vacuum conditions did not lead to any degradation of the prepared films. The thin mica sheets were attached to a steel plate via tantalum wires, which was heated resistively. The temperature was controlled by a Ni-NiCr thermocouple spot-welded to the back of the steel plate. This allowed a controlled heating of the steel plate and hence of the mica sample for thermal desorption spectroscopy (TDS), typically with heating rates of 1 K/s. With additional LN_2 cooling, the temperature of the steel plate could be varied between 100 K and 1000 K. Unfortunately, a considerable temperature difference existed between the front mica surface and the heating plate, due to the low heat conductivity of mica normal to the (001) plane. However, a calibration of the temperature can be performed by comparing the multilayer peak maximum of desorbing 6P from mica with that from the tantalum fixation wires, as described in more detail elsewhere.[33] For thermal desorption spectroscopy a multiplexed quadrupole mass spectrometer (QMS) (0–500 amu) was used. In addition to the mass of the 6P molecules ($m = 458.6$ amu) typically the mass $m = 61$ amu was measured, because this showed the largest signal of the cracking pattern in the QMS. Furthermore, it was verified that no cracking of the 6P molecules occurred at the surface.

For the quantitative determination of the 6P film thickness a quartz microbalance that was positioned next to the sample was used. The reliability of this device was checked in two ways: (a) by comparing with corresponding AFM images of submonolayer films of standing molecules and (b) by thermal desorption spectroscopy, as outlined in more detail elsewhere.[33] Typically, evaporation rates of about 0.02 monolayers (ML)/min were applied. For the modification of the mica surface to obtain exclusively layers with standing 6P molecules, the surface was sputtered for about 10 min by Ar^+ ions with 600 eV at an argon partial pressure of 5×10^{-5} mbar. The result of this procedure was verified by TDS: 6P desorbing from the freshly installed mica surface exhibit two desorption peaks, indicative of desorption from the multilayer and desorption from the more strongly bound wetting layer. In contrast, 6P desorption from the modified mica surface does not show the wetting layer peak.[33] Auger electron spectroscopy and x-ray photoelectron spectroscopy (XPS) were used to check the chemical composition of the mica substrate. After the *in situ* preparation and characterization of the 6P films on mica, the samples were investigated *ex situ* by atomic force microscopy in the tapping mode (Digital Instruments MultiMode IIIa), using PPP-NCHR cantilevers from NanoSensors with 300-kHz resonance frequency, guaranteed tip radius $<8 \pm 2$ nm, and an opening angle of 10°.

III. THEORETICAL METHODS

The structure and the energetics of 6P islands containing up to 20 molecules were obtained by molecular dynamics simulations using the simulated annealing method. Since the interaction of the 6P molecules with the sputter-modified mica(001) surface is difficult to capture in such an atomistic

approach, the substrate was replaced by a 6P(001) surface that corresponds to a standing 6P film ensuring the desired, relatively weak molecule/substrate interaction. Implications of the simplified treatment of the substrate will be discussed below. Molecular dynamics simulations were performed using Allinger's MM3 force field[34–36] and the TINKER code.[37] The 6P(001) surface was simulated by a supercell employing periodic boundary conditions. The surface unit cell was taken to be 12 × 8 6P(001) except for the largest clusters containing 12, 16, and 20 lying molecules, for which the substrate surface was increased to 20 × 14 ($n = 12$) and 25 × 15 ($n = 16, 20$), respectively. A vacuum distance of 100 Å was chosen in the direction perpendicular to the surface.

The equilibrium structure of 6P islands containing n molecules adsorbed on the 6P(001) surface was obtained by using the simulated annealing technique as implemented in TINKER's program "anneal." Following a 100-ps molecular dynamics equilibration step at a temperature of 400 K, the system temperature was decreased to 0 K with a linear cooling rate of 2 K/ps. Dynamic trajectories were propagated by a modified Beeman's integration algorithm[37] with a time step of 1 fs. The whole procedure was repeated several times with different initial molecular arrangements to ensure stable results for the predicted cluster geometries and corresponding binding energies. In particular, two sets of data corresponding to "lying" and "standing" 6P islands, respectively, were obtained by choosing initial configurations with parallel and perpendicular orientations of the long molecular axes with respect to the substrate surface.

The binding energy of an island containing n 6P molecules is defined as the energy required to break the island into n 6P monomers adsorbed on the substrate. Islands consisting of 1, 2, and 3 "standing" 6P molecules were found to be unstable, that is, after a finite simulation time (typically within the first 5 ps) they were transforming into the lying configurations. Therefore, to obtain the energy of these "unstable" configurations, we optimized the cluster shapes by using the local minimization technique as implemented in TINKER's "optimize" routine. As above, the simulations were performed several times for different starting configurations. The rms gradient cutoff criterion of 0.01 was used as a stopping criterion for the minimization procedure. Lower values of the criterion led, as in the case of molecular dynamics, to the lying cluster orientations.

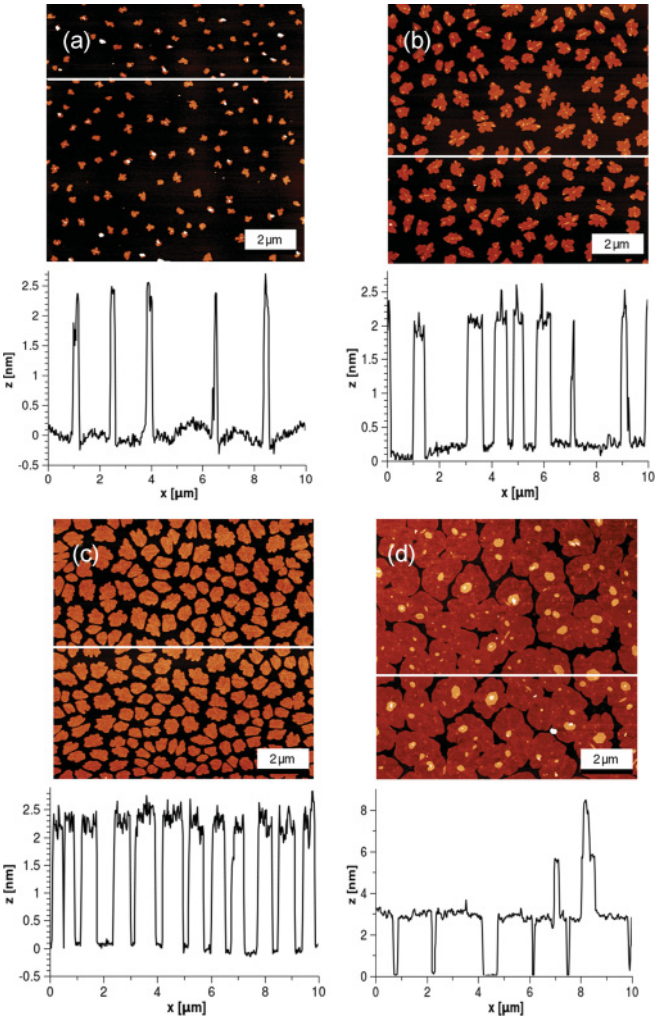

FIG. 1. (Color online) AFM images (10 μm × 10 μm, z-scale: 5 nm in (a-c), 10 nm in (d)) which show the coverage dependence of 6P on amorphous mica: (a) 0.08 ML, (b) 0.32 ML, (c) 0.60 ML, (d) 0.98 ML. $T = 300$ K. Deposition rate: 0.02 ML/min. The height profiles shown are taken from the lines indicated in the corresponding AFM images. In images (d)already coalescence and second layer growth is observed.

IV. RESULTS AND DISCUSSION

A. Coverage dependence of film formation and island-size distribution

In Fig. 1(a)–1(d) selected AFM images of 6P submonolayer films on amorphous mica(001) are presented as a function of the coverage Θ (Θ = 0.08, 0.32, 0.60, and 0.98 ML, respectively), prepared at room temperature with an evaporation rate of 0.02 ML/min. In all cases cross section measurements revealed island heights of about 2.5 nm. In Fig. 1(d) already some second-layer islands of the same height were observed. This demonstrates that the islands consist of standing molecules, most probably arranged as in the 6P(001) plane, where the molecules with a van der Waals length of 2.85 nm are inclined by 17° with respect to the (001) plane.[31,38] The coverage, the island density, and the island-size distribution can easily be determined from the AFM images using appropriate software.[39] In all the following evaluations of the island density and island-size distribution typically five AFM images from different sample areas were used for averaging, if not stated otherwise. From a series of AFM images as a function of coverage (including those in Fig. 1), we determined the aggregation regime (where the island density remains nearly constant) to be between 0.2 and 0.7 ML. Above 0.7 ML coalescence of the 2D islands and island formation in the second layer already starts [1 ML ≡ molecule density in the 6P(001) plane: 4.4×10^{14} molecules/cm^2]. The saturation island density for the given experimental conditions ($T = 300$ K, $R = 0.02$ ML/min) amounts to $n_i \approx 2$ mm^{-2}. The shape of the islands is slightly dendritic, but becomes more compact with increasing coverage.

TABLE I. The constants a_i and C_i in Eq. (2), for $i = 1$–6.

i	a_i	C_i
1	0.2715	1.1091
2	0.2976	1.9678
3	0.3086	3.2385
4	0.3145	5.1214
5	0.3182	7.9036
6	0.3207	11.9963

TABLE II. The constants a_β and b_β in Eq. (3), for $\beta = 2$–7.

β	a_β	b_β
2	3.24	1.27
3	6.25	1.77
4	11.60	2.26
5	21.05	2.76
6	37.62	3.26
7	66.50	3.76

In the aggregation regime (between 0.2 and 0.7 ML) information can be obtained from the island-size distribution $N_s\Theta$. According to the dynamic scaling assumption[40] the scaled island-size distribution $f_i(s/S)$ should be independent of the coverage Θ and the mean island size S and should only be determined by the critical island size i, which is defined as the largest unstable island that becomes stable when just one more particle is added:

$$f_i\,(s/S) = N_s(\Theta)S^2/\Theta, \tag{1}$$

with s being the island size and S the average island size.

Amar and Family[13] proposed an analytical expression for the scaling function in the form

$$f_i(u) = C_i u^i \exp\left(-ia_i u^{1/a_i}\right), \tag{2}$$

with $u = s/S$ and C_i,a_i defined by implicit geometrical equations:

$$(ia_i)^{a_i} = \frac{\Gamma\left[(i+2)\,a_i\right]}{\Gamma\left[(i+1)\,a_i\right]}, \quad C_i = \frac{(ia_i)^{(i+1)a_i}}{a_i\Gamma\left[(i+1)\,a_i\right]}. \tag{2a}$$

For the most realistic critical sizes $i = 1$ through 6 the values C_i and a_i are listed in Table I. In Fig. 2 the scaled island-size distribution for different film thicknesses in the aggregation regime ($\Theta = 0.22$, 0.32, 0.60 ML) are shown and compared with the scaling functions for different critical island size, $i = 1 - 6$. The best fit, as obtained by a least squares method, yields $i = 3 \pm 1$.

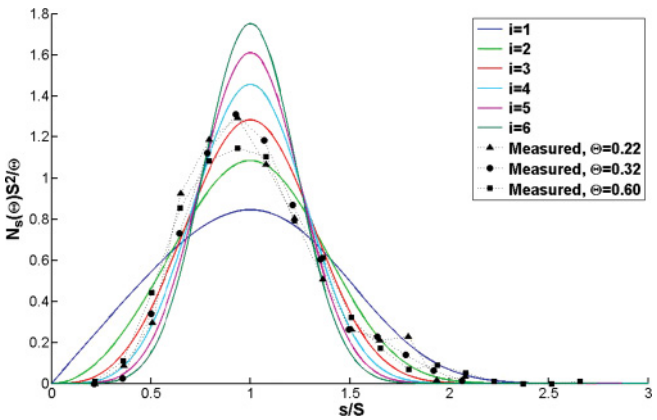

FIG. 2. (Color online) Scaled island-size distribution for three different coverages ($\Theta = 0.22$, 0.32, and 0.60 ML) of 6P on modified mica(001), and comparison with scaling functions for different critical island size (i = 1–6), according to Eq. (2). T = 300 K. Deposition rate $R = 0.02$ ML/min.

Pimpinelli and Einstein[41] have recently proposed an alternative method where the critical island size can be derived from the capture zone distribution. By capture zone one understands the region of the substrate from which monomers are more likely to diffuse to this particular island than to any other in the system. The capture zones can be roughly described by Voronoi polygons.[42] It is assumed that the capture zone distribution P can be described by a simple expression based on the generalized Wigner surmise, that is, being the product of a power-law rise and a Gaussian decay:

$$P_\beta(s) = a_\beta s^\beta \exp(-b_\beta s^2), \tag{3}$$

where $\beta = i + 2$,[43,44] $s = v/V$, v is Voronoi polygon size, V is mean value of v, and a_β and b_β are constants fixed by normalization and unit-mean conditions:

$$a_\beta = 2\Gamma\left(\frac{\beta+2}{2}\right)^{\beta+1} \Big/ \Gamma\left(\frac{\beta+1}{2}\right)^{\beta+2},$$
$$b_\beta = \left[\Gamma\left(\frac{\beta+2}{2}\right) \Big/ \Gamma\left(\frac{\beta+1}{2}\right)\right]^2. \tag{3a}$$

These values are listed for β ranging from 2 to 7 in Table II. In Fig. 3(a) the island-size distribution for a 0.19-ML film prepared at 300 K with an evaporation rate of 0.04 ML/min and in Fig. 3(b) the corresponding Voronoi tessellation is presented. Figure 3(c) shows the capture-zone distribution together with the calculated functions for i ranging from 0 to 5. The value of $i_{\text{fit}} = 2.8$ was estimated from a direct fit using the method of least squares with the Levenberg-Marquardt algorithm. Thus, both methods can be applied equally to determine the critical cluster size. It seems that the fits in Fig. 2 and Fig. 3(c) are quite different. There are several reasons for that: First, for Fig. 2, as for all other data evaluation [except that for Fig. 3(c)], AFM images were recorded at five different areas on the surface close to all four corners and at the surface center. On the one hand this procedure averages over a possible surface inhomogeneity as well as over slightly different surface coverages. On the other hand, it yields, however, the rather large scattering of the data points in Fig. 2. For the application of the capture zone method we recorded ten AFM images in a small area in the middle of the sample surface. This leads to the much better statistics in Fig. 3(c). Besides that, the fit function as proposed by Einstein and Pimpinelli [Eq. (3)] gives a better fit to the slightly asymmetric shape of the island-size and capture zone distribution than the function as described in Eq. (2).

According to the definition of the critical island size it would mean that for $i = 3$, 6P tetramers would already be

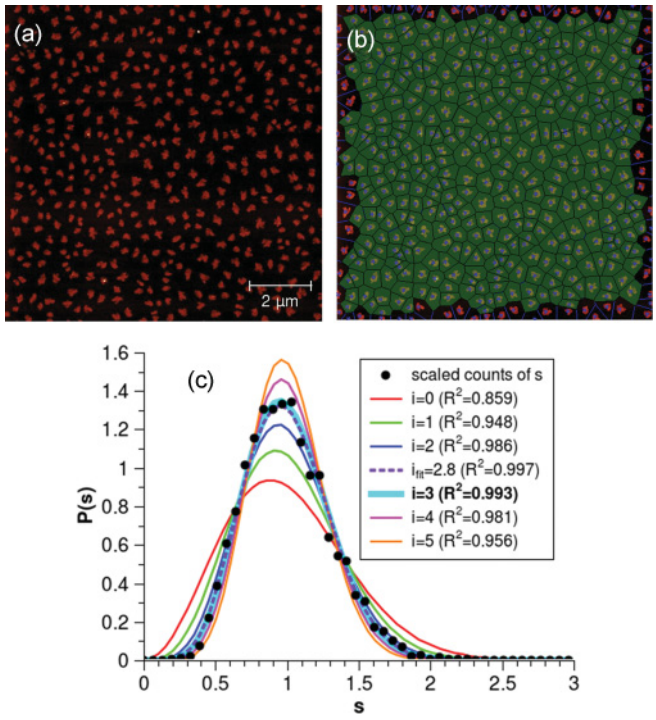

FIG. 3. (Color online) (a) Island-size distribution of 6P on amorphous mica: Coverage: 0.19 ML, $T = 300$ K. Deposition rate: 0.04 ML/min. (b) Corresponding Voronoi tessellation. (c) Distribution of capture zones as shown in (b), and comparison with the scaling functions, according to Eq. (3). The bin width was optimized according to a model by Scott (Ref. 56).

stable entities. At this stage the question arises whether the critical nuclei already consist of standing molecules or if they are still composed of lying molecules, which would rotate into the standing configuration only at a later stage. For this purpose, we have calculated the binding energy E(n) of an island containing n 6P molecules, which we define as the energy difference between the n-molecule cluster adsorbed on the substrate compared to the energy of n adsorbed, but well-separated, lying 6P molecules. For the calculation we have modeled the surface by the (001) plane of a 6P crystal. Unfortunately, the atomic structure of the ion-bombarded mica surface is not known, precluding a force-field simulation of the 6P deposition on this substrate. The replacement of the modified mica by the 6P(001) surface is rationalized as follows: We were aiming at a reasonably simple substrate surface with a rather weak molecule/substrate interaction since this is a prerequisite for the appearance of the experimentally observed standing islands. Here, 6P(001) was a natural choice. We expect our simulation results, concerning the cluster shapes of standing and lying islands, to be rather insensitive to the exact nature of the substrate/molecule interaction as long as it remains in this weakly interacting regime. Qualitatively, a stronger substrate/molecule interaction will energetically favor "lying clusters" due to the larger adsorption energy of lying molecules compared to standing ones. On the other hand, a weaker substrate/molecule interaction will favor islands composed of standing molecules due to their lower surface energy. Thus, tuning the strength of the substrate/molecule interaction will result in a relative shift of the binding energy curves for the standing and lying clusters, respectively, thereby modifying the cluster size where the transition from lying to standing clusters occurs.

In Fig. 4 the binding energy E_n is plotted vs the cluster size n, for clusters of lying molecules and of standing molecules, respectively. The binding energy is defined as the cluster energy minus the energy of n molecules adsorbed lying on the surface. It can be seen that for small cluster size, in particular for $n < 4$, the standing formation is completely unstable. For $4 < n < 14$ the clusters consisting of standing molecules are still energetically less favorable than those with lying molecules, but they would be at least metastable with respect to the isolated molecules. Only above $n = 14$ do the clusters of standing molecules become more favorable. However, the binding energy for the lying clusters strongly depends on the molecule/substrate interaction, as discussed above, thus the crossover could be at a somewhat different cluster size for 6P on the amorphized mica surface. Nevertheless, from these results we have to conclude that the critical clusters ($n = 2, 3$) are still composed of lying molecules and that

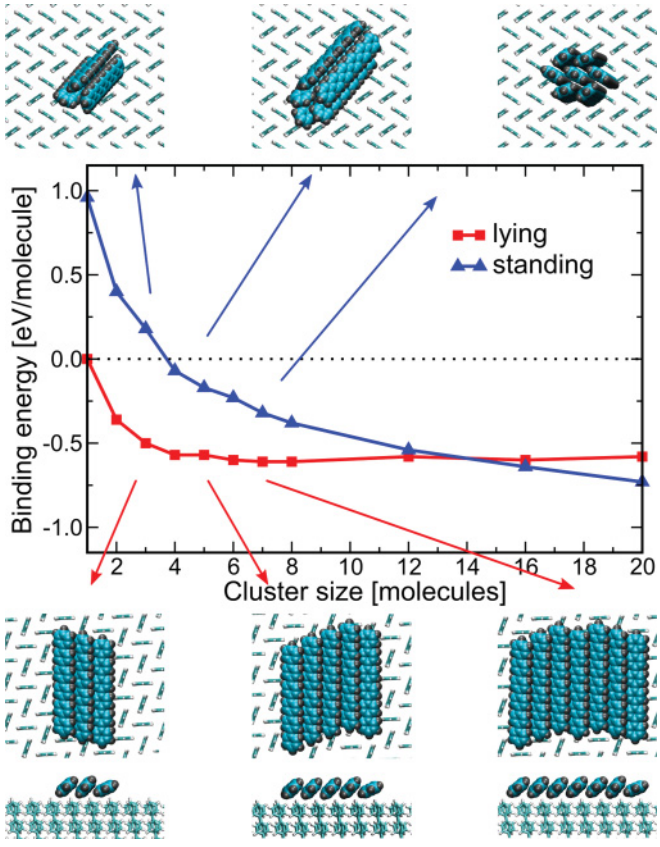

FIG. 4. (Color online) 6P cluster binding energy on a 6P(001) plane as a function of cluster size for clusters with standing and lying molecules, respectively. The conformation of the stable clusters, starting from standing (upper row) and lying molecules (lower row), respectively, are depicted. For the lying clusters, an offset of neighboring molecules is observed which is caused by the π-π interaction of the aromatic molecules. The lattice mismatch with the substrate causes that only a maximum of 4 molecules exhibit this offset in the same direction. For the standing islands (top), the molecular packing systematically adopts the bulk-like herringbone formation with increasing cluster size.

only after further island growth do the molecules switch to the standing configuration. How this change proceeds in detail is not yet clear, and only further molecular dynamic studies could elucidate this process.

B. Deposition rate dependence of film formation and critical island size

The saturation island density N_x in the aggregation regime is a function of the deposition rate R and the surface temperature T. When complete condensation can be assumed, that is, when desorption of the monomers can be ignored, then the critical island size can be extracted from the saturation island density as a function of the deposition rate. In order to verify whether this condition is fulfilled for the present system, we have measured the adsorbed amount of 6P on the amorphous mica surface with the help of TDS as a function of the exposed 6P amount as obtained from the quartz microbalance. This is compiled in Fig. 5 for substrate temperatures of 150, 300, and 400 K. For surface temperatures of 150 and 300 K the correlation is linear within the experimental error, indicating a constant sticking coefficient. At 400 K, however, the sticking coefficient is slightly smaller, in particular at an evaporated amount of about 15 Hz. According to the calibration via AFM images this corresponds to a coverage of slightly less than one monolayer (inset in Fig. 5). This shows that for very large islands some of the molecules already desorb before they reach the island border, where they can be incorporated by surmounting the Ehrlich-Schwöbel barrier, or before they can form a new nucleus in the second layer. Nevertheless, at low coverage, even in the case of 400 K nearly complete condensation can be assumed.

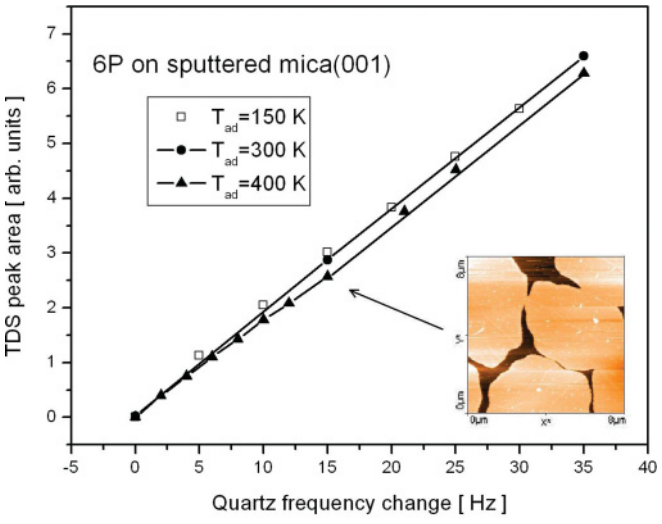

FIG. 5. (Color online) Adsorbed amount of 6P on amorphous mica(001), obtained by TDS, vs the amount of impinging molecules, obtained by the frequency change of a quartz microbalance, for various substrate temperatures: 150, 300, and 400 K. Deposition rate: 0.02 ML/min. In the inset an AFM image (8 μm × 8 μm) of a film with an evaporated amount of 15 Hz at 400 K is shown, corresponding to a coverage of close to 1 monolayer,

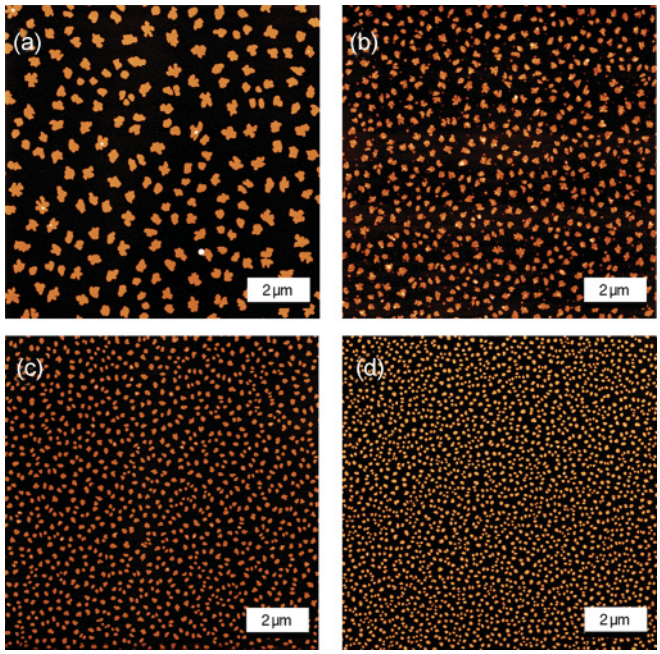

FIG. 6. (Color online) AFM images (10 μm × 10 μm, z scales: 5 nm) that show the deposition rate dependence of 6P on amorphous mica: (a) 0.021 ML/min, (b) 0.045 ML/min, (c) 0.117 ML/min, (d) 0.481 ML/min, $T = 300$ K, coverage: 0.25 ML.

The saturation island density N_x in the aggregation regime for a rectangular lattice can be described in the case of complete condensation in the following form:[5,45]

$$\frac{N_x}{N_0} = \eta(\Theta, i)\left(\frac{4R}{\nu_0 N_0}\right)^{i/(i+2)} \exp\left(\frac{i E_d + E_i}{(i+2)kT}\right), \qquad (4)$$

where N_0 is the number of surface sites per unit area [4.4×10^{14} 6P molecules·cm^{-2} in the 6P(001) plane], η is a weak function of Θ and i, with $\eta \sim 0.2$–0.3,[5] R is the deposition rate, ν_0 is the attempt frequency for surface diffusion, E_d is the activation barrier for diffusion, and E_i is the binding energy of the critical cluster.

A plot of $\ln N_x$ vs $\ln R$ for constant substrate temperature and coverage allows the determination of the critical cluster size i from the slope α_{0R}, and the intercept with the y axis (y_{0R}) yields information on the energies involved:

$$\alpha_R = \frac{i}{i+2}, \qquad (5)$$

$$y_{0R} = \ln(\eta N_0) + \frac{i}{i+2}\ln\left(\frac{4}{\nu_0 N_0}\right) + \frac{i E_d + E_i}{(i+2)kT}. \qquad (6)$$

Figures 6(a)–6(d) show selected AFM images of 6P films with a mean coverage of about 0.25 ML, prepared at 300 K with different deposition rates. Qualitatively, the saturation island density increases with increasing deposition rate, as expected. In Fig. 7, the plot of $\ln N_x$ vs $\ln R$ is depicted. From the slope of the straight line ($\alpha_R = 0.55 \pm 0.05$) a critical island size of $i = 2.5 \pm 0.5$ can be obtained. This result is in good agreement with the data obtained from scaling theory within the experimental error. However, the evaluation procedure based on the variable deposition rate is more accurate, and therefore the result of the noninteger critical island size $i = 2.5$ has to be assumed

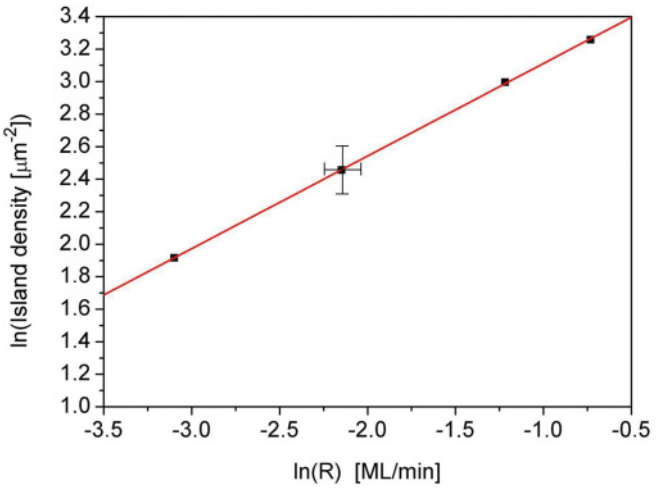

FIG. 7. (Color online) Island density as a function of deposition rate for 6P on amorphous mica. $T = 300$ K, $\Theta = 0.25$ ML. The slope corresponds to $i = 2.5$.

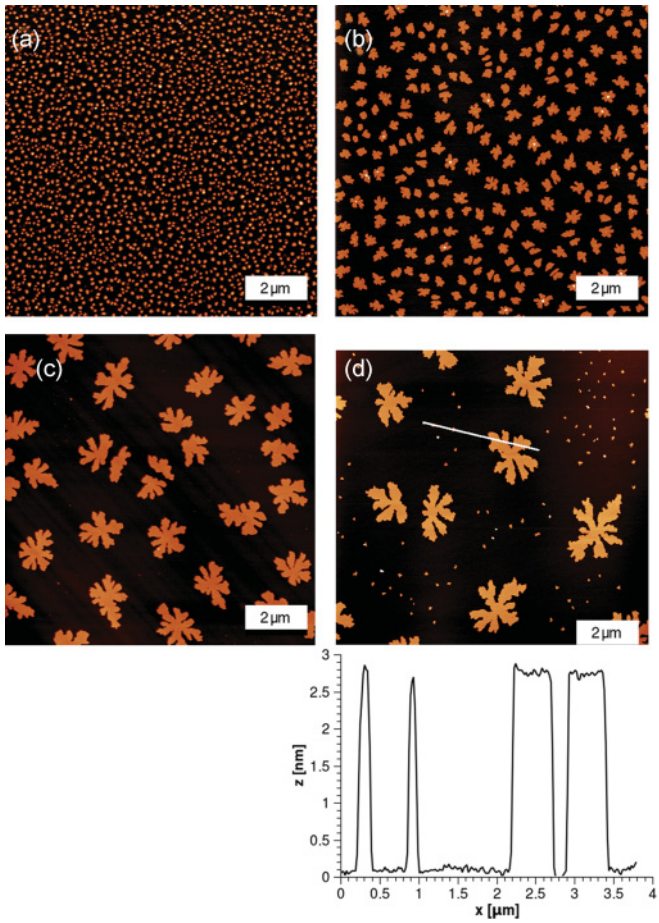

FIG. 8. (Color online) AFM images (10 μm $\times$ 10 μm, z-scale: 5 nm) which show the temperature dependence of 6P growth on amorphous mica: (a) 150 K, (b) 250 K, (c) 350 K, and (d) 400 K. Mean coverage: 0.22 ML. Deposition rate: 0.02 ML/min. The height profile shown is taken from the line indicated in the AFM image of (d).

to be the more reliable one. This would mean that both trimer ($i = 2$) and tetramer ($i = 3$) clusters of 6P molecules are of similar stability. Actually, this feature is not implausible. Compared to the clustering of single atoms, where a trimer is a quite well-defined entity, a trimer of lying rodlike entities can have a variety of different conformations. Thus, one can imagine that a special arrangement of three 6P molecules is already stable, whereas for another arrangement four molecules are necessary to become a stable cluster. In fact, it would be better to characterize the stability of a cluster by its lifetime. If the lifetime of a special cluster is longer than the time that elapses until a further monomer can be incorporated in the cluster, then the cluster tends to be stable. A detailed discussion of the critical island size can be found in Ref. 46.

C. Substrate temperature dependence of film formation and nucleation parameters

According to Eq. (4), the saturation island density should be influenced by the substrate temperature even more strongly than by the deposition rate, because the temperature shows up in the exponential term. Also from the experimental point of view the substrate temperature can be varied over a wide range more easily than the deposition rate. In Fig. 8 selected AFM images of 6P films on amorphous mica(001) are shown as a function of the substrate temperature, for mean coverages of 0.22 ML and deposition rates of 0.02 ML/min. Whereas up to 350 K [see also Fig. 1(b)] the number of islands and the island-size distribution behave as expected, at 400 K a bimodal island size distribution is observed [Fig. 8(d)]. Few large islands with pronounced dendritic behavior are surrounded by small islands of nearly identical size, as shown by the cross section in Fig. 8(d). However, the existence of the small islands is not well reproducible. There exist AFM measurements for films grown under similar experimental situations, where only little or no small islands can be observed. Actually, we believe that these small islands are in some way correlated with not well amorphized areas on the surface. Therefore, we will ignore this feature for the following data evaluation, because their contribution to the total coverage is not significant.

A plot of the island density as a function of temperature in the form of $\ln N_x$ vs $1/T$ is shown in Fig. 9. The most pronounced feature is a bend in the straight lines around 300 K. We will return to this point later. At the moment we want to emphasize that there are strong indications that only above 300 K are the experimental conditions for diffusion-limited aggregation fulfilled. Thus we will concentrate first on the evaluation of this part of the slope. Again, useful information can be gained from the slope α_T and the intercept y_{0T} with the y axis:

$$\alpha_T = \frac{i E_d + E_i}{(i+2)k}, \tag{7}$$

$$y_{0T} = \ln(\eta N_0) + \frac{i}{i+2}\ln\left(\frac{4}{N_0}\right) - \frac{i}{i+2}\ln \nu_0 + \frac{i}{i+2}\ln R. \tag{8}$$

Since the critical island size i is already known from Eq. (5), the evaluation of ν_0 is possible from Eq. (8).

In addition, the combination of Eq. (5) through Eq. (8) yields the following relationship:

$$y_{0R} + \alpha_R \ln R = y_{0T} + \frac{\alpha_T}{T}. \quad (9)$$

Although this relationship does not yield new information on the parameters contained in Eq. (4), it is a valuable measure for the quality of the two independent experimental data sets $N(R)$ and $N(T)$. Indeed, the evaluation of the graphs in Fig. 7 ($\alpha_R = 0.55$, $y_{0R} = 5.64$) and Fig. 9 (high-temperature slope: $\alpha_T = 3.890$ K, $y_{0T} = 6.45$) yields an agreement within 2% between the left- and right-hand sides of Eq. (9). (Note the used units of cm^2 and s for the evaluation of the graphs.) For the low-temperature part of the slope, Eq. (9) is not fulfilled with the same accuracy. Therefore we believe that for temperatures below 300 K the conditions for diffusion-limited aggregation are not fulfilled and a different physics is responsible for the growth behavior (see below). One could, of course, speculate whether a possible contamination in the low-temperature regime might be responsible for this unusual behavior. However, AES and XPS investigations did not reveal any significant contamination. Besides the elements contained in muscovite mica (Si, Al, K, O), only carbon was detected. However, this carbon content remained the same, within the experimental error, for all sample temperatures used.

From Eq. (8) we can obtain the attempt frequency for surface diffusion of the 6P monomers on the mica substrate (which can be assumed to diffuse as lying molecules) of $\nu_0 = 2 \times 10^{17 \pm 0.5} s^{-1}$. This is a rather high value when compared with typical diffusion frequencies of surface atoms in the order of 10^{13} s^{-1}. However, this can easily be understood in the context of transition state theory (TST).[47] Within this theory the preexponential factor (frequency factor) is interpreted as the ratio of the partition functions of the particles in the transition state for surface diffusion and in the adsorbed state:

$$\nu_0 = \frac{kT}{h} \frac{Q^{\oplus}}{Q}, \quad (10)$$

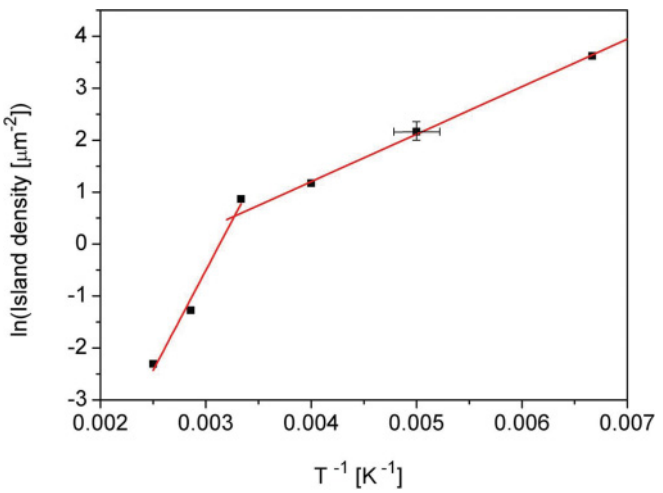

FIG. 9. (Color online) Island density of 6P on amorphous mica(001) as a function of temperature, $\Theta = 0.22$ ML, $R = 0.02$ ML/min.

where $Q^{\oplus}$ is the partition function for all modes (translation, rotation, vibration) of the transition complex (without that of the reaction coordinate, which is $kT/h \approx 6 \times 10^{12}$ s^{-1} at room temperature) and Q is the partition function of all modes in the adsorbed site.[48] It is obvious that only for single-atom diffusion, where the partition functions are similar in the adsorbed and the transition state, the hopping frequency is close to 10^{13} s^{-1}. However, for large organic molecules many more rotational and vibrational modes can be excited in the transition state than in the adsorbed state and hence the preexponential factor can be considerably higher. This is similar to the desorption of large organic molecules from surfaces, where also unusually large preexponential factors for the desorption rate have been experimentally observed[49–51] and theoretically explained along TST.[52] For example, a frequency factor of 5.6×10^{25} s^{-1} has been measured for 6P desorption from Au(111).[53]

From Eq. (7) we can only obtain information on the combined energies E_d and E_i involved in the island formation. However, we have recently calculated the diffusion barrier for flat lying molecules which resulted in an activation energy barrier for 6P diffusion of 0.02 eV.[17] Taking this into account we determine a binding energy of the critical 6P cluster of $E_i = 1.5$ eV. From our calculations we obtain a cluster energy for an adsorbed dimer with lying molecules ($i = 2$) of 0.74 eV and for a trimer ($i = 3$) of 1.53 eV. (Note that in Fig. 4 the cluster energies are given in eV/molecule.) By applying the same evaluation procedures to the low temperature slope yields completely unrealistic values of $\nu_0 = 20\,s^{-1}$ and $E_i = 0.23$ eV. This is another strong indication that a different physics governs the layer growth at low temperature.

Actually, a bend in the curves $\ln N_x$ vs. 1/T has also been observed by other groups. For the inorganic system Cu on Ni(100)[54] such a bend has been assigned to a change of the critical cluster size from $i = 3$ to $i = 1$ with decreasing temperature. With respect to organic molecules such a behavior has been described for pentacene on SiO_2,[24] pentacene on polystyrene[23] and 6P on SiO_2.[9] However, different explanations were given for this particular behavior. Tejima *et al.*[24] attributed it also to a transition of the critical island size from $i = 3$ to $i = 2$ at around 260 K. Ribic *et al.*[23] explained the bend in their results as being due to a transition of complete condensation into incomplete condensation above 320 K. Finally, Yang *et al.*[9] proposed that in their case a different growth mechanism exists below 330 K. In this temperature range the impinging molecules should be immediately freezing when they hit the surface, which would lead to a metastable disordered film. Because of the high surface free energy, however, the disordered film should relax in the course of time to an energetically more favorable state. This would explain the existence of the compact islands formed at low temperature.

A thorough analysis of our data also brings us to the conclusion that a different growth mechanism at low substrate temperature is the reason for the bend in Fig. 9. An attempt to evaluate the data by assuming initially incomplete condensation completely fails. Also an assumed change of the critical island size in the low-temperature regime to $i = 2$ or $i = 1$ leads to unrealistically high diffusion energies for the lying monomers. Thus, we suggest that at low temperatures the conditions for DLA are just not fulfilled and

a different growth mechanism must be considered. However, our explanation of the observed behavior is somewhat different to that described by Yang *et al.*[9] In particular we have seen that the surface mobility of the 6P monomers is very high, even at low temperature. From the diffusion energy $E_i \approx 0.02$ eV and the pre-exponential factor $\alpha_0 = 2\times10^{17}$ s^{-1}, the calculated hopping frequency ν at 150 K is still 4×10^{16} s^{-1}. Thus, the formation of a frozen amorphous layer by a hit-and-stick process is not reasonable in the temperature range used.

We rather believe that the main issue in the nucleation process of rodlike organic molecules is the kinetics of critical nuclei formation. In the classical examples of metal film growth the monomers are zero-dimensional objects. In the case of a critical nucleus size $i = 1$, as frequently observed for metal film growth, the encounter of two atoms will already lead to a stable nucleus, independent of the relative impact angle. Furthermore, it can safely be assumed that the capture probability is unity, throughout the growth. However, for large organic molecules the situation for critical cluster formation and further growth is significantly different. It is known that rodlike molecules will only bind when they are parallel to each other. A head-on or T-shaped configuration would be energetically unfavorable. Furthermore, it is known that the rodlike molecules diffuse preferentially in directions parallel to the long axis.[55] This also decreases the probability that two molecules would approach each other in a favorable orientation. For the proper rotation into the favorable conformation an activation barrier has to be overcome, which is only possible at sufficiently high temperature. It is obvious that the capture probability will no longer be independent of the orientation of the individually approaching molecules and is most probably much smaller than unity (rotational hindering). This effect of steric constraints for cluster formation results in a much higher monomer density. In the classical DLA film growth the monomer density is exceedingly small in the aggregation regime, which leads to the formation of dendritic islands via the hit-and-stick process at the island borders. In the case of steric hindering of critical cluster formation from flat-lying monomers, a supersaturated two-dimensional monomer gas phase will develop. However, as soon as stable clusters of lying molecules have been formed, which soon afterwards transform into small clusters of standing molecules, the probability for the incorporation of approaching molecules into these clusters might be significantly increased, due to less steric constraints. Consequently, a rapid condensation of the supersaturated two-dimensional gas phase would occur, leading to the observed compact islands. Further growth of the islands in the aggregation regime, where the monomer concentration is again quite small, would no longer change their shape considerably.

V. SUMMARY AND CONCLUSIONS

Submonolayers of hexaphenyl (6P) grown by physical vapor deposition on sputter modified muscovite mica(001) consist of islands with standing molecules. It was experimentally shown that at room temperature complete condensation can be assumed, that is, the desorption rate is negligible, and that the aggregation regime, that is, where the number of islands remains essentially constant, lies between 0.2 and 0.7 monolayers. The island density was determined as a function of the surface temperature and the deposition rate, as well as the island-size and capture-zone distribution, which allowed a quite comprehensive description of the nucleation process. A critical island size of 2 to 3 was deduced, indicating that trimers and tetramers of 6P are already stable islands. However, calculations of the cluster energy and cluster conformation have shown that small clusters ($n < 5$) are only stable when the molecules are lying on the surface. Thus, one has to conclude that the critical islands consist of lying molecules and that the conversion into standing islands takes place at a later stage ($n \approx 14$). From the island density as a function of temperature and deposition rate also the preexponential factor for surface diffusion can be obtained, which was calculated to be 2×10^{17} s^{-1}. This rather large value can be understood in terms of transition-state theory, because for the large 6P molecules many rotational and vibrational modes can be excited in the transition state for diffusion. Furthermore, the energy for nucleation can be deduced, which actually consist, in case of complete condensation, of the activation energy for diffusion and the binding energy of the critical nuclei. Using the calculated value of 0.02 eV for the diffusion energy, we obtain a binding energy for the critical cluster of 1.5 eV. This is in good agreement with our calculated binding energy for a cluster consisting of three lying molecules. The shape of the clusters, which is rather compact at low surface temperature, changed to a more pronounced dendritic shape above room temperature. This behavior, which is in contrast to the frequently observed temperature dependence of the island shape for metal films, can be explained by the steric hindering of nucleation at low temperature, which leads to a supersaturation of the monomer density. This means that the conditions for diffusion-limited aggregation of 6P, on which the nucleation theory is based, are not sufficiently fulfilled at low surface temperature.

ACKNOWLEDGMENTS

This work was financially supported by the Austrian Science Fund (FWF), Projects No. P19197, S9707, and S9714.

*Corresponding author: a.winkler@tugraz.at

[1]H. E. Katz and J. Huang, Ann. Rev. Mat. Res. **39**, 71 (2009).

[2]S. R. Forrest and M. E. Thomson, Chem. Rev. **107**, 923 (2007).

[3]T. B. Singh and N. S. Sariciftci, Ann. Rev. Mat. Res. **36**, 199 (2006).

[4]R. Ruiz, D. Choudhary, B. Nickel, T. Toccoli, K.-C. Chang, A. C. Mayer, P. Clancy, J. M. Blakely, R. L. Headrick, S. Iannotta, and G. G. Malliaras, Chem. Mat. **16**, 4497 (2004).

[5]J. A. Venables, G. D. T. Spiller, and M. Hanbücken, Rep. Prog. Phys. **47**, 399 (1984).

[6]R. Ruiz, B. Nickel, N. Koch, L. C. Feldman, R. F. Haglund Jr., A. Kahn, F. Family, and G. Scoles, Phys. Rev. Lett. **91**, 136102 (2003).
[7]B. Stadlober, U. Haas, H. Maresch, and A. Haase, Phys. Rev. B **74**, 165302 (2006).
[8]M. Campione, S. Caprioli, M. Moret, and A. Sassella, J. Phys. Chem. C **111**, 12741 (2007).
[9]J. Yang, T. Wang, H. Wang, F. Zhu, G. Li, and D. Yan, J. Phys. Chem. B **112**, 7816 (2008).
[10]C. Ratsch and J. A. Venables, J. Vac. Sci. Technol. A **21**, S96 (2003).
[11]H. Brune, Surf. Sci. Rep. **31**, 121 (1998).
[12]T. Michely and J. Krug, *Islands, Mounds and Atoms*, Springer Series in Surface Sciences, Vol. 42 (Springer Verlag, Berlin, 2004).
[13]J. G. Amar and F. Family, Phys. Rev. Lett. **74**, 2066 (1995).
[14]J. G. Amar and F. Family, Thin Solid Films **272**, 208 (1996).
[15]H. Yanagi and S. Okomato, Appl. Phys. Lett. **71**, 2563 (1997).
[16]F. Balzer and H. G. Rubahn, Adv. Funct. Mater. **15**, 17 (2005).
[17]G. Hlawacek, P. Puschnig, P. Frank, A. Winkler, C. Ambrosch-Draxl, and C. Teichert, Science **321**, 108 (2008).
[18]F.-J. Meyer zu Heringdorf, M. C. Reuter, and R. M. Tromp, Nature **412**, 517 (2001).
[19]K. Puntambekar, J. Dong, G. Haugstad, and C. D. Frisbie, Adv. Funct. Mater. **16**, 879 (2006).
[20]Y. Wu, T. Toccoli, J. Zhang, N. Koch, E. Iacob, A. Pallaoro, S. Iannotta, and P. Rudolf, Appl. Phys. A **95**, 21 (2009).
[21]Y. Wu, T. Toccoli, N. Koch, E. Iacob, A. Pallaoro, P. Rudolf, and S. Iannotta, Phys. Rev. Lett. **98**, 076601 (2007).
[22]S. Pratontep, F. Nüesch, L. Zuppiroli, and M. Brinkmann, Phys. Rev. B **72**, 085211 (2005).
[23]P. R. Ribic, V. Kalihari, C. D. Frisbie, and G. Bratina, Phys. Rev. B **80**, 115307 (2009).
[24]M. Tejima, K. Kita, K. Kyuno, and A. Toriumi, Appl. Phys. Lett. **85**, 3746 (2004).
[25]A. S. Killampalli, T. W. Schroeder, and J. R. Engstrom, Appl. Phys. Lett. **87**, 033110 (2005).
[26]B. R. Conrad, E. Gomar-Nadal, W. G. Cullen, A. Pimpinelli, T. L. Einstein, E. D. Williams, Phys. Rev. B **77**, 205328 (2008).
[27]E. Gomar-Nadal, B. R. Conrad, W. G. Cullen, E. D. Williams, J. Phys. Chem. C **112**, 5646 (2008).
[28]T. A. Witten Jr. and L. M. Sander, Phys. Rev. Lett. **47**, 1400 (1981).
[29]F. Balzer and H. G. Rubahn, Appl. Phys. Lett. **79**, 3860 (2001).
[30]A. Andreev, G. Matt, C. J. Brabec, H. Sitter, D. Badt, H. Seyringer, and N. S. Sariciftci, Adv. Mater. **12**, 629 (2000).
[31]R. Resel, J. Phys. Cond. Matt. **20**, 184009 (2008).
[32]C. Teichert, G. Hlawacek, A. Y. Andreev, H. Sitter, P. Frank, A. Winkler, and N. S. Sariciftci, App. Phys. A. **82**, 665 (2006).
[33]P. Frank, G. Hlawacek, O. Lengyel, A. Satka, C. Teichert, R. Resel, and A. Winkler, Surf. Sci. **601**, 2152 (2007).
[34]N. L. Allinger, Y. H. Yuh, and J. H. Lii, J. Am. Chem. Soc. **111**, 8551 (1989).
[35]J. H. Lii and N. L. Allinger, J. Am. Chem. Soc. **111**, 8566 (1989).
[36]J. H. Lii and N. L. Allinger, J. Am. Chem. Soc. **111**, 8576 (1989).
[37]J. W. Ponder, TINKER–Software tools for molecular design, 5.1 ed. [http://dasher.wustl.edu/tinker/].
[38]K. N. Baker, A. V. Fratini, T. Resch, H. C. Knachel, W. W. Adams, E. P. Socci, and B. L. Farmer, Polymer **34**,1571 (1993).
[39][http://gwyddion.net/].
[40]T. Vicsek and F. Family, Phys. Rev. Lett. **52**, 1669 (1984).
[41]A. Pimpinelli and T. L. Einstein, Phys. Rev. Lett. **99**, 226102 (2007).
[42]P. A. Mulheran and J. A. Blackman, Phys. Rev. B. **53**, 10261 (1996).
[43]A. Pimpinelli and T. L. Einstein, Phys. Rev. Lett. **104**, 149602 (2010).
[44]M. Li, Y. Han, and J. W. Evans, Phys. Rev. Lett. **104**, 149601 (2010).
[45]K. Oura, V. G. Lifshits, A. A. Saranin, A. V. Zotov, and M. Katayama, *Surface Science: An Introduction* (Springer Verlag, Berlin, 2003).
[46]C. Ratsch, P. Smilauer, A. Zangwill, D. D. Vvedensky, Surf. Sci. **329**, L599 (1995).
[47]V. P. Zhdanov, Surf. Sci. Rep. **12**, 183 (1991).
[48]P. W. Atkins, *Physical Chemistry* (Oxford University Press, Oxford, United Kingdom, 1988).
[49]A. Winkler, Springer Proc. Phys. **129**, 107 (2009).
[50]K. R. Paserba and A. J. Gellman, Phys. Rev. Lett. **86**, 4338 (2001).
[51]S. L. Tait, Z. Dohnalek, C. T. Campbell, and B. D. Kay, J. Chem. Phys. **122**, 164708 (2005).
[52]K. A. Fichthorn and R. A. Miron, Phys. Rev. Lett. **89**, 196103 (2002).
[53]S. Müllegger and A. Winkler, Surf. Sci. **600**, 1290 (2006).
[54]B. Müller, L. Nedelmann, B. Fischer, H. Brune, and K. Kern, Phys. Rev. B **54**, 17858 (1996).
[55]K. Müller, A. Kara, T. K. Kim, R. Bertschinger, A. Scheybal, J. Osterwalder, T.A. Jung, Phys. Rev. B **79**, 245421 (2009).
[56]D. W. Scott, Biometrika **66**, 605 (1979).

5. Summary

The organic molecules (6P, 5A) were deposited on sputter amorphized mica by physical vapor deposition in ultra-high vacuum (UHV). A quartz microbalance was used to quantify the deposited amount. Thermal desorption spectroscopy (TDS) was applied to obtain information on the energetics and kinetics of adsorption, nucleation and desorption. Ex-situ atomic force microscopy (AFM) was used to determine the morphology, island density and island size distribution of the sub-monolayer films. Both types of molecules formed islands, composed of standing molecules, on the sputter amorphized mica surface [P3, P6]. This is typical for organic film growth on weakly interacting substrates, e.g. on mica or silicon dioxide, as frequently used in fundamental and application studies.

The first issue concerns the adsorption process. It is usually assumed in the literature that organic molecules, at sufficiently low temperature, adsorb with a probability of one. We could unequivocally demonstrate that this is not generally the case. The sticking coefficient for 6P at low, sub-monolayer coverage is clearly smaller than for higher coverage. Also a smaller sticking coefficient of s_0 = 0.2 has been published for rubicene on SiO_2 [19]. Another important issue is the nucleation process itself. It is nearly exclusively assumed that film growth can be described by diffusion-limited aggregation (DLA). According to the seminal paper by Venables et al. [1] the island density N can be described by a power-law function of the deposition rate R, $N \sim R\alpha$, with $\alpha = i/(i+2)$, i being the critical island size. Thus, one can in principle determine i by preparing sub-monolayer films at different deposition rates, counting the island density in the AFM image and plotting $\ln N$ vs $\ln R$. The slope of this line, which is predicted to be between 0.33 and 1, allows the calculation of i. However, it turns out that for both, pentacene and hexaphenyl on amorphous mica, these lines are bent and change from $\alpha = 0.7$ to $\alpha = 1.3$. The latter slope is inconsistent with DLA, however, can be explained by so-called attachment-limited aggregation (ALA) [6, 20, P1]. In this case $\alpha = 2i/(i+3)$. One can easily understand why this is a reasonable assumption for large organic molecules. On the one hand the diffusion coefficient is very high, due to low diffusion barriers, but on the other hand it can be argued that the incorporation of the molecules at the rim of the islands is sterically hindered because of the necessary reorientation.

A further aspect is the accommodation of the molecules upon adsorption and prior to nucleation. In the Venables model it is assumed that the molecules are instantaneously equilibrated and perform random hops before nucleation. We could show that the molecules may exist in a hot-precursor state after adsorption and move ballistically for some time before full accommodation [3]. This process has been modelled through an effective molecular temperature higher than the substrate temperature, which leads to a bend in the plot of $\ln N$ vs $1/T$. This explains some puzzling results of the literature [P6, 19, 20]. The scaling of the island size distribution (ISD) and/or the capture zone distribution (CZD) can also be used to determine i, but so far analytic functions for ISD [3] and CZD [21] exist only for DLA. For CZD the scaling function is $P_\beta(s) = a_\beta s^\beta exp(-b_\beta s^2)$, with $ß = i+2$. We have extended the CZD also to attachment-limited aggregation; for this

case we obtain $ß = (i+3)/2$. Furthermore, we could prove that for compact islands the "exponent equality" $\alpha \cdot \beta = i$ holds, independent of the aggregation mechanism [P 4]. This important finding should help experimenters to better characterize nucleation and growth of thin films.

Another exciting issue is that atomic force microscopy (AFM) revealed a bimodal island size distribution for the films on both surfaces [2]. On freshly cleaved mica long needle-like islands exist, which are surrounded by small crystallites. On the sputter-amorphized substrates, large dendritic islands exist which are again surrounded by small, compact islands. We could prove by thermal desorption spectroscopy that the small islands are the result of adsorbate-induced subsequent nucleation, when the films were exposed to air. In case of the freshly cleaved mica, islands grow on a wetting layer in vacuum. This layer dewets and forms the small islands upon venting, due to the adsorption of water. In the case of the amorphous mica substrate an equilibrium exists between the islands and a two-dimensional gas phase in the sub-monolayer regime. Again, the latter phase nucleates after venting. In a particular coverage range, islands due to nucleation during deposition and subsequent nucleation coexist on the substrate, leading to the bimodal island size distribution. Kinetic Monte Carlo (KMC) simulations were performed to model the nucleation process after venting on the sputter-modified mica substrate. The density of the subsequently nucleated islands just depends on the initial coverage and the critical island size. A critical cluster size of $i = 7$ molecules was determined for 6*P* on amorphized mica, by comparing the KMC results with the AFM images in case of adsorbate-induced nucleation.

Bibliography

[1] J.A. Venables, G.D.T. Spiller, and M. Hanbucken. Nucleation and growth of thin films. *Reports on Progress in Physics*, 47:399–459, 1984.

[2] R. Ruiz, B. Nickel, N. Koch, L. Feldman, R. Haglund, A. Kahn, F. Family, and G. Scoles. Dynamic scaling, island size distribution and morphology in the aggregation regime of submonolayer pentacene films. *Physical Review Letters*, 91:136102, 2003.

[3] J.G. Amar and F. Family. Critical cluster size: Island morphology and size distribution in submonolayer epitaxial growth. *Physical Review Letters*, 74:2066–2069, 1995.

[4] T. Vicsek and F. Family. Dynamic scaling for aggregation of clusters. *Physical Review Letters*, 52:1669–1672, 1984.

[5] B. Stadlober, U. Haas, H. Maresch, and A. Haase. Growth model of pentacene on inorganic and organic dielectrics based on scaling and rate-equation theory. *Physical Review B*, 74:165302, 2006.

[6] A. Pimpinelli and T.L. Einstein, Phys. Rev. Lett. 99, 226102 (2007).

[7] P.W. Palmberg, G.E. Riach, R.E. Weber, and N.C. MacDonald. Handbook of Auger electron spectroscopy. *Physical Electronics Industries, Inc.*, 1972.

[8] G. Ertl and J. Küppers. Low energy electrons and surface chemistry. *Verlag Chemie*, 1974.

[9] D. Briggs, M.P. Seah, *Practical Surface Analysis by Auger and X-ray Photoelectron Spectroscopy*. John Wiley & Sons, Chichester/ NewYork/ Brisbane/ Toronto/ Singapore (1983).

[10] K. Oura, V.G. Lifshits, A.A. Saranin, A.V. Zotov, M. Katayama, *Surface Science*. Springer Verlag, Berlin (2003).

[11] H. Bubert, H. Jenett, *Surface and Thin Film Analysis: Principles, Instrumentation, Applications*. Wiley-VCH, Weinheim (2002).

[12] http://www.wsu.edu/~scudiero/, 2009.

[13] SecretDisc. http://de.wikipedia.org/wiki/Cantilever(Mikroskop). 2008.

[14] S. Schröder and M. Gottfried. Temperature programmed desorption (TPD)/ thermal desorption spectroscopy (TDS). *FU Berlin*, 2002.

[15] P. Frank. Thin film growth of rod-like and disc-shaped organic molecules on insulator and noble metal surfaces. *PhD thesis, TU Graz*, 2009.

[16] Nanosurf. Operating instructions, easyScan 2 AFM. 2005.

[17] Nanosurf. Software reference, easyScan 2. 2005.

[18] P. Klapetek, D. Necas, and C. Anderson. Gwyddion user guide. 2009.

[19] B. Scherwitzl, W. Lukesch, A. Hirzer, J. Albering, G. Leising, R. Resel, and A. Winkler, J. Phys. Chem. C 117, 4115 (2013).

[20] D. Kandel, Phys. Rev. Lett. 78, 499 (1997).

[21] J.A. Venables and H. Brune, Phys. Rev. B 66, 195404 (2002).

[22] G. Berlanda et al., Phys. Rev. B 69, 085409 (2004).

[23] J. Yang et al., J. Phys. Chem. 112, 7816 (2008).